moisture capacity curve, which gives:

$$R = \frac{S_I}{S_T} M_e + \frac{S_T - S_I}{S_T} \int_w^{M_e + w} x(\xi)\, d\xi \quad \text{if} \quad M_e + w < w_m \tag{3.32}$$

or

$$R = \frac{S_I}{S_T} M_e + \frac{S_T - S_I}{S_T} \left\{ M_e - \int_w^{w_m} [1 - x(\xi)]\, d\xi \right\} \quad \text{if} \quad M_e + w \geq w_m. \tag{3.33}$$

Equations (3.32) and (3.33), can also be expressed in terms of the catchment average soil moisture content (W) and that at saturation (Wm) and after integration they become:

$$\begin{cases} R = M_e + \dfrac{S_T - S_I}{S_T} \left\{ (W_m - W) - W_m \left[\left(1 - \dfrac{W}{W_m} \right)^{\frac{1}{b+1}} - \dfrac{M_e}{(b+1) W_m} \right]^{b+1} \right\}, \\ \qquad\qquad \text{for} \quad 0 < M_e < (b+1) W_m \left(1 - \dfrac{W}{W_m} \right)^{\frac{1}{b+1}} \\ R = M_e - \dfrac{S_T - S_I}{S_T} (W_m - W) \quad \text{for} \quad M_e \geq (b+1) W_m \left(1 - \dfrac{W}{W_m} \right)^{\frac{1}{b+1}} \end{cases} \tag{3.34}$$

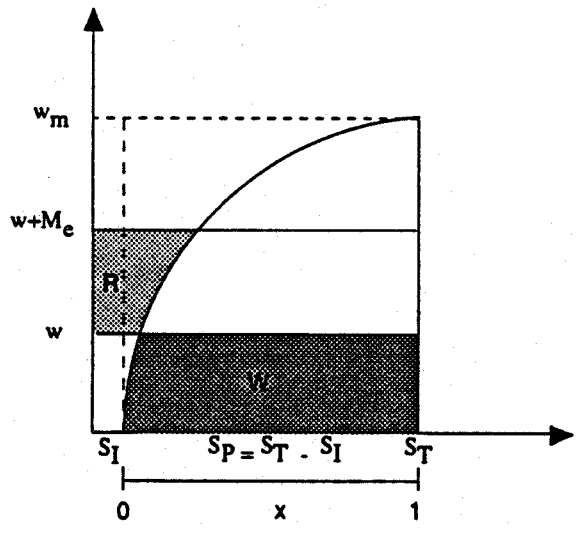

Figure 3.3.4 Runoff R generated by an effective meteorological input $M_e>0$.

If the precipitation P is smaller than the potential evapotranspiration ET_p the effective meteorological input M_e, becomes negative:

$$M_e = P - ET_p < 0 \tag{3.35}$$

which implies that the runoff R is zero. The actual evapotranspiration is then computed as the precipitation P plus a quantity which depends upon M_e reduced by the average degree of saturation of the soil, which gives:

$$ET_a = P + \left(ET_p - P\right)\frac{\left(S_T - S_I\right)}{S_T}\frac{\left(1+\frac{W}{W_m}\frac{1}{b}\right)-\left(1-\frac{W}{W_m}\right)^{\frac{1}{b+1}}}{\left(1+\frac{1}{b}\right)-\left(1-\frac{W}{W_m}\right)^{\frac{1}{b+1}}} \tag{3.36}$$

These equations, which represent the average surface runoff produced in the sub-catchment, must be associated with an equation of state in order to update the mean water content in the soil. This equation takes the form:

$$W(t+\Delta t) = W(t) + P(t,t+\Delta t) - ET_a(t,t+\Delta t) - R(t,t+\Delta t) - D(t,t+\Delta t) - I(t,t+\Delta t) \tag{3.37}$$

where:

$W(t+\Delta t)$ is the soil moisture content at time $t+\Delta t$;

$W(t)$ is the soil moisture content at time t.

$P(t,t+\Delta t)$ is the area precipitation between t and $t+\Delta t$;

$ET_a(t,t+\Delta t)$ is the loss through evapotranspiration between t and $t+\Delta t$;

$R(t,t+\Delta t)$ is the total runoff between t and $t+\Delta t$;

$D(t,t+\Delta t)$ is the loss through drainage between t and $t+\Delta t$;

$I(t,t+\Delta t)$ is the percolation loss to groundwater between t and $t+\Delta t$;

All the quantities representing averages over the sub-basin are expressed in mm.

The non-linear response of the unsaturated soil to precipitation, represented by the shape of the distribution curve given by equation (3.29), is strongly affected by the horizontal drainage and vertical percolation losses. The drainage loss D is an important quantity to be reproduced in a hydrological model, since on the one hand it affects the soil moisture storage and on the other hand it controls the hydrograph recession. Experience derived from applications suggested the use of the following empirical relationship to express also the drainage loss D as a non-linear function of the soil moisture content:

$$D = D_{min}\frac{W}{W_m} \qquad \text{for} \quad W < W_d$$

$$D = D_{min}\frac{W}{W_m} + (D_{max} - D_{min})\left(\frac{W - W_d}{W_m - W_d}\right)^c \qquad \text{for} \quad W \geq W_d \qquad (3.38)$$

where:

c = exponent of the variation law;

D_{min}, D_{max} = drainage parameters at saturation;

W_d = moisture content threshold value;

The percolation loss I, which feeds the groundwater module, which will control the base flow in the model, varies less significantly over time if compared with the other terms; nevertheless a non-linear behaviour is also assumed as follows:

$$I = 0 \qquad \text{for} \quad W < W_i$$

$$I = \alpha(W - W_i) \qquad \text{for} \quad W \geq W_i \qquad (3.39)$$

where W_i represents the moisture content threshold value below which the percolation may be considered negligible, and α is an empirical coefficient.

The total runoff per unit area produced by the precipitation P is finally expressed as:

$$R_{tot} = R + D + B \qquad (3.40)$$

where:

B is the base flow generated by the presence of a groundwater table fed by the percolation, and computed by the groundwater module.

The Evapotranspiration Module

Although the Penman-Monteith equation is the most rigorous theoretical description for this component, in practice many simplifications are necessary because in most countries the required historical data for its estimation are not extensively available, and, in addition, apart from a few meteorological stations, almost nowhere are real time data available for flood forecasting applications. Moreover it should be clearly understood that evapotranspiration plays a major role in the rainfall-runoff process not really in terms of its instantaneous impact, but in terms of its cumulative temporal effect on the soil moisture volume depletion; this reduces the need for an extremely accurate expression, provided that its integral effect be well preserved. In the ARNO model, the effects of the vapour pressure and wind speed are explicitly ignored and evapotranspiration is calculated starting from of a simplified equation known as the radiation method (Doorembos et al., 1984):

$$ET_{0d} = C_v W_{ta} R_s = C_v W_{ta}\left(0.25 + 0.50\frac{n}{N}\right)R_a \qquad (3.41)$$

where:

ET_{0d} is the reference evapotranspiration, i.e. evapo-transpiration in soil saturation conditions caused by a reference crop (mm/day) ;

C_v is an adjustment factor obtainable from tables as a function of the mean wind speed;

W_{ta} is a compensation factor that depends on the temperature and altitude;

R_s is the short wave radiation measured or expressed as a function of R_a in equivalent evaporation (mm/day);

R_a is the extraterrestrial radiation expressed in equivalent evaporation (mm/day);

n/N is the ratio of actual hours of sunshine to maximum hours of sunshine (values measured or estimated from mean monthly values).

Hence the calculation of R_s requires both knowledge of R_a, obtainable from tables as a function of latitude, and knowledge of actual n/N values, which may not be available. In the absence of the measured short wave radiation values R_s or of the actual number of sunshine hours otherwise needed to calculate R_s as a function of R_a (see equation (3.41)), an empirical equation was developed that relates the reference potential evapotranspiration ET_{0d}, computed on a monthly basis using one of the available simplified expressions, to the compensation factor W_{ta}, the mean recorded temperature of the month T and the maximum number of hours of sunshine N. The developed relationship is linear in temperature (and hence additive), and permits the dissaggregation of the monthly results on a daily or even on an hourly basis, while most other empirical equations are ill-suited for time intervals shorter than one month.

The relation used, which is structurally similar to the radiation method formula in which the air temperature is taken as an index of radiation, is:

$$ET_0 = \alpha + \beta N W_{ta} T_m \tag{3.42}$$

where:

ET_0 is the reference evapotranspiration for a specified time step Δt (in mm/Δt);

α,β are regression coefficients to be estimated for each sub-basin;

T_m is the area mean air temperature averaged over Δt;

N is the monthly mean of the maximum number of daily hours of sunshine (tabulated as a function of latitude).

W_{ta} for a given sub-basin can be either obtained from tables or approximated by a fitted parabola:

$$W_{ta} = A\overline{T}^2 + B\overline{T} + C \tag{3.43}$$

where:

A, B, C are coefficients to be estimated;

$\bar{T}$ is the long term mean monthly sub-basin temperature (°C).

The Snowmelt Module

Again, for reasons of limited data availability, the snowmelt module is driven by a radiation estimate based upon the air temperature measurements; in practice the inputs to the module are the precipitation, the temperature, and the same radiation approximation which is used in the evapotranspiration module.

Given the role that altitude may play in combination with the thermal gradient, the sub-catchment area is subdivided into a number of equi-elevation zones (snow-bands) according to the hypsometric curve, and for each zone simplified mass and energy budgets are continuously updated. For each snowband the following steps, similar to those adopted in SHE (Abbott et al., 1986), are followed:

- Estimation of radiation at the average elevation of the snowband;
- Decide whether precipitation is solid or liquid;
- Estimation of the water mass budget based on the hypothesis of zero snowmelt;
- Estimation of the energy budget based on the hypothesis of zero snowmelt;
- Comparison of the total available energy with that sustained as ice by the total available mass at 273 °K;
- Computation of the snowmelt produced by the excess energy;
- Updating of the water mass budget;
- Updating of the energy budget.

Estimation of radiation at the average elevation of the snowband

The estimation of the radiation is performed by re-converting the latent heat (which has already been computed as the reference evapotranspiration ET_0) back into radiation, by means of a conversion factor C_{er} (Kcal Kg^{-1}) which can be found in any thermodynamics textbook as:

$$C_{er} = 606.5 - 0.695\ (T - T_0) \tag{3.44}$$

where T_0 is the temperature of fusion of snow (273 °K).

In addition, in order to account for albedo which plays an extremely important role in snowmelt, it is necessary to apply an efficiency factor which will be assumed approximately as $\eta = .6$ for clear sky and $\eta = .8$ for overcast conditions: this leads to the following estimate for the driving radiation term:

$$Rad = \eta\ \left[606.5 - 0.695(T - T_0)\right] ET_0 \tag{3.45}$$

Given the lack of information concerning the status of the sky when simulating with historical data, for practical purposes it is generally assumed in the ARNO model that the sky is clear if there is no precipitation and overcast if precipitation is being measured.

Decision on whether the precipitation is solid or liquid

Information concerning the status of precipitation (solid or liquid) is rarely available as a continuous record; therefore it is necesary to define a mechanism, mainly based upon the air temperature measurements and the historical precipitation. If one plots the frequency of the usually scattered observations with which precipitation was observed to be liquid or snow as a function of the air temperature, a Gaussian distribution is generally obtained, with a mean value T_s which very seldom will coincide with T_0. For this reason, the following rules are adopted:

- Precipitation is taken as liquid if the air temperature $T > T_s$;
- Precipitation is taken as snow otherwise.

The value of T_s (which generally ranges between 271 and 275 °K) must be derived, as previously mentioned, by plotting the frequency of the status of historically recorded precipitation as a function of the air temperature.

Estimating the water mass

The water equivalent mass is estimated with the following simple mass balance equation, where all quantities are expressed in mm of water:

$$Z^*_{t+\Delta t} = Z_t + P \tag{3.46}$$

The water equivalent at the end of the time step is designated with a star because it is a tentative value which does not yet account for the eventual snowmelt.

Estimating the energy

Similarly to the mass, the energy is estimated in the following way, by computing the increase (or decrease) of total energy E:

- if the precipitation is zero:

$$E^*_{t+\Delta t} = E_t + Rad \tag{3.47}$$

-if the precipitation is non-zero and the precipitation is in the solid phase ($T \leq T_{sn}$)

$$E^*_{t+\Delta t} = E_t + Rad + C_{sg}\, T_0\, P \tag{3.48}$$

-if the precipitation is non-zero and the precipitation is in the liquid phase ($T > T_{sn}$)

$$E^*_{t+\Delta t} = E_t + Rad + \left[C_{si}\, T_0 + C_{lf} + C_{sa}(T - T_0)\right]P \tag{3.49}$$

Again the total energy at the end of a time step is designated with a star to denote a tentative value; in the previous equations C_{si} is the specific heat of ice (0.5 Kcal °K^{-1} Kg^{-1}), C_{lf} the heat of fusion of water(79.6 Kcal Kg^{-1}) and C_{sa} the specific heat of water(1 Kcal °K^{-1} Kg^{-1}).

Estimation of snowmelt and updating of mass and energy state variables

If the total available energy is smaller or equal to that required to maintain the total mass in the solid phase at the temperature T_0 i.e; $C_{si}Z^*_{t+\Delta t}T_0 \geq E^*_{t+\Delta t}$,it means that the available energy is not sufficient to melt part of the accumulated water, and therefore:

$$\begin{cases} R_{sm} = 0 \\ Z_{t+\Delta t} = Z^*_{t+\Delta t} \\ E_{t+\Delta t} = E^*_{t+\Delta t} \end{cases} \tag{3.50}$$

where R_{sm} is the snowmelt expressed in mm. If the total available energy is larger than that required to maintain the total mass in the solid phase at the temperature T_0, it means that part of the accumulated water will melt, and therefore the following energy balance equation holds:

$$C_{si}\left(Z^*_{t+\Delta t} - R_{sm}\right)T_0 = E^*_{t+\Delta t} - \left(C_{si}T_0 + C_{lf}\right)R_{sm} \tag{3.51}$$

from which the snowmelt and the mass and energy state variables can be computed as:

$$\begin{cases} R_{sm} = \dfrac{E^*_{t+\Delta t} - C_{si}T_0Z^*_{t+\Delta t}}{C_{lf}} \\ Z_{t+\Delta t} = Z^*_{t+\Delta t} - R_{sm} \\ E_{t+\Delta t} = E^*_{t+\Delta t} - \left(C_{si}T_0 + C_{lf}\right)R_{sm} \end{cases} \tag{3.52}$$

The Groundwater Module

The groundwater module represents the overall response of its storage by means of a cascade of linear reservoirs, characterised by two parameters: the number of reservoirs n and their time constant K, a model which is well known in hydrology as the Nash model (Nash, 1958). For practical reasons, instead of using the Gamma distribution function to express the impulse response, a numerical procedure has been adopted. The expression to be used can easily be derived from the assumption of a cascade of linear

reservoirs where the volume of the ith reservoir is proportional to its outflow, i.e. $S_t = K B_t^i$; thus, the continuity equation written for the generic ith reservoir becomes:

$$K \frac{\partial B_t^i}{\partial t} = B_t^{i-1} - B_t^i \tag{3.53}$$

which, after discretization in time with a finite difference scheme centred at time $t+\Delta t/2$, becomes:

$$\frac{K}{\Delta t}\left(B_{t+\Delta t}^i - B_t^i\right) = \frac{B_{t+\Delta t}^{i-1} + B_t^{i-1}}{2} - \frac{B_{t+\Delta t}^i + B_t^i}{2} \tag{3.54}$$

and the required expression is then obtained by making $B_{t+\Delta t}^i$ explicit:

$$B_{t+\Delta t}^i = \frac{2K - \Delta t}{2K + \Delta t} B_t^i + \frac{\Delta t}{2K + \Delta t}\left(B_{t+\Delta t}^{i-1} + B_t^{i-1}\right) \tag{3.55}$$

where:

B^i is the outflow from the ith reservoir

$B^0=I$ is the percolation given by the soil moisture balance equation

$B^n=B$ is the resulting base flow

Equation (3.55) is then recursively solved n times at each time step.

The Parabolic Routing Module

In the ARNO model hillslope routing and channel routing of distributed inflows are both performed using a distributed inflow linear parabolic model, while channel routing of upstream inflows to a sub-basin is performed by means of a concentrated input parabolic model. The parameters of the two linear parabolic transfer functions can be estimated as a function of the slope, the length of the drainage system and the roughness, as is shown below.

Routing of upstream inflows

The propagation of inflows from upstream is carried out by means of a linear model consisting of a parabolic unit hydrograph deriving from the analytical integration of the unsteady flow equations when the inertia effects are ignored and the coefficients are linearised around mean outflow values. In this case the following differential equation is obtained:

$$\frac{\partial Q}{\partial t} = D\frac{\partial^2 Q}{\partial x^2} - C\frac{\partial Q}{\partial x} \tag{3.56}$$

where D and C are the diffusivity and the convectivity coefficient respectively. The discrete time solution of equation (3.56) for mean values of the coefficients C and D is (Todini and Bossi, 1986):

$$\overline{U}_{\Delta x}(t, t+\Delta t) = \frac{1}{\Delta t^2}\left[IF(t+\Delta t) - 2IF(t) + IF(t-\Delta t)\right] \tag{3.57}$$

where

$$IF(t) = \int_0^t F(\vartheta)\,d\vartheta = \int_0^t \int_0^{\vartheta} u_{\Delta x}(\tau)\,d\tau\,d\vartheta \tag{3.58}$$

with $u_{\Delta x}$, the impulse response relevant to equation (3.58), which can be written as:

$$u_{\Delta x}(\tau) = \frac{\Delta x}{\sqrt{4\pi D\tau^3}} e^{-\frac{(\Delta x - C\tau)^2}{4D\tau}} \tag{3.59}$$

Integrating equation (3.58), after substitution from equation (3.59) one obtains:

$$IF(t) = \frac{1}{C}\left[(Ct - \Delta x)N\left(-\frac{\Delta x - Ct}{\sqrt{2Dt}}\right) + (Ct + \Delta x)e^{\frac{\Delta x C}{D}} N\left(-\frac{\Delta x + Ct}{\sqrt{2Dt}}\right)\right] \tag{3.60}$$

where N(•) is the value of the Standard Normal probability distribution in (•), and Δx is the length of the channel reach.

Diffuse lateral inflow routing

The runoff generated in each sub-basin moves first along the slopes and then reaches the drainage network as diffuse inflow that, for simplicity, may be considered uniformly distributed. In this case the following differential equation applies:

$$D\frac{\partial^2 Q}{\partial x^2} - C\frac{\partial Q}{\partial x} - \frac{\partial Q}{\partial t} = -Cq \tag{3.61}$$

where q is the lateral inflow per unit length. The discrete time solution of equation (3.61) for mean values of the coefficients C and D is (Franchini and Todini, 1988):

$$\overline{UL}_{\Delta x}(t, t+\Delta t) = \frac{1}{\Delta t^2}\left[IG(t+\Delta t) - 2IG(t) + IG(t-\Delta t)\right] \tag{3.62}$$

where:

$$IG(t) = \frac{C}{2}\left[t^2 - IIF(t)\right] \tag{3.63}$$

with

$$IIF(t) = \int_0^t IF(\xi)\,d\xi = \int_0^t \int_0^\xi F(\vartheta)\,d\vartheta\,d\xi = \int_0^t \int_0^\xi \int_0^\vartheta u_{\Delta x}(\tau)\,d\tau\,d\vartheta\,d\xi \tag{3.64}$$

Integration of equation (3.64), after substitution of $u_{\Delta x}$ from equation (3.59), yields:

$$\begin{aligned} IG(t) = {} & \frac{C}{2}\left\{t^2 - \left(t^2 + \frac{\Delta x^2}{C^2}\right)\left[N\left(-\frac{\Delta x - Ct}{\sqrt{2Dt}}\right) + N\left(-\frac{\Delta x + Ct}{\sqrt{2Dt}}\right)e^{\frac{\Delta x C}{D}}\right]\right\} + \\ & + \frac{C}{2}\left\{\frac{2\Delta x}{C}\left(t - \frac{\Delta x}{C^2}\right)\left[N\left(-\frac{\Delta x - Ct}{\sqrt{2Dt}}\right) - N\left(-\frac{\Delta x + Ct}{\sqrt{2Dt}}\right)e^{\frac{\Delta x C}{D}}\right]\right\} + \\ & + \frac{C}{2}\left\{\frac{2\Delta x}{C^2}\sqrt{\frac{Dt}{\pi}}e^{-\frac{(\Delta x - Ct)^2}{4Dt}}\right\} \end{aligned} \tag{3.65}$$

The results provided by equation (3.62) when substitued for $IG(t)$ given by equation (3.65), differ from the ones obtained by Naden (1992), in that they represent the response of a discrete time system to a time discretised input (see Todini and Bossi, 1986)

As mentioned earlier the parameters of each of the models are naturally composed of the two convectivity (C) and diffusivity (D) coefficients for each response function which are related to the dimensions, slopes and lengths of the individual sub-basins. In general very small values for D are assumed for the hillslopes, given the marked kinematic nature of the phenomenon; generally, D increases with the size of the river and with the inverse of the bottom slope. Table 3.3.1 gives an indication of the orders of magnitude of C and D.

	C (m/s)	D(m^2/s)
Hillslopes	1-2	1-100
Brooks	1-3	100-1000
Rivers	1 - 3	1000-10000
Large rivers	1 - 3	10000-100000

Table 3.3.1 - Approximate initial guess for parameters C and D.

3.4 ANALYSES AND FURTHER MODEL DEVELOPMENTS

3.4.1 Using TOPMODEL on Real Data

Alternative formulation of TOPMODEL equations.

The 'soil column' is modeled with two interconnected reservoirs. Evapotranspiration is taken from the root zone storage. Actual evapotranspiration (*AET*) is computed as a variable fraction of the potential evapotranspiration (*PET*):

$$AET = PET\, SRZ / SRMAX \tag{3.66}$$

where *SRZ* is the state variable describing the root zone storage and *SRMAX* is the maximum capacity. The 'gravity' reservoir includes two storages. The upper one controls the unsaturated zone while the bottom one represents the behavior of the saturated zone. The upper storage is controlled by the saturation deficit of the saturated store S_i which is equivalent to the quantity of water required to fill completely this upper reservoir.

Vertical drainage q_{vi} to the saturated reservoir is delayed as a function of the unsaturated storage SUZ_i and a mean residence time per unit of deficit (Beven and Wood, 1983):

$$q_{vi} = SUZ_i / (t_d . S_i) \; with \; q_{vi} \leq SUZ_i \tag{3.67}$$

where t_d is a time delay parameter per unit of deficit. This time delay t_d is assumed to be constant for the catchment and represents the second parameter of the model. Local lateral subsurface flow q_i from the saturated zone is assumed to be (Beven, 1986):

$$q_i = K_i \tan\beta \exp(-S_i / m) \tag{3.68}$$

where K_i is a soil lateral transmissivity parameter, $tan\beta$ is the local slope and m is a model parameter. This assumption is consistent with a set of more physically based hypotheses: local hydraulic gradient equal to the local topographic slope, exponentially decreasing with depth hydraulic conductivity, and constant with depth 'effective' porosity. According to these assumptions, the model parameters m and K_i can be expressed as follows:

$$m = \Delta\theta_s / f \tag{3.69}$$

$$K_i = K_o / f \tag{3.70}$$

where $\Delta\theta_S$ is the soil 'effective' (readily drainable) porosity, K_O is the saturated hydraulic conductivity at the soil surface and f is the parameter that characterizes the exponential decay of hydraulic conductivity with depth.

To step from the 'soil column' to the catchment scale, Beven and Kirkby (1979) introduced some simplifying assumptions in order to integrate over the whole catchment the behavior of the saturated zone: steady state subsurface flow, catchment averaged inputs to the saturated zone (R), and spatially constant m parameter. Using these assumptions a one-to-one relationship between the catchment areally averaged saturation deficit $\bar{S}$ and local saturation deficits can be derived (Beven, 1986):

$$\bar{S} = S_i - m\left(\gamma - ln(a / K_i \tan\beta)_i\right) \tag{3.71}$$

where $\gamma$is a constant for the basin which can be separated in a topographic part and a soil part:

$$\gamma = \frac{1}{A}\int_A ln(a / tan\beta)_i - \frac{1}{A}\int_A ln(K_i) \qquad (3.72)$$

The first integral is the topographic constant λ (Beven and Kirkby, 1979). In equation (3.71), $ln(a / K_i tan\beta)$ is called the soil-topographic index which also shows two components respectively related to topography and soil properties:

$$ln(a / K_i tan\beta)_i = ln(a / tan\beta)_i - ln(K_i) \qquad (3.73)$$

where $ln(a / tan\beta)_i$ is called the topographic index. If soil transmissivity is assumed to be constant over the catchment, equation (3.71) drops to the initial formulation of Beven and Kirkby (1979):

$$\bar{S} = S_i - m\left(\lambda - ln(a / tan\beta)_i\right) \qquad (3.74)$$

Since the actual pattern of soil transmissivity is seldom known in most practical applications, including that of Haute-Mentue catchment, it was decided to use equation (3.74).

Subsurface flow contribution Q_b is expressed as (Beven and Kirkby, 1979):

$$Q_b = Q_o \exp(-\bar{S} / m) \qquad (3.75)$$

A theoretical expression for Q_O can be obtained by integration of local subsurface flow given by (3.68) along stream banks (Beven, 1986):

$$Q_o = \exp(-\gamma) \qquad (3.76)$$

Parameter estimation

The version of TOPMODEL described above is parameterized by the topographic index distribution and five single valued parameters: the root zone maximum storage SRMAX (mm), the vertical drainage parameter t_d (h/mm), the subsurface flow at zero mean deficit Q_O (mm/h), the m (mm) parameter characterizing the decrease of hydraulic conductivity with depth and the kinematic wave velocity (m/s).

The topographic index was derived from a raster digital terrain model (DTM) with a grid spacing of 10 m using the multiple flow direction algorithm proposed by Quinn et al. (1991). Given the fact that in the Haute-Mentue catchment stream beds generally lie on the low permeability bedrock, the method was modified in order to account for the stream network. In the case of "river" gridcells the upslope draining area was not routed to the downslope gridcells. This is consistent with the assumption made to derive (3.76): the integral of upslope draining area along stream banks is equal to the catchment area. The effect of this modified approach is shown in Fig. 3.4.1b for Corbassière. It is obvious that differences become larger as catchment area (and thus the draining area of 'river' gridcells) increases.

The sensitivity of topographic index cumulative curves to gridcell size was analyzed. The accuracy of the topographic support used to derive the DTM was also studied. Gridcells of 5 and 10 meters were used for a DTM derived from the 1 m equidistance contour lines obtained from a precise leveling. Gridcells of 10 and 25 m were used for a DTM developed from the 10 m equidistance contour lines of a 1/5000 topographic map. A systematic trend was observed (Fig. 3.4.1a). The 'position' parameter (λ) becomes higher and the spread of the distribution is reduced with increasing grid-size and decreasing accuracy of the map support. Grid size acts as a threshold for upslope draining area (a) in near to divide locations. Larger grid sizes together with a less accurate DTM smooth the topography, thus reducing the variability of $\tan\beta$ but also decreasing its geometric mean (which is equivalent to an increase in the 'position' parameter). Sensitivity of topographic index maps to the above mentioned factors is even more dramatic than that of cumulative distribution curves (Jordan, 1992, 1994a).

Using the topographic index instead of the complete soil-topographic index also affects the shape of the distribution curve used in model calculations. If the spatial pattern of transmissivity is not positively correlated with topographic index, soil-topographic index curves will always be more spread out than those of the topographic index alone. Theoretical considerations show that model results, in particular the location of contributing areas, are strongly dependent on the sub-catchment definition. This is of considerable concern when one is interested in the prediction of actual location of contributing areas. However for the forecasting problem this drawback seems less relevant as numerical experiments have shown that the total outflow is much less influenced by the sub-catchment definition.

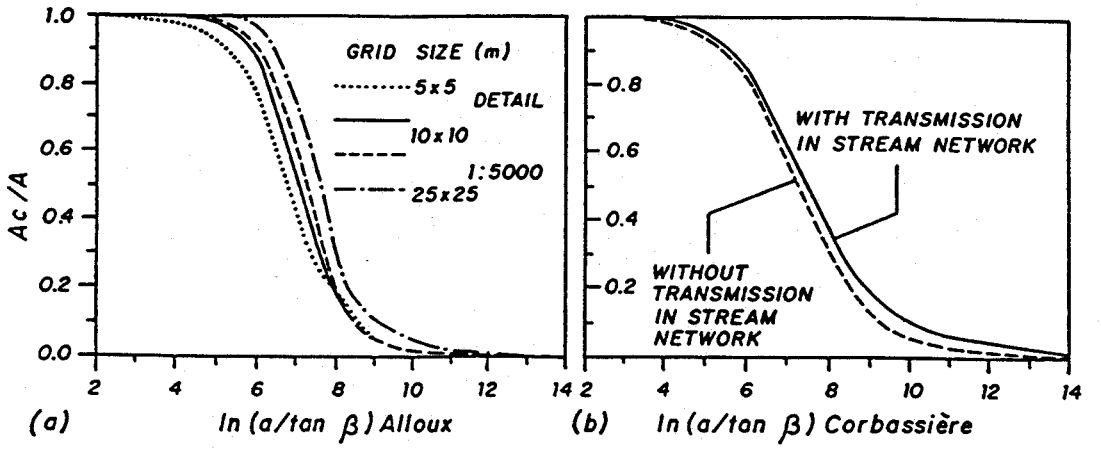

3.4.1 Sensitivity analysis of topographic index cumulative distribution with respect to a) gridcell size and map accuracy and b) to treatment of 'stream' gridcells.

These remarks, together with problems related to the numerical algorithm itself suggest that, for routine calculations of the topographic index distribution curve, errors are likely to be systematic. This may bias model results. From (3.76), it can be seen that an overestimation of the 'position' parameter of the topographic index distribution (λ) together with field estimates of lateral saturated conductivity underestimates Q_o. Conversely, using a calibrated Q_o value and the estimated λ value leads to an overestimation of lateral transmissivity. From (3.73) it can be seen that errors in the 'spread' of the topographic index curve affect calculations of saturated areas. The same relation suggests that there may be some interaction between the 'spread' of topographic index curve and the m parameter. The effect of a reduced 'spread' can be partly compensated by an increase in the m parameter.

SRMAX was estimated from soil water content profiles as the difference between the equivalent water content in saturated conditions when 'gravity' drainage is no longer active and the water content during the severe 1989 drought.

Since the actual variation of hydraulic conductivity with depth is not known, the m parameter was derived from several recessions using equation (3.75) for two successive time steps and the continuity equation for the saturated reservoir. It was noted that estimates made for the initial period of the recessions were consistently lower than those at the end of the period. This trend can not be attributed to overland flow recession since calculations started after three hours without rain, nor to the assumption of zero drainage since accounting for it would have an inverse effect on m. This results seem to indicate that relation (3.75) may not be adequate to describe recession characteristics for the Haute-Mentue catchment. As it was pointed out in the preceding sections, relation (3.75) was derived assuming an exponential decrease of lateral transmissivity with increasing saturation deficit. In the Haute-Mentue catchment saturated hydraulic conductivity generally decreases with depth in approximately the first 50 cm. However, where the bottom moraine cover is thin, hydraulic conductivity increases in the weathered sandstone. It is not an easy decision to reject the hypothesis of exponential decrease of saturated hydraulic conductivity with depth. Changing it would imply changing relation (3.71) and topographic index definition. Currently efforts are made in order to allow other formulations for the variation of hydraulic conductivity with depth. However, situations in the field are variable and complex. No other simple rule for the variation of lateral hydraulic conductivity with depth could be derived. Moreover, recession data analysis did not permit to formulate a one-to-one relation between baseflow and a single state variable as the mean storage deficit.

Parameter Q_o was estimated for Alloux using a relation between watertable levels and baseflow (Iorgulescu and Jordan, 1994). This produced an estimate of lateral hydraulic conductivity at the surface which is probably several times greater than the actual average value. However, it must also be noted that the estimation procedure is quite sensitive with respect to the local topographic index value and to the hypothesis of a constant transmissivity. It was also observed that the relationship between measured watertable depths and baseflows is not unique, both intercept and slope being significantly different between individual recessions.

Modeling of two sub-catchments

The model was applied on a continuous basis over periods of approximately one month on Corbassière (185 ha) and Alloux (3.6 ha) sub-catchments. The two selected periods present wet antecedent moisture conditions, a series of rainfall-runoff events followed by a relatively long recession. The October 1988 period, used for model calibration, includes an event with a return period of about 2 years for peak-flow and greater for storm-flow volume for the Haute-Mentue catchment. It is the largest recorded event for both Alloux and Corbassière. This period is characterized by a low evapotranspirative demand and long duration, generally low intensity rainfalls. Total precipitation was about 200 mm from the 1st to 12th of October. In the period of June to July 1990, used for model validation, evapotranspirative demand was much higher and rain events were shorter although more intense. Total rainfall between the 27th of June and the 5th of July was equal to 120 mm.

In the case of conceptual rainfall-runoff models, periods of one month might be too short for a reliable assessment of parameters. Sorooshian et al. (1983) suggested that at least a one year period is necessary to calibrate 'conceptual' models. They also stressed the importance of activating all model components during calibration. It can be argued that the available information on the studied catchment can, when using a model with some physical basis, guarantee an adequate estimation of parameters even if calibration periods remain relatively short. Because the principal aim was to test the adequacy of the TOPMODEL conceptualization of the saturated overland flow mechanism in this catchment, the use of events in which partial-area infiltration excess overland flow or riparian area contributions might have been of major importance was avoided.

A time-step Δt of 1 h was selected for the simulations. This value is considered to be a reasonable compromise between the assumption of steady state subsurface flow and the need to accurately simulate the characteristics of storm hydrographs as well as the dynamics of contributing areas.

With the estimated parameters described above, simulated stormflow volumes and peak-flows were consistently overestimated (3 to 4 times for peak-flows). Storm-flow was simulated almost entirely by the saturation overland flow component. Subsurface flows showed little variation. In general, simulations were very poor. This implied the

rejection of field estimations as a suitable parameter set for modeling purposes.

As a consequence parameters have to be calibrated. Three parameters were calibrated: t_d, m and Q_O. It was decided not to calibrate *SRMAX* since during the simulation periods *AET* can be considered close to *PET*. Therefore *SRMAX* was not sufficiently activated. The quality of the numerical fit between observed and simulated hydrographs, was evaluated with the Nash and Sutcliffe (1970) efficiency criteria.

Identification of the set of optimal parameters was performed through the exploration of the response surface of the above numerical criteria. Although this approach is computer-time consuming, it is still feasible for short length records and for a small number of parameters. It avoids the problem of 'local optima' and might offer useful insights into model structure (Sorooshian and Gupta, 1983). Ranges for the parameters were selected in order to encompass acceptable values: $1<m<50$ mm, $0.01<Q_O<1000$ mm/h and $0.001< t_d<100$ h/mm.

At a first stage the objective function was calculated in the nodes of a 100x100x100 regular grid for m, $\log(Q_O)$ and $\log(t_d)$. The numerical criteria was not sensitive for both the lower and the upper ranges of t_d. This can be explained by the structure of the model (3.67). The unsaturated storage is not active when t_d is low and all water percolates during the same time-step to the saturated store. On the other hand, percolation becomes negligible when t_d is high. The global optimum appears in a well defined zone that falls in the range where t_d is inactive. A number of 'local optima' (defined as grids where all neighbouring nodes present lower values of the criteria) were identified in the middle range of t_d (0.1-10 h/mm). However, the values of the criteria in these grids were consistently lower than those in the global optimum zone. Tests performed on parameter sub-spaces with denser grids gave similar results.

As a result of this investigation, the calibration effort concentrated on the two remaining parameters: m and Q_O. Fig. 3.4.2 shows the response surface of the objective function for the calibration records. There is a large domain around the global optimum in which the response surface is quite flat and where several combinations of parameters would be numerically acceptable. The response surfaces for both watersheds show the existence of some parameter interaction. The orientation of this interaction can be roughly explained by the effect of parameters on simulated flows

since reducing m or Q_o generates more quickflow. Flatness of global optimum zone may be partly due to the reduced calibration data set or to the type of objective function used. It can also be noted that the model is more sensitive when the parameters vary in the lower range. This effect is apparent even when the scale of Q_o is distorted.

The overall shapes of the response surfaces presented above are quite similar to those obtained by Sorooshian and Gupta (1983) for a simple two-parameter reservoir model, with Q_o behaving like a threshold-type parameter and m like a recession coefficient. Since TOPMODEL is a non-linear model, interpretation is not straight forward, but from (3.75) it is obvious that m is governing recession shape. In (3.75) high values of Q_o, for a given value of Q_b, imply high values of average saturation deficit. From (3.71) it appears that if $\bar{S}$ is high enough (according to the value of m, difference between maximum topographic index and λ, and inputs), all local deficits will be positive. This means that the saturation overland flow component is not active. Consequently, the topographic index distribution is no longer significant. In this case with no overland flow and no time delay in the unsaturated zone, input to the saturated reservoir R^t varies only with surface inputs and the root zone storage. According to (3.1) subsurface flow is no longer a function of Q_o. It is interesting to note that for Alloux a high efficiency (>0.70) can be obtained with the subsurface component alone.

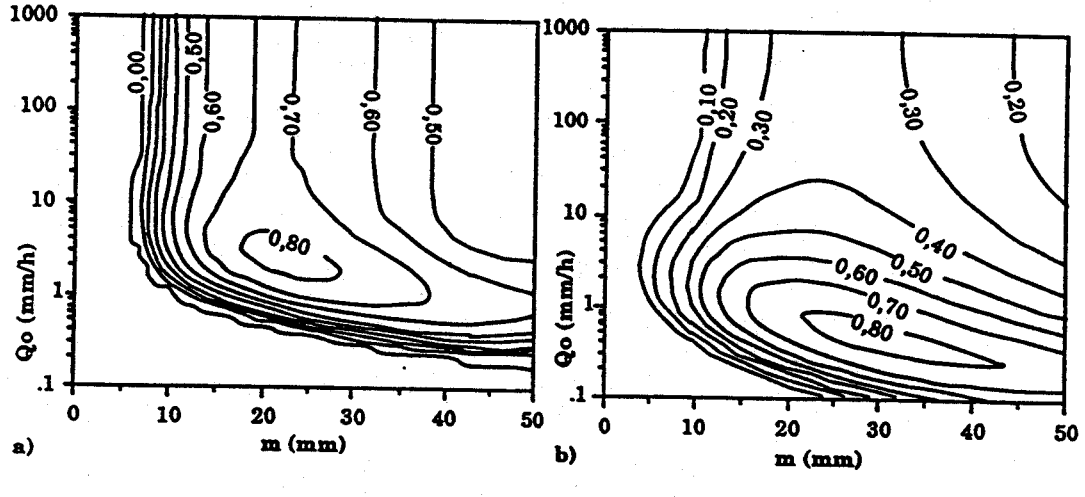

Figure 3.4.2 Response surfaces of Nash criteria with respect to parameters m and Qo a) Alloux and b) Corbassière (only positive values represented.

The overall shape of the response surfaces as well as the best efficiency values compare well between both watersheds although the global optimum zone for Corbassière is shifted towards lower values of Q_o and larger values of m. If the differences in Q_o can be qualitatively explained by differences between the topographic index average value λ, no apparent reason could be advanced at this stage for m, especially when it is realized that estimates from recession data are relatively close and no major differences in soil cover between the two catchments are documented. Following the calibration procedure the 'best' parameter sets for both catchments are the following:

Q_o=2.2 mm/h, m=22.1 mm and t_d =0.001h/mm (inactive) for Alloux
Q_o=0.4 mm/h, m=31.0 mm and t_d=0.001 h/mm (inactive) for Corbassière.

A ten-fold increase in Q_o with respect to the field-estimated value can be noted for Alloux. Using equation (3.76) this increase has similar effects on transmissivity which already yielded to a high surface saturated hydraulic conductivity. For Alloux, parameter m is close to the recession estimated value. Figure 3.4.3 shows the simulations results for the calibration period. Efficiency values of around 0.84 for both catchments are acceptable. Consequently the overall fit between observed and simulated hydrographs is satisfactory.

It appears that the dominant runoff generating mechanisms computed by the model are different in each catchment. The response of Alloux (especially in volume) is modeled mainly by subsurface flow while for Corbassière, saturation excess overland flow is dominant. These differences correspond to the perceived basin reaction. However, their magnitude seems exaggerated. A close look at the simulated hydrograph for Alloux shows that variations in subsurface flow (and accordingly in saturated areas) are too slow. The first peak between the 10th and the 12th of October is underestimated while the remaining ones are overestimated. For this event, rapid rise and decline of watertable could be monitored in the piezometers. The watertable depth data recorded on several dates during the calibration period for a 29 piezometer network in the Alloux sub-catchment are presented in Figure 3.2.5. It can be seen that the number of piezometers showing saturated or near saturated conditions (0-9 cm class) drops from 20 on October 10th to only 6 on October 13th. No spatial pattern of saturation could be identified from this set of piezometer data. The watertable depth evolution during October 1988 is presented in Fig. 3.4.4 b) for a continuously recording piezometer

located near the center of the Alloux sub-catchment. Rapid watertable rise can be observed for the events during this period. During recessions watertable drops at a nearly constant rate of about 10 cm/day.

The overestimation of flows from the beginning of the recession is offset by a prolonged underestimation later on. The trend of m parameter estimations, described above, appears to be the most obvious reason for such a behavior. For Corbassière successive events are better simulated but the subsurface flow recession is too slow.

For the validation period (Fig. 3.4.4), efficiency decreases only marginally for Alloux (0.80). Simulated saturation overland flow is negligible in volume but quite important in determining peak flows. The latter are acceptably simulated. The last recession is remarkably well simulated (and has an important impact on overall efficiency). This is in sharp contrast with the previous recessions for which simulated flows do not match the quick decay of subsurface flow. For Corbassière the efficiency is consistently lower than that of the calibration period (0.63). The underestimation of subsurface flow dynamics is evident. For short, high intensity, rainfalls, simulated overland flow recessions do not match observed ones. Peak-flows are acceptably estimated but storm-flow volumes are underestimated. It may also be noted that these results are comparable to those of the events on the 5th to the 7th of October which are similar in magnitude.

Modeled subsurface responses and claims for quick variations in subsurface storm flow may seem inconsistent with measured hydraulic conductivities. Numerical simulations performed by Freeze (1972a) indicate that subsurface storm-flow (including return flow) can be significant only under specific soil and topographic conditions. Evidence from environmental isotope tracing studies in humid temperate climate, including those for Alloux, strongly support the existence of large fractions of 'pre-event' water in the storm hydrograph. Field studies (Dunne and Black, 1970; Dunne 1978) suggest that return flow can represent a major contribution (about 50%) to flood hydrographs when the saturated overland flow mechanisms is dominant. The response characteristics of 'return flow' were found to be quite similar to those resulting from precipitation onto saturated areas. Bernier (1985) using a physically based storm-simulator failed to accurately simulate field documented characteristics of exfiltrated water, attributing this to spatial resolution which obliterates micro-topographic features that may be essential for this process.

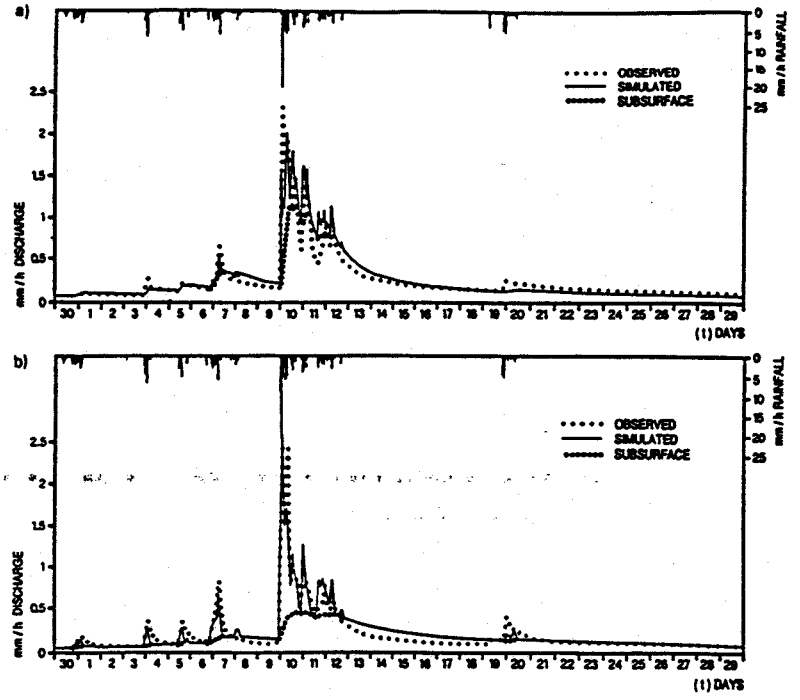

Figure 3.4.3. October 1988 (calibration period) simulation with the calibrated parameters: a) Alloux; b) Corbassière.

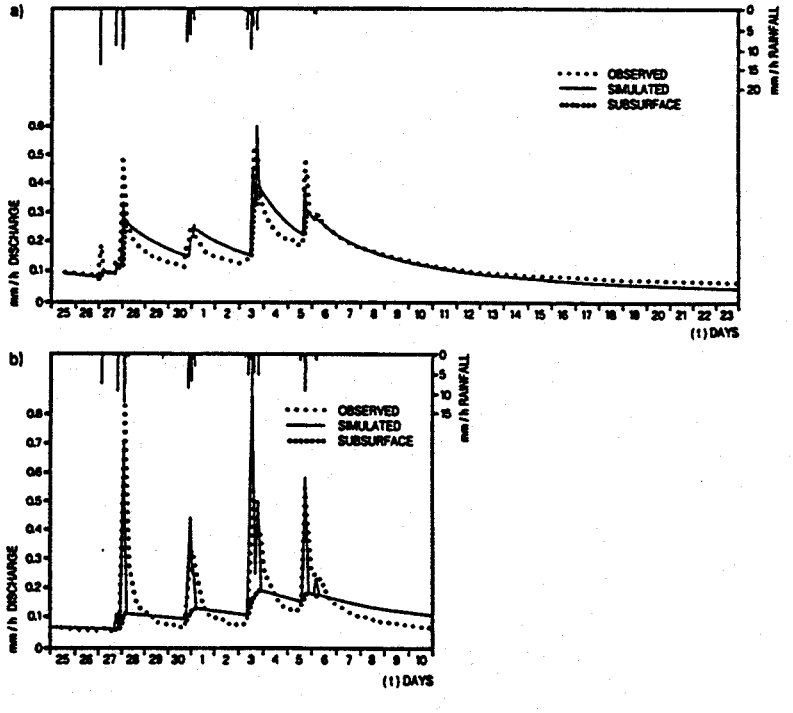

Figure 3.4.4 June-July 1990 (validation period) simulation with the calibrated parameters: a) Alloux; b) Corbassière (Note change in scale with respect to Fig. 3.4.3)

The quick subsurface response for Alloux is well documented by field evidence and especially by isotope tracing (Jordan 1992a). For small events, such as that of October 4th, isotope tracing showed that 'pre-event' water dominates the storm hydrograph, but the observations did not permit to identify the precise mechanisms involved. It seems that areas adjacent to the stream are the most probable source. Direct observations, made at Alloux during the October 10th to 12th 1988 event after the bulk of rainfall, indicate a wide spread of overland flow in a form which might be related to 'return flow'. Small seeps could be observed over practically all of the basin. Flow was soon concentrated in rivulets. Large macropores, especially rodent holes, provided concentrated discharge. About three-quarters of the 29 piezometers showed watertable either at the surface or at a few cm from the surface. Runoff coefficient was about 30%. For this event the model simulated a maximum extent of saturated areas equal to 25%.

The subsurface flow model component might be adequate for many modeling objectives but appears to be insufficient for an accurate process-based simulation in the Haute-Mentue catchment. Under-parameterization as well as over-parameterization may cause problems in process identification. A one to one relation between subsurface flow and reservoir content is unable to model the rapid transitory subsurface flows. The need to model 'return flow', with the same relationship makes the problem more difficult. 'Return flow' seems to be an important mechanisms in the studied catchment, and therefore needs special consideration.

The sizes and the physical characteristics of the studied catchments may be in the range of those where hillslope routing is important, especially for events involving large contributing areas. In such circumstances, separating between overland flow and quick subsurface response (including return flow) is extremely complex. If channel routing parameters are calibrated beyond their 'physical' range, a better numerical fit can be obtained by spreading the 'precipitation onto saturated area' component and allowing subsurface flow to simulate only the slowflow component. Dunne and Black (1970) measured overland flow velocities as low as 0.15 cm/s and considerable depression and detention storage for low-angled topography and dense vegetation. A crude attempt to explicitly consider hillslope routing for the elementary catchment of Alloux was considered. A fixed percentage (30%) of saturation overland flow was delayed during an hour. Use of the previously calibrated parameters resulted in an increased efficiency

for both the calibration and the validation periods, respectively 0.86 and 0.83.

Further investigation of the modeled mechanisms in the two catchments indicates that differences can not be explained only by topographical factors. The ratio between optimized Q_o values for both catchments is 3.4 times higher than that given by the theoretical formulation in equation (3.76) when considering equal lateral transmissivities and the calculated λ in each case. This discrepancy is too significant to be attributed to topographic index estimation or to differences in catchment average transmissivities. However, the response surfaces in Figure 3.4.7 show that the criteria of equal transmissivity can be matched with only marginal loss of efficiency. This would have the additional advantage of bringing the m parameter values closer. The model was run again with m=25 mm for both catchments and Q_o values of 1.32 mm/h and 0.85 mm/h for Alloux and Corbassière respectively. For Alloux, efficiencies are 0.80 and 0.78 for October 1988 and June-July 1990 respectively. For Corbassière values of 0.81 (October 1988) and 0.66 (June-July 1990) were obtained. For the first three cases efficiency marginally decreased while for Corbassière there is slight increase in the validation period. It is interesting to note that for Alloux this set of parameters and use of 'hillslope routing' resulted in a substantial increase in efficiency (0.88 for October 1988 and 0.87 for June-July 1990). It is difficult to state whether this 'joint-calibration' validates the topographic index or whether it represents an improvement in model calibration. The gain in efficiency for Corbassière is only marginal and the absolute value is still unsatisfactory.

Comparative modeling of four sub-catchments

It must be stressed that the objective of this modeling exercise is to use TOPMODEL as a tool for identifying catchment scale physical controls of hydrological response and for explaining spatial and temporal variability in streamflow generation processes. Model calibration and validation are only steps towards this objective. TOPMODEL was applied in a continuous mode with an hourly time step from August the 19th till October the 27th 1993. Precipitation was 490 mm and potential evapotranspiration about 160 mm. During this period catchments passed from dry to wet moisture conditions. Several significant rainfall-runoff events as those on 8-14 September and

5-8 October occurred during this period.

Details of the procedure used in this study for parameter estimation can be found in Tarantola (1987). It is considered that the most general way to describe the information on a parameter set is by defining a probability on the parameter space. A convenient and consistent way for defining this probability is by the interpretation of a likelihood function as a measure of probability. Following these lines normalized response surfaces as those in Figure 3.4.2 can be interpreted as probability distribution functions of the parameters. These concepts are quite similar to the GLUE method of Beven and co-workers (e.g. Beven and Binley, 1992). In order to map the likelihood function a regular grid was used in the parameter space, the same procedure as in the previous section. For sake of simplicity the results are presented mainly by their maximum likelihood values (expressed as Nash efficiency) and are summarized in Table 3.4.1. Most of this section will concentrate on the discussion of these results.

Catchment Model	Bois-Vuacoz (λ=7.92)	Corbamont (λ=6.76)	Ruzillon (λ=7.65)	Esserts (λ=7.12)
M I	+1.00	-0.03	+0.74	-0.84
M II	+0.84	+0.76	+0.82	+0.77
M III	+0.84	+0.03	+0.57	-0.68
M IV	+0.79	+0.74	+0.78	+0.61
M V	+0.49*	+0.17	+0.61	-0.66

Table 3.4.1 Summary of numerical results expressed using Nash efficiency criterion. *Models: M I- Specific discharge of Bois-Vuacoz; M II-TOPMODEL with best fit parameters for each catchment independently; M III-TOPMODEL with parameters calibrated on Bois-Vuacoz data; M IV-TOPMODEL with parameters calibrated on Bois-Vuacoz and Corbamont data.; M V-TOPMODEL with parameters calibrated on Bois-Vuacoz and Corbamont and using Bois-Vuacoz topographic index curve for the other catchments. (* For Bois-Vuacoz the topographic index curve of Corbamont was used)*

The specific discharge model (M I) is used as a reference. It basically offers a concise numerical measure of the significant differences in hydrological response between the four catchments. Specific discharge of Bois-Vuacoz can be considered an acceptable simulator only for Ruzillon catchment which has the topographic index curve closest to that of Bois-Vuacoz. M II is another reference. It represents the best fit values obtained

with TOPMODEL by calibrating the soil parameters m and T_o on each catchment separately. It indicates the best numerical results which can be obtained using the present version of TOPMODEL being thus an indicator of model and data errors. It can be observed that for all catchments this value is about 0.8. These figures are in the same range as the results of a previous modeling exercise with the same model on two other sub-catchments in the same area (Iorgulescu and Jordan, 1994). These results are not particularly good but may be considered as satisfactory. Note that they were obtained by tuning only two parameters.

M III is obtained by applying the best fit soil parameters (m and T_o) to the three other catchments. The rationale behind this approach is that, if topography is a dominant factor for variability in hydrologic response, then topographic characteristics alone should be able to explain a large part of differences in reaction between the catchments. This should give a measure of the importance of topography as a control of hydrological response and also of the ability to model its effect. The success of such an approach beside its theoretical implications would have an important impact for more practical problems as it would allow for more reliable distributed predictions inside a catchment and open the possibility of using TOPMODEL for regionalization purposes. The adoption of such an approach is reasonable also considering that these catchments are nearby and have a similar geology. However, results of M III are not encouraging. If they are compared with M I only a rather marginal improvement is noted for Corbamont and Esserts. For Ruzillon, even if in absolute terms this catchment has the best fit, one can note that M III is worse than M I. If efficiency values are compared with those obtained with M II, a sharp decline with respect to optimum values is noted for all three catchments.

At this stage one may conclude that either topography is not the dominant factor for catchment response or that TOPMODEL does not accurately account for it. However, as it was suggested in the previous sections by visual comparison or by simple analysis techniques, differences in responses at the catchment scale qualitatively agree with the topographic control theory (Kirkby and Chorley, 1967). Moreover, the experience with TOPMODEL during previous work reported in this study strongly suggested that the interaction between the m and To parameters could be responsible for the poor model prediction on independent data sets. Beven and Binley (1992) suggested that when parameters are not well estimated by the data, the quality of prediction on independent

data sets can be seriously affected.

In the present study the possibilitiy of adding additional information for parameter estimation in order to improve their identifiability was explored. Following this objective Model IV was obtained by combining the information on parameters derived from Bois-Vuacoz and Corbamont data sets. If the numerical results are compared with M II only marginal decrease is noted for three out of four catchments (including Ruzillon which was used for validation). For Esserts the drop is more important, but compared with M I and M III this catchment has the best performance in relative terms. The significant improvement on an independent data set suggests an increased predictive capacity as a result of better estimated parameters. In order to substantiate these affirmations the simulations with M I, M III and M IV and the observed hydrograph at Esserts are hown in Fig.3.4.5 for a representative sequence of events in September.

It is acknowledged that this approach beside potentially adding information on parameters may also imply some parameter 'averaging' between the two catchments. Consequently individual best fit parameter sets may be better simulators for each catchment not only numerically but even from a 'physical' point of view. Nevertheless, considering the results obtained, the implication is that in efficiency terms much more was gained by reducing interaction between parameters than by averaging them. It may also be argued that more averaging is implied by taking catchment scale effective parameters than by considering the four neighboring catchments as having similar soil parameters. Moreover, in the perspective of the objectives of extracting the significance of the topographic factor and that of assessing the predictive power of TOPMODEL, it seems that this method had favorable effects as it helped to obtain more stable parameters.

Finally, M V was constructed using for Esserts, Ruzillon and Corbamont the m and T_o parameters from M IV and the topographic index distribution of Bois-Vuacoz. For the latter catchment the topographic index distribution of Corbamont was employed. The objective pursued was to assess the sensitivity of the 'jointly calibrated' parameter set with respect to the topographic information. It may be noted that numerical performance significantly dropped for all catchments. This confirms that the information carried by the topographic index curve is significant for model parameterization.

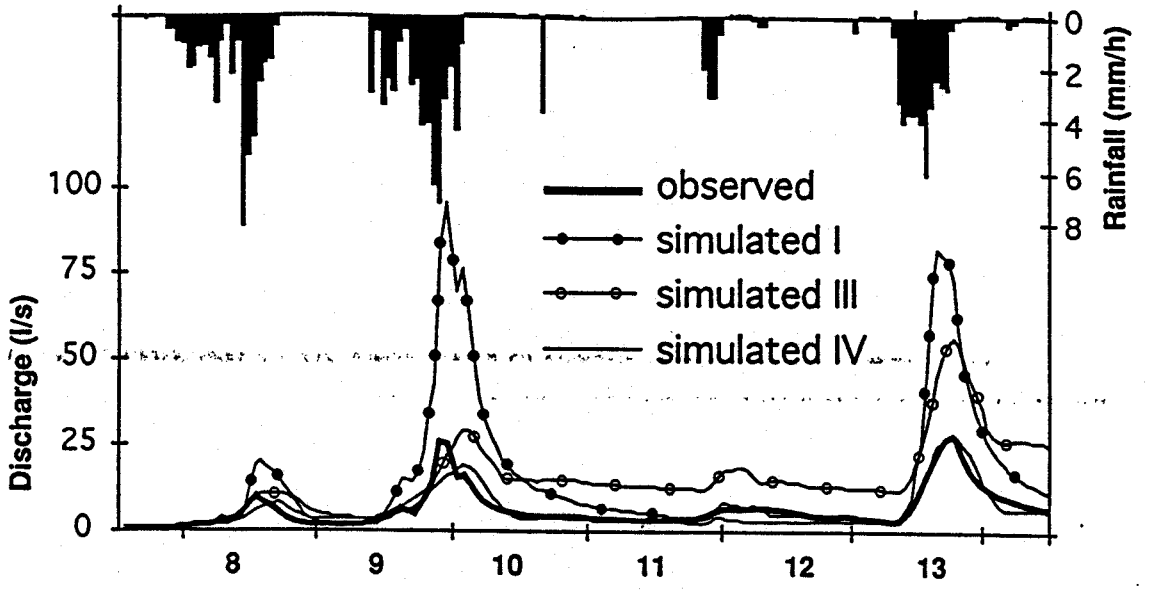

Figure 3.4.5 Esserts 7-14 September 1993. Simulation with different models.

Summary

Infiltration excess overland flow is active but its importance is less than it was previously accepted for this type of physio-climatical environment. Consequently it can not be expected that models parameterized on the basis of the hortonian concept of flood generation give good results. It appears that even a simple forecasting model should account for the variable contributing area concept.

Saturation overland flow and shallow subsurface flow (interflow) have been found dominant for the Haute-Mentue catchment. The most important physical factors which control flood generation processes have been found to be soil and topography. In contrast to the Hortonian concept in which soil is parameterized by its infiltration capacity at the surface, it has been found that one should characterize it mainly by its available storage capacity and by the ability of soil horizons to transmit fluxes laterally. Topography exerts also a strong control on contributing areas by its effect on the rate of lateral drainage and by convergence or divergence of flow paths. In the Haute-Mentue catchment, contrary to what has been until recently a common belief, steeper slopes produce less stormflow than gentler ones.

Integrative measurement techniques such as environmental tracing have important potential for process identification and parameter estimation. Environmental tracer results in the Haute-Mentue have an important impact on the problem of process identification in humid temperate forests. In contrast with most other studies only relatively small fractions of pre-event baseflow are found in stormflow. It is also one of the first comprehensive studies in which soil-water was found to have important, even dominant, contributions. This soil-water is, previous to event in unsaturated or only partly saturated conditions. When applying this method important attention has to be paid to the problem of spatial and temporal variability in end-member signature.

Identification of parameters for operational models is mainly performed with rainfall-runoff data. However the problems related to this exercise are widely acknowledged in literature. As TOPMODEL's parameterization is parsimonious it was possible to perform a quite exhaustive study by using the complete exploration of the response surface of an objective function. Parameter interaction and multiple optima problems can be conveniently handled. Useful insights in model structure can be obtained quite easily. The use of this calibration procedure for TOPMODEL is strongly recommend. As it is largely acknowledged that even for models with a large number of parameters, only 4-5 need to be optimized, this procedure could find a wide use. Interpretation of surface response as probability density functions of parameter estimates allows for the evaluation of the effect of additional data as well as they permit to consider model result uncertainty. As an example, in this study it was able to be demonstrated that the use of multiple catchments improves model performance on independent data sets.

It has also been shown that, at least for the Haute-Mentue data, there is a well defined zone of global optimum. Some local optima could be identified outside this zone, but the value of the optimization criteria was considerably smaller than for the global optimum. An important interaction between the two main parameters of TOPMODEL was found. Consequently equivalent numerical fits were obtained with rather different combinations of parameters which imply totally different dominant processes. It is not clear yet to what extent this affects model performance in extrapolation mode. Use of tracer data would help to improve identifiability by imposing constraints when splitting between subsurface and surface processes. It was also found that two parameters are inactive in a part of the domain in which they may take values. A search optimization based on gradient methods starting in such a zone of the parameter space would fail to leave it.

Parameters estimated from field data gave poor results (Nash-Sutcliffe efficiencies below 0.00). Rather unrealistic simulations were obtained, with storm flows being consistently overestimated and peak flows from a small 3.6 ha catchment being overestimated 4-5 times. This and the results presented before suggest that the physical basis of the model is questionable and that independent estimates of some important model parameters from field data are not of significant use.

Optimum parameter set yielded satisfactory efficiency values (>0.83). Validation on an independent data set showed a decrease in efficiency. This decrease can be considered reasonable as the validation period data set reflected hydrological conditions significantly different from those of the calibration data set. Considering that such results were obtained in a continuous simulation by tuning only two parameters it can be stated that TOPMODEL has a good parametric efficiency and that the stability of outflow prediction is quite satisfactory.

It is expected to have a significant gain in process representation by an explicit or implicit description of topography. Topographic factors have been found to be able to explain a large part of the variability in the rainfall-runoff process. The description of topography should be at the best accuracy possible. The trade-off between accuracy in the description of topography and that of soil-related processes, has not been explicitly considered in this study, but should be an area of future interest. The efforts to interpret soil parameters and especially to relate soil parameters as hydraulic conductivity or transmissivity with independently measured values have been much less successful.

These conclusions recommend the use of TOPMODEL for flood forecasting. The model also demonstrated some potential for purposes of regionalization and making distributed predictions inside a catchment. These are justified by TOPMODEL's ability to parameterize the topographic factor. However, it must be stressed again, that the physical basis of model results is not guaranteed and that the generally available data (rainfall and runoff) are not, by any means, sufficient to assess it. Data as discharge in several sub-catchments and environmental tracing seem to be the most effective information for validating the model.

3.4.2 Practical Refinements to TOPMODEL

The main purpose was the application of TOPMODEL to an experimental basin of the French Méditerranean zone: the Réal Collobrier (71km^2). This work was done by INPG-RHE at Grenoble. The approach was to use the most refined version of the model to maximise its performances, and to test the effect of simplifications that might be necessary for operational catchments.If necessary, some adjustments in the processes modeled were planned to fit the Mediterranean environment. A special paragraph on the role of spatially varying precipitation input is given in section 3.5 of this chapter.

The available data have been organised to test the model both on an event per event basis, as usually done in operational use, and on a continuous basis (usually a whole rainy season of 2 or 3 months). In both cases, the samples have been split into a calibration sample used to optimise the parameters and a validation sample for independent evaluation.

The time-step selected is one hour and the basin has been subdivided into 20 land units for soil moisture accounting. The generation of the different flow components (i.e. groundwater baseflow, saturation excess overland flow or eventually infiltration excess flow) makes extensive use of the catchment topography, which has been processed from a Digital Terrain Model with a 60 m meshsize.

The model has been processed first in its semi-distributed TOPMODULAR version, involving the 20 land units although with a uniform rainfall input over the basin taken from five well scattered raingages. This has immediately raised a problem of water balance, since a significant volume in excess has led to a reconsideration of the different water losses included in the model. After rejection of the gauge estimate of rainfall as a potential source for this discrepancy, particular attention has been devoted to evaporative losses. In the initial version, only the evapotranspiration at potential rate could be withdrawn from the topsoil reservoir. For those winter events, it hardly allows more than 2 or 3 mm/day, not to say that it was often considered that under rainy conditions, the saturation of the atmosphere would probably bring these values to lower actual ones.

However, recent works (e.g. Calder, 1990 or Kelliher et al., 1992) have suggested that the interception losses during rain events might contribute much more to enhance this component . Figures of up to 0.4 mm/h or 8 mm/day have been proposed. Although further experimental works was needed at that time to verify this hypothesis, it had already been noticed that the conjunction of a rainy event with sustained wind and the location of the basin on the leeward side of the mountain range could favor those large values. So a subtractive correction has been introduced in the model allowing withdrawal of .2 to .3 mm/h during rainy periods, (day and night). This suggested the setting up of a specific experiment, financed by another EEC project EV5V-CT91-0039), that fully confirms that order of magnitude.

Next some simplifications were introduced to allow an easier and more economical use of the model having in mind operational conditions:

- It was first tested in a lumped version, showing no real decrease in performance as compared to the semi-distributed one. There is no need to provide every land unit with its own topographic index distribution curve, which in fact do not differ so much from one unit to another.

- The routing of the water available for runoff, initially performed by an isochrone routine, was also reconsidered. It appeared that a transfer function approach introduced significant improvements, whether it was obtained by optimisation of a functional form (usually a 2 parameter Gamma function) or by forcing an externally optimised response function (identified by the FDTF - ERUDHIT approach, briefly described in Chapter 4)

- It also appeared that the topographic index distribution function, usually obtained from a tedious geometric analysis of the DTM, could be economically parameterised first by a 3 parameter Gamma function, with little or no loss in efficiency as compared to the empirical one. This has opened quite nice practical perspectives for the adaption of TOPMODEL to an efficient operational use (See paragraph 4.2.2). This confirm the results obtained by Franchini et al. (1996)

- This has also raised some theoretical issues to understand the interaction between the DTM used, essentially its meshsize, the topographic index curve derived, and

the value of the parameters required. This interaction, very close to numerical diffusion in partial differential equation treatment, allows one to understand why the values of the saturated conductivity K_0 must take irrealistic values when compared with physical ones, and how this effect can be partly "corrected". This has been described in in the next paragraph 3.4.3 and by Franchini et al., 1996.

A rather simple understanding of this numerical effect may be got by remembering that increasing the meshsize will tend to make the basin flater, while the smallest areas drained are fairly large. Therefore, the values of the topographic index, which expresses in some way the capacity of a given point to become saturated, become larger than with a smaller meshsize, and the basin as seen through this DTM will tend to develop more saturated areas, probably more than required by the reproduction of observed discharges. An automatic way to avoid that drawback is to increase artificially the average transmissivity of the soil profile, and therefore the surface saturated conductivity K_0 but this usually comes out automatically in calibration.

This leads to the following summary conclusions:

a) First, the Réal Collobrier data (with the Sieve, Arno, Reno data), have allowed a fairly exhaustive test of TOPMODEL capacities. There has been obviously some trade-off between goals and available informations (like in the choice of the time-step used), but its application to a typical Mediterranean environment is acceptable.

b) A second conclusion is that TOPMODEL has appeared well adapted to operational purposes. It has proved to work very well in an Event context within which it had not been used before, specifically because its initialisation at the start of an event appears very easy and the results not very sensitive to this initialisation. However, like most other existing models, the conceptual non linear structure shows sensivity of the optimised parameter sets to sample size and context of use (whether events or continuous periods). It has been verified that stability and robustness in validation require a substantial calibration sample, whether event or continuous based, but that parameter sets optimised on continuous periods still do well on the simulation of events only.

c) A third conclusion concerns the routing of excess water, initially done by

isochrone or kinematic wave. The transfer function approach as developed in the FDTF-ERUHDIT method has been easily introduced and proved very efficient when connected with TOPMODEL.

d) The fourth conclusion is less encouraging: The capacity of TOPMODEL to provide objectively some hints on the physical functioning of the catchment have remained a little disappointing. For example, the separation of discharge water into surface and groundwater components may vary significantly with similar performances on the total discharge. Similarly, good performances have been reached with rather different sets of parameters depending for example if the calibration had been made on events or on continuous samples.

This may obviously be caused by the lack of detailed information as for example the soil characteristics in space (like depth). Although some of this information can be distributed spatially (like the Kirkby index) their worth may have been cancelled by the fact that some others were not. Similarly, good performances have been reached with rather different levels for the baseflow component, depending for example on whether if the calibration had been made on event or continuous samples.

Another more optimistic example is provided by the detection of a significant volume of water in excess when the only loss allowed by the model was by evapotranspiration. It has suggested that the interception losses in these forested Mediterranean catchments needed further consideration and recent experimental results show that the figures for interception during rainy events are surprisingly high, and much in line with our optimised guess (0.2 to 0.4 mm/h)

e) The fifth conclusion is about the use of TOPMODEL as a semi-distributed model. This capacity of the model, and therefore its capacity to tackle some aspects of the spatial variability of input variables or basin characteristics, has not proved essential in the experiments. The lumped versions have systematically done better than the semi-distributed ones.

In conclusion, TOPMODEL has appeared as a very practical tool to test the sensitivity of simulated response to various hypotheses. It therefore keeps the drawbacks of all hydrologic models at this time, whether semi- or fully distributed. It does not suggest

what important process has been forgotten in the modelling, nor does it solve the inverse problem of suggesting, from a limited set of observed data, what the only acceptable hypothesis should be among several proposed. Unfortunately, if it exists, this philosopher's stone of Hydrology is yet to be found elsewhere.

3.4.3 Improving rainfall-runoff models' physical representation - TOPMODEL and ARNO to TOPKAPI

The UNIBO Bologna contribution to rainfall-runoff modelling has been the investigation on an alternative model formulation that, take advantage of the capabilities of the two conceptual models mainly addressed under the AFORISM Project, namely the TOPMODEL and the ARNO model, would lead to an improved physical representation of the phenomena involved.

The pros and cons of these two models can be summarised as follows:

The main advantage of the TOPMODEL is that it offers a theoretical possibility of estimating the topographic index curve from the topography of a basin (Quinn et al., 1991); in addition all the other parameters are physically related to the soil and porous media characteristics of the basin, where no direct calibration of parameters is really possible.

The major disadvantage of the TOPMODEL lies in the steady state assumption which is advocated in order to derive the model integral equations. This assumption, which corresponds to a null travel time from one side to the other of an elementary grid cell (pixel) of the digital terrain model used in the derivation of the Topographic Index Curve, becomes unrealistic for cells of the order of magnitude of hundreds of meters. As a consequence, in order to obtain a correct travel time, the horizontal saturated permeability parameter must be artificially increased by orders of magnitude, which in turn makes the infiltrated water immediately drop to the saturated zone leaving the unsaturated zone mostly depleted, with a general underestimation of the actual evapotranspiration (Franchini et al., 1996).

By contrast, the main advantage of the ARNO model is the fact that it is entirely driven by the total soil moisture storage, which is functionally related by means of simple analytical expressions to the directly contributing areas, to the drainage and to the percolation amounts. This makes the model extremely useful in evaluating the total amount of soil moisture available for evapotranspiration losses, which permits a continuous time running mode and the possibility of automatically updating the initial conditions.

The major disadvantage of the ARNO model is the lack of physical grounds for establishing some of the parameters which have to be estimated on the basis of the available precipitation and runoff data. This is not particularly critical in hydrological applications but it prevents its extention to ungauged catchments.

A shopping list for a new lumped model

From the description of the two models (Sections 3.3.2 and 3.3.3) and of their advantages and disadvantages outlined above, it seems reasonable to define the following properties to be included in a new rainfall-runoff model formulation, as was proposed by Todini (1995).

In the following list the properties reflected by the ARNO and the TOPMODEL are marked (A) and (T) respectively; the new ideal properties are marked (N):

i) When dealing with mesh sizes of the order of magnitude of hundreds of metres, the precipitation always infiltrates into the soil, unless the soil has already reached saturation (A,T);

ii) The total water storage in the first soil layer is responsible for the control of the saturated surface dynamics, which must also depend on topography, soil properties and soil moisture content (A,T), and for the control of the actual evapo-transpiration losses (A);

iii) The total water stored in the soil is explicitly accounted for at each step in time (A,T) and the actual evapo-transpiration will depend upon it (A);

iv) The total catchment area must be described by means of elementary areas (pixels) which are small compared to the overall catchment area (A,T);

v) The position of a pixel must not be relevant: what matters is the total probability distribution which is used for obtaining the surface average value (A,T);

vi) Drainage and percolation must follow physical laws (T) and not empirical ones (A);

vii) The digital elevation model should provide information on the horizontal flow driving mechanism (T);

viii) The local horizontal flow as well as the local transmissivity must depend upon the overall soil moisture content obtained as the integral along the vertical direction of the soil moisture profile (N);

ix) Model parameters must be determined on physical grounds (T) and their values must be of physically meaningful orders of magnitude (A);

x) The discrete space model must be expressed in terms of a non-linear reservoir model invariant in its essential structure, with only the parameters varying from small to larger scales (N).

The first hypothesis, which is the same expressed by both ARNO and TOPMODEL, is a reasonable hypothesis mainly due to the extremely large values of permeability in the first soil layer (Dunnian infiltration); but even if Hortonian infiltration holds, this property tends to be true with the increasing size of the pixel, due to the characteristic travel time needed to cross the pixel itself, which is no longer infinitesimal.

In addition, the major idea for the development of the new model is the concept of lumping. The original problem is obviously a three dimensional problem which can be reduced to a two dimensional problem if property (viii) applies and then reduced to a zero dimensional problem if property (v) applies.

These points raise the following two major questions:

(a) Is it possible to lump the horizontal flow properties in the vertical dimension? In other words can one express the total horizontal permeability (generally called transmissivity) as a function of the total soil moisture content?

(b) Is the succession of hill-slopes important or can it be disregarded, while only the overall frequency distribution or its integral are retained?

These questions must be answered by comparing errors originating from other sources of uncertainty with the order of magnitude of the error one makes assuming that (a) and (b) are correct.

The answer to question (a) is: yes it is possible to lump the phenomenon in the vertical dimension without a significant loss of accuracy. This was demonstrated by showing that the integral of the horizontal permeability along the vertical dimension can be related to the vertically integrated soil moisture content, without great loss of accuracy.

The answer to question (b) is also in the affirmative, and in fact both models (the ARNO and the TOPMODEL) already implicitly assume it.

In the next sub-sections the description of the results from single experiments set up in order to demonstrate the validity of the assumptions, will be outlined.

The vertical lumping

Description of horizontal flow in unsaturated conditions can be made based upon the knowledge of the vertical moisture content profile in the soil. Due to the high conductivity value, caused by macropores in the top of the soil (Beven and Germann, 1982), gravity will be the dominant mechanism driving water from the top of the soil to the bottom (impermeable or semi-impermeable lower boundary). The latter mentioned boundary will create a perched water table. In this zone a not negligible horizontal propagation (also involving unsaturated flow), will occur.

Nevertheless, the depth of this high conductive soil (one or two metres) will be negligible with respect to the horizontal grid dimensions (> 100x100 m^2). By assuming a number of vertical soil moisture profiles it was shown that the horizontal flow (or hydraulic conductivity) evaluated starting from a real vertical profile and that deriving from the integral moisture content were comparable. This allows the transient phase of vertical infiltration to be neglected; in other words, when interested in the horizontal movement of water, it is possible to avoid (within the range of reasonable errors) the integration of the unsaturated soil vertical infiltration equation (namely Richards equation) by assuming a transmissivity which is a function of the total soil moisture content.

In order to clarify the point, assume that the relative permeability $\tilde{\vartheta}$ can be expressed, with a more or less simple relationship, as a function of the reduced soil moisture content defined as:

$$\tilde{\vartheta} = \frac{\vartheta - \vartheta_r}{\vartheta_s - \vartheta_r} \tag{3.77}$$

where:
- ϑ is the soil moisture content
- ϑ_r is the residual soil moisture content
- ϑ_s is the saturation soil moisture content

and where all the quantities are point values varying with the downward directed vertical co-ordinate z.

The hypothesis is that the horizontal transmissivity T can be expressed in terms of the integral, along the vertical, of the reduced soil moisture and that the shape of this function, apart from the parameter values, is the same as the one relating the point relative permeability to the point reduced soil moisture content, namely:

$$T = \int_0^L k\left(\tilde{\vartheta}(z)\right) dz \tag{3.78a}$$

$$\tilde{T} = k_s L \tilde{\Theta}^{\alpha} \qquad (3.78b)$$

where:

T	is the horizontal transmissivity calculated from the intagral of the permeability
$k(.)$	is the point relative permeability
$\tilde{T}$	is the suggested approwimation to T
$\tilde{\Theta} = \frac{1}{L}\int_0^L \tilde{\vartheta}(z)dz$	is the mean relative moisture content and
k_s	is the permeability at saturation.

To demonstrate the validity of the hypothesis that $\tilde{T}$ is approximately equal to T, two different but very well known relationships describing hydraulic conductivity with moisture content were used; the first one due to Brooks and Corey (1964) and the second one given by van Genuchten (1980).

Using the Brooks and Corey expression, namely $k(\tilde{\vartheta}) = k_s \tilde{\vartheta}^a$, with a a parameter, the hydraulic permeability was calculated from a number of different approximated vertical profiles having a variation in moisture content with depth while keeping the same mean integral moisture content $\tilde{\Theta}$. Note the similarity of form of the Brooks and Corey expression and equation (3.78b). A number of different $\tilde{\Theta}$ values were taken into account, ranging from 0 to 1.

The results of this calculation for a wide range of soil moisture profiles, both increasing and decreasing with depth, are shown in Figure 3.4.6 where the flux index T / k_s given by equation (3.78a) is plotted against $\tilde{\Theta}$. These appear as scattered points. Also plotted is the relationship $\tilde{T} / k_s$ from equation (3.78b) plotted as a solid curve versus $\tilde{\Theta}$, clearly demonstrating that, given the range of uncertainty in the soil properties, the assumption of equality holds.

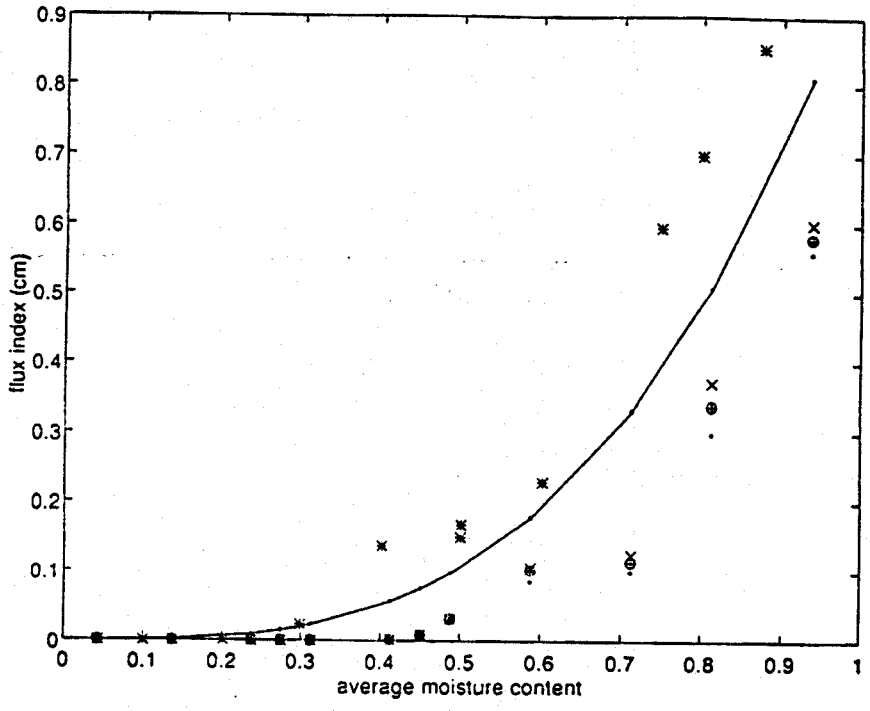

Figure 3.4.6 - The different values of the flux index, calculated as the integral of the point relative permeability for different soil moisture profiles T / k_s (points) from equation (3.78a) and $\tilde{T} / k_s$ (solid curve) from equation (3.78b) plotted against average soil moisture content $\tilde{\Theta}$.

A similar analysis was done (Benning, 1994) by using a suitable approximation of the van Genuchten expression (suitable in that it allowed for analytical integration); Figure 3.4.7 shows a number of different water profiles for a given terrain, and Table 3.4.2 shows a comparison of the two expressions, here matched in terms of transmissivity.

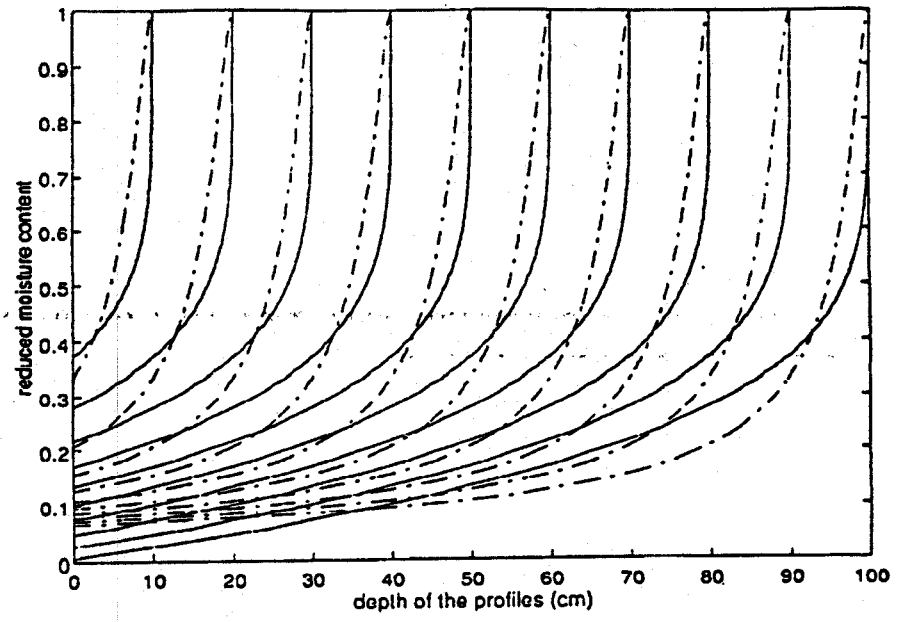

Figure 3.4.7 -Different soil moisture profiles, calculated with the van Genuchten expression (solid curves) and the approximate one (dashed/dotted curves) allowing for analytical integration.

depth of profiles	moisture content van Genuchten	moisture content appr. expr.	transmiss. van Genuchten	transmiss approx. expression
	%	%	(cm^2/s)	(cm^2/s)
100 cm.	16.8089	17.0488	0.0121	0.0269
90 cm.	21.0549	26.9006	0.2000	0.2267
80 cm.	28.4701	36.5355	0.4000	0.4262
70 cm.	36.6885	45.9320	0.6000	0.6254
60 cm.	45.2917	55.0630	0.8000	0.8242
50 cm.	54.1264	63.8934	1.0000	1.0225
40 cm.	63.1180	72.3755	1.2000	1.2204
30 cm.	72.2239	80.4400	1.4000	1.4175
20 cm.	81.4173	87.9757	1.6000	1.6138
10 cm.	90.6803	94.7661	1.8000	1.8087
0 cm.	100.0000	100.0000	2.0000	2.0000

Table 3.4.2 - Values of reduced moisture content and transmissivity as a function of depth, calculated with the van Genuchten expression and the approximated one.

In this case, from the following expression which was adopted for the point relative permeability:

$$k(\tilde{\vartheta}) = k_s\left[1-(1-\tilde{\vartheta})^c\right] \tag{3.79}$$

the following similar expression can be derived for the transmissivity as an alternative to (3.78b), by analytical integration (Benning, 1994):

$$\tilde{T} = k_s L\left[1-\lambda(1-\tilde{\Theta})^\gamma\right] \tag{3.80}$$

where γ and λ are two parameters that can be derived from the original ones, and again one can see that the form of the function remains more or less unchanged.

It is worth noting thedifferences between (and similarities of) equations (3.79) and (3.80). The first is the equation for permeability, while the second is an equation for transmissivity. Although they have the same form and many practitiones adopt the second, the use of (3.80) is only justifiable in the light of the proceeding argument.

In conclusion, on the basis of the results obtained above, it is possible to assume a simplified expression in terms of the total vertical soil moisture content for the description of the horizontal transmissivity, thus reducing what was initially a three dimensional problem to a two dimensional one, after lumping in the vertical dimension.

The succession of slopes

If one assumes that the horizontal transmissivity is very high in the top soil layer and that it can be described as equation (3.78b) (via the Brooks and Corey expression) namely $\tilde{T} = k_s L\tilde{\Theta}^\alpha$, it is easy to show that the horizontal movement of water in the unsaturated zone (using the same assumptions as does TOPMODEL) can be approximated by a kinematic wave model, which gives:

$$(\vartheta_s - \vartheta_r)L\frac{\partial\tilde{\Theta}}{\partial t} = p + \frac{\partial q}{\partial x} = p + \alpha k_s L\, tan(\beta)\tilde{\Theta}^{(\alpha-1)}\frac{\partial\tilde{\Theta}}{\partial x} \tag{3.81}$$

where :

	$tan(\beta)$	represents the terrain slope;
	q	is the interflow
	p	is the precipitation

The model is written in one dimension because it is thought that the movement of water will proceed in the direction of steepest descent of the surface topography along the hillslopes towards the closest drain, and afterwards it will proceed along the drainage network. This allows for reduction by an additional dimension and reduces the original problem to the solution of a one dimensional kinematic wave problem.

The basic idea of a higher conductivity in the first layer of limited dimension (the rootzone) expressed in TOPMODEL, which was stated by Freeze (1972b) and Sloan and Moore (1984), is clearly preserved in this formulation. However, the exponential decay formulation in which this phenomenon is presented in TOPMODEL is replaced by an equation that gives the relation of the transmissivity to the total moisture content while neglecting, after the vertical lumping, the dependence of saturated hydraulic conductivity with depth. This means that the kinematic model considers a vertical layer of limited dimensions characterised by a high constant saturated conductivity, but with a corresponding transmissivity varying with total moisture content.

Kinematic wave equations have been extensively used to model surface propagation. It was the American hydrologist, Horton who in 1933 carried out the earliest recorded scientific studies of surface runoff. Later Keulegan (1945) applied the continuity and momentum equations conjunctively for surface runoff analysis. He investigated the magnitude of the various terms in the dynamic equation of St. Venant and indicated that a simplified form of the equation, now termed the kinematic equation, would be adequate for surface runoff.

Starting with the formulation of the kinematic wave theory by Lighthill and Whitham (1955), kinematic surface runoff models have been utilised increasingly in hydrologic investigations. The first application of kinematic wave routing to surface runoff and groundwater flow was by Henderson and Wooding (1964). The conditions under which the kinematic flow approximation holds for surface runoff were first investigated by Woolhiser and Liggett (1967); they found it is an accurate approximation to the full equations for most surface runoff cases (cf. Stephenson et al., 1986).

In an earlier study, Henderson and Wooding (1964) provide solutions for horizontal kinematic subsurface flow through a porous medium of constant permeability both for steady state and a rising water-table. They compare the extended Dupuit-Forchheimer

equation to a further simplification of the flow equation in which it is assumed that the hydraulic gradient at any point within the saturated zone is equal to the bed slope. Beven (1981, 1982), in two papers about kinematic subsurface storm flow, gave a kinematic wave equation valid in a sloping soil mantle of constant saturated hydraulic conductivity overlying a relative impermeable bedrock sloping surface. In the first article, mainly devoted to the study of horizontal propagation, Beven stated that this equation was a good approximation to the more correct extended Dupuit-Forchheimer equation (see Beven (1981) for further details). In the second article, the vertical propagation in the unsaturated zone was also taken into account by Beven to evaluate the time at which the wetting front reaches the bottom of the profile. In addition a kinematic approximation in subsurface flows (both in vertical and horizontal directions) has been successfully tested by several other authors (see Borah et al. 1980; Charbeneau 1984; Sloan and Moore, 1984; Hurley and Pantelis, 1985; Stagnitti et al., 1986, Steenhuis et al., 1988).

In TOPMODEL a topographic index curve is used in order to synthesise the topographical information of the catchment. In doing so there is an implicit assumption that the overall behaviour does not depend upon the arrangement of individual slopes but alternatively on the overall distribution of the slopes. In the case of the kinematic wave approach a similar assumption is made, therefore it was felt essential to prove that the flow at the end of a cascade of slopes is not strongly modified by their relative position.

In order to prove this property of the kinematic scheme several slopes were generated at random in the range 0-10%, and the relevant resulting flows at the end of the different cascades are compared as in Figures 3.4.8 (a,b).

Given the results, one can see in Figures 3.4.8 (a,b) that the alternative successions of slopes produce differences that can hardly be separated from other sources of errors, thus justifying the hypothesis that slopes can be treated in terms of their probability distribution, rather than in terms of their actual arrangement This would be true if the successive elements of the slopes behaved as linear storage elements, adding justification to the (linear) kinematic, or distribution-based, model.

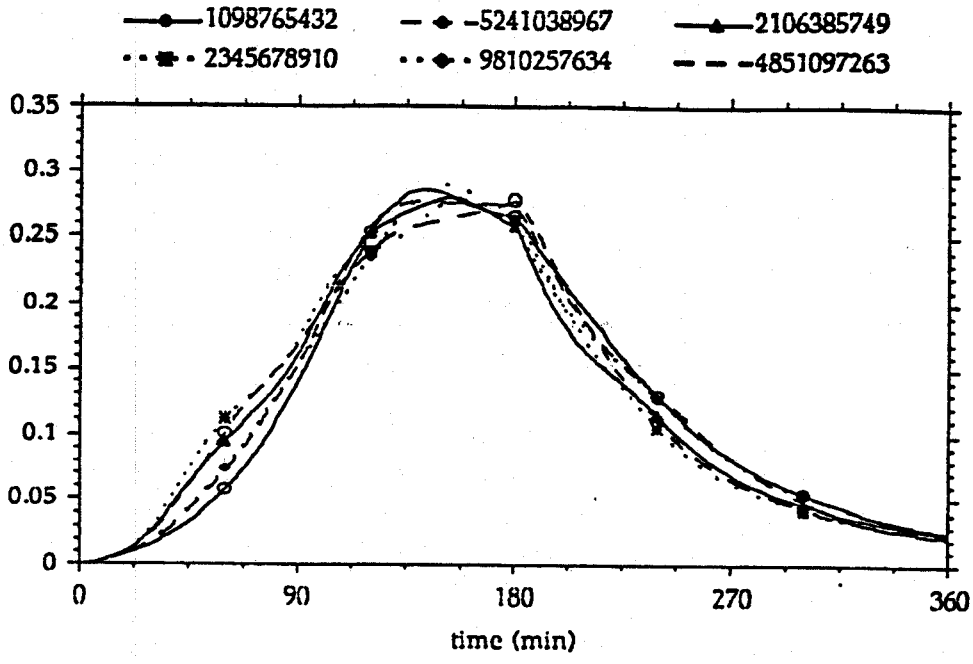

(a)

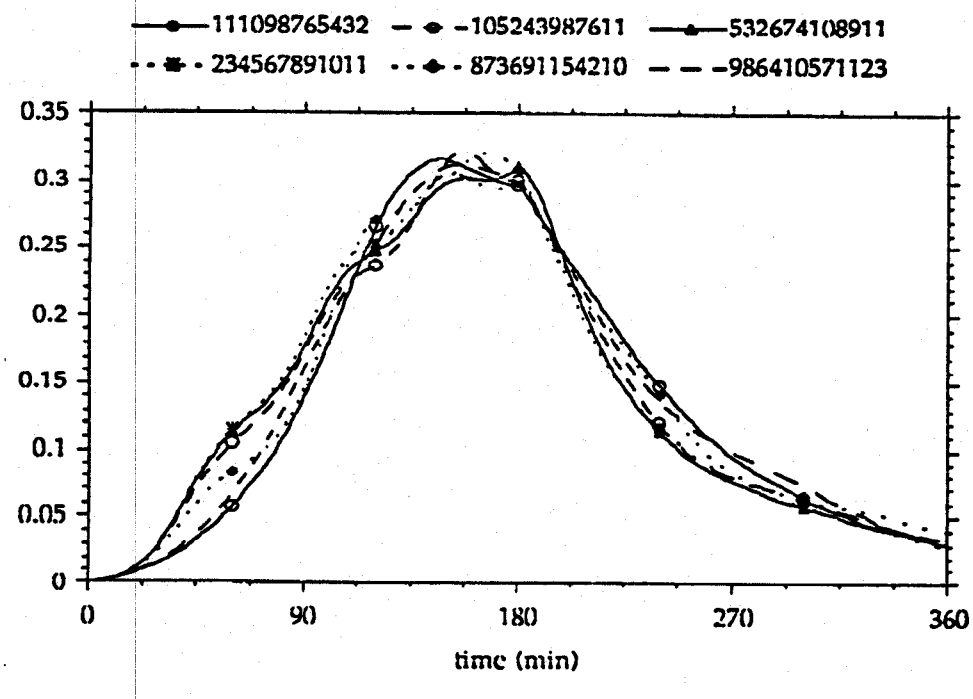

Figure 3.4.8 Different kinematic waves resulting from random permutation of 9 slopes (a) and 10 slopes (b).

The proposition of a new model: the TOPKAPI

The development of a new modelling approach at catchment scale is here sketched, in that it is not yet a real model but it constitutes a logical synthesis of what has previously been analysed.

The model name TOPKAPI derives from its main features, i.e. TOPographic Kinematic APproximation and Integration. Its development originates in fact from the integration of the kinematic approximation presented above over increasing size domains.

The continuity of mass can be expressed as:

$$(\vartheta_s - \vartheta_r) L \frac{\partial \tilde{\Theta}}{\partial t} + \frac{\partial q}{\partial x} = p \tag{3.82}$$

where p is the precipitation taken as constant in space and time, and in line with what expressed above, is considered to entirely infiltrate in the soil until it reaches saturation;

q is the flow, given as:

$$q = tan(\beta) T\left(\tilde{\Theta}\right) = tan(\beta) k_s L \tilde{\Theta}^{\alpha} \tag{3.83}$$

where, similarly to the assumption made in TOPMODEL, the surface slope is taken instead of the head slope.

The main idea is then to combine the kinematic model with the topography, which is described by means of a number of elementary cells of fixed size (for instance 100×100 m or 400×400 m).

For this purpose, it is convenient to rewrite equations (3.82) and (3.83) in terms of the actual total vertical soil moisture content η, defined as $\eta = (\vartheta_s - \vartheta_r) L \tilde{\Theta}$ as described in Beven et al.(1988), to give:

$$\begin{cases} \dfrac{\partial \eta}{\partial t} = p - \dfrac{\partial q}{\partial x} \\ q = T\, tan(\beta) = L k_s\, tan(\beta)\, \tilde{\Theta}^{\alpha} = \dfrac{L k_s\, tan(\beta)}{(\vartheta_s - \vartheta_r)^{\alpha} L^{\alpha}} \eta^{\alpha} = C \eta^{\alpha} \end{cases} \tag{3.84}$$

where the following substitution was applied for the sake of clarity:

$$C = \frac{L k_s \tan(\beta)}{(\vartheta_s - \vartheta_r)^{\alpha} L^{\alpha}} \tag{3.85}$$

The two equations (3.84) can then be combined together, to give the following kinematic wave model:

$$\frac{\partial \eta}{\partial t} = p - \frac{L k_s \tan(\beta)}{(\vartheta_s - \vartheta_r)^{\alpha} L^{\alpha}} \frac{\partial \eta^{\alpha}}{\partial x} = p - C \frac{\partial \eta^{\alpha}}{\partial x} \tag{3.86}$$

In the TOPMODEL, after integrating in space a similar expression, the time derivative is set to zero, thus implying that stationarity is immediately reached, which may be reasonable for small mesh sizes (in the range of one or few meters), but it is not when dealing with mesh sizes of hundreds of meters. Equation (3.86) can in fact be integrated by means of the method of characteristics (Eagleson, 1970) over a mesh of size x, and it is possible to derive the concentration time corresponding to a precipitation that equals the maximum possible discharge $p = L k_s \tan(\beta)$, which gives:

$$t_c = x^{1/\alpha} \frac{(\vartheta_s - \vartheta_r)}{k_s \tan(\beta)} \tag{3.87}$$

Unfortunately the solution provided by the method of characteristics is only valid along the characteristic lines and, given the non-linearity, does not provide an explicit solution in time and space, which is required to find a relationship between the point water content and the total volume stored in the mesh. It is therefore necessary to integrate equation (3.86) over the mesh on the basis of a reasonable simplifying assumption.

On these lines it is reasonable to assume that, although the water content η varies in space, its time partial derivative $\frac{\partial \eta}{\partial t}$ does not vary strongly in space at a given time t; therefore its space integral can also be approximately considered constant in space, which gives:

$$p - \frac{1}{x} \int_0^x \frac{\partial \eta}{\partial t} \, dx \equiv q_s \tag{3.88}$$

with q_s a specific yield, which varies in time, but at any time is assumed practically constant in space. Under this assumption the flow at any time increases linearly in space, but not necessarily by an increment equal to the precipitation p as in TOPMODEL; this will only happen at saturation when $\frac{\partial \eta}{\partial t}$ is null. It should also be noted that this formulation is applicable when p is null and the specific yield q_s becomes negative.

At the end of a mesh of size x the discharge thus becomes:

$$q_x = q_0 + \int_0^x \left[p - \frac{\partial \eta}{\partial t} \right]_\xi d\xi = q_0 + q_s x \tag{3.89}$$

which, substituted for in the second of equation (3.84), allows for the derivation of the soil moisture horizontal profile:

$$\eta(\xi) = \left(\frac{q_\xi}{C} \right)^{1/\alpha} = \left(\frac{q_0 + q_s x}{C} \right)^{1/\alpha} \tag{3.90}$$

The total volume stored in a single mesh can thus be computed as:

$$\begin{aligned}
&V_x = \int_0^x \eta(\xi) d\xi = \int_0^x \left(\frac{q_0 + q_s \xi}{C} \right)^{1/\alpha} d\xi \\
&y = \frac{q_0 + q_s \xi}{C} \qquad \xi = \frac{C y - q_0}{q_s} \qquad d\xi = \frac{C}{q_s} dy \\
&\begin{cases} \xi = 0 & \Rightarrow \quad y = \frac{q_0}{C} \\ \xi = x & \Rightarrow \quad y = \frac{q_0 + q_s x}{C} \end{cases} \\
&V_x = \int_{\frac{q_0}{C}}^{\frac{q_0 + q_s x}{C}} \frac{C}{q_s} y^{1/\alpha} dy = \frac{\alpha C}{(\alpha + 1) q_s} \left[y^{\frac{\alpha+1}{\alpha}} \right]_{\frac{q_0}{C}}^{\frac{q_0 + q_s x}{C}} = \frac{\alpha C}{(\alpha + 1) q_s} \left[\left(\frac{q_0 + q_s x}{C} \right)^{\frac{\alpha+1}{\alpha}} - \left(\frac{q_0}{C} \right)^{\frac{\alpha+1}{\alpha}} \right]
\end{aligned} \tag{3.91}$$

V_x can also be written as:

$$V_x = \frac{\alpha C^{-1/\alpha}}{(\alpha + 1) q_s} \left[(q_0 + q_s x)^{\frac{\alpha+1}{\alpha}} - (q_0)^{\frac{\alpha+1}{\alpha}} \right] \tag{3.92}$$

Up to this point the integration has been carried out on a single mesh. By extending the hypothesis of constancy of the specific yield to all the meshes contributing to a downstream one, it is possible to write an expression relating the outflow discharge from the i^{th} mesh, to its contributing surface and to the specific yield.

For the sake of clarity the derivation will be done for meshes in series as in a hillslope, but a similar result holds for the general case of meshes in series and in parallel.

Given the constancy of the specific yield one easily gets for the i^{th} mesh in series:

$$q_i = i\,x\,q_s \tag{3.93}$$

and bearing in mind the relationship between the discharge and the water content:

$$\eta_i = \left(\frac{i\,x\,q_s}{C_i}\right)^{1/\alpha} \tag{3.94}$$

which can be written as:

$$x\,q_s = \frac{\eta_i^{\alpha}\,C_i}{i} \tag{3.95}$$

The total volume of water stored in i^{th} mesh becomes:

$$\begin{aligned} V_i &= \frac{\alpha\,C_i^{-1/\alpha}}{(\alpha+1)q_s}\left[\left(q_{(i-1)}+q_s x\right)^{\frac{\alpha+1}{\alpha}}-\left(q_{(i-1)}\right)^{\frac{\alpha+1}{\alpha}}\right]=\frac{\alpha\,C_i^{-1/\alpha}}{(\alpha+1)q_s}\left[\left(i\,x\,q_s\right)^{\frac{\alpha+1}{\alpha}}-\left((i-1)\,x\,q_s\right)^{\frac{\alpha+1}{\alpha}}\right] \\ &= \frac{\alpha}{(\alpha+1)}x\left(\frac{x\,q_s}{C_i}\right)^{1/\alpha}\left[i^{\frac{\alpha+1}{\alpha}}-(i-1)^{\frac{\alpha+1}{\alpha}}\right] \end{aligned} \tag{3.96}$$

while the total volume stored in n meshes can finally be estimated as:

$$V_n = \frac{\alpha}{\alpha+1}x\left(x\,q_s\right)^{1/\alpha}\sum_{i=1}^{n}\frac{i^{\frac{\alpha+1}{\alpha}}-(i-1)^{\frac{\alpha+1}{\alpha}}}{C_i^{1/\alpha}} \tag{3.97}$$

In order to find a relationship between the outflow discharge and the total volume stored as well as with the average soil moisture content, one has to recall that equation (3.93) also applies to the n^{th} mesh, which gives:

$$x q_s = \frac{\eta_n^{\alpha} C_n}{n} \tag{3.98}$$

Equation (3.98) can then be substituted for into equation (3.97) to give:

$$V_n = \frac{\alpha}{\alpha+1} \frac{x C_n^{1/\alpha}}{n^{1/\alpha}} \eta_n \sum_{i=1}^{n} \frac{i^{\frac{\alpha+1}{\alpha}} - (i-1)^{\frac{\alpha+1}{\alpha}}}{C_i^{1/\alpha}} = \frac{\alpha}{\alpha+1} \frac{n x C_n^{1/\alpha}}{n^{\frac{\alpha+1}{\alpha}}} \eta_n \sum_{i=1}^{n} \frac{i^{\frac{\alpha+1}{\alpha}} - (i-1)^{\frac{\alpha+1}{\alpha}}}{C_i^{1/\alpha}}$$

$$= \frac{\alpha}{\alpha+1} n x C_n^{1/\alpha} \eta_n \sum_{i=1}^{n} \frac{\left(\frac{i}{n}\right)^{\frac{\alpha+1}{\alpha}} - \left(\frac{i-1}{n}\right)^{\frac{\alpha+1}{\alpha}}}{C_i^{1/\alpha}} \tag{3.99}$$

Recalling the meaning of C_i which was defined in equation ('3.85), the summation term in equation (3.99) represents an average equivalent resistance weighted by a topological density function, given by the i/n terms (which will also contain summations for the parallel connections), and can be replaced with:

$$\frac{1}{\overline{C}_n} = \left[\sum_{i=1}^{n} \frac{\left(\frac{i}{n}\right)^{\frac{\alpha+1}{\alpha}} - \left(\frac{i-1}{n}\right)^{\frac{\alpha+1}{\alpha}}}{C_i^{1/\alpha}} \right]^{\alpha} \tag{3.100}$$

where $1/\overline{C}_n$ is the TOTOPS index, which can be computed on the basis of both the TOpography of the surfaces and the TOpology of the meshes connection graph, as well as on the Physical Soil properties.

Substituting for equation (3.100) into equation (3.99), the sought-for expression, relating the outlet water content to the total volume stored, can be finally given as:

$$V_n = \frac{\alpha}{\alpha+1} n x \eta_n \left(\frac{C_n}{\overline{C}_n} \right)^{1/\alpha} \tag{3.101}$$

or as:

$$\eta_n = \frac{\alpha+1}{\alpha n x} \left(\frac{\overline{C}_n}{C_n} \right)^{1/\alpha} V_n \tag{3.102}$$

On the other hand the spatial integration of equation (3.86) to all the contributing area gives:

$$\frac{\partial V_n}{\partial t} = n x p - C_n \eta_n^{\alpha} \tag{3.103}$$

Substitution of equation (3.102) into equation (3.103) allows for the derivation of a non-linear reservoir model at the scale of the hillslope whose parameters are entirely derived from the physical as well as from the topographical and topological characteristics:

$$\frac{\partial V_n}{\partial t} = n x p - \left(\frac{\alpha+1}{\alpha n x}\right)^{\alpha} \overline{C}_n V_n^{\alpha} \tag{3.104}$$

Equation (3.104) shows that the kinematic model assumption results in the derivation of a zero dimensional non-linear reservoir model which extends its validity beyond the size of the elementary grid cells (pixels) spatially describing the geographical information, to larger sizes provided that the soil properties, the topographical and topological characteristic are appropriately synthesised. Integration of equation (3.104) allows for the determination of the volume stored in the soil at any time and can be used in the same form for all the contributing areas, only requiring the computation of the TOTOPS index for the different areas contributing to the drainage network, as is done by the TOPMODEL combined topography-soil index. Note that the TOTOPS index contains more information than the TOPMODEL index, in that it includes the topology of the drainage channel connections, thus allowing for a geomorphological interpretation.

Finally, although the explicit integration of equation (3.104) only exists in the form of an infinite series, an approximated solution can be found in order to compute the volume stored in the soil at any time. Given the volume, it is then possible, by means of equation (3.102), to compute the local soil moisture and to compare it with the maximum amount that can be locally stored in order to estimate the saturated areas, for which a similar kinematic model will be used in order to express the surface runoff.

3.5 MODEL SENSITIVITY TO RAINFALL INFORMATION

3.5.1 Experiments involving SHETRAN and MTB Rainfall Model

3.5.1.1 Application of SHETRAN to the Reno River

SHETRAN description

SHETRAN is a physically based, spatially distributed modelling system for water flow, sediment transport and contaminant migration, applicable at the scale of the river basin, which has been developed by the University of Newcastle upon Tyne, Figure 3.5.1. It is based on an enhanced version of the Systeme Hydrologique Europeen (SHE) hydrological modelling system (Abbott et al, 1986a, b), which provides an integrated surface and subsurface representation of water movement through a river basin, incorporating the major elements of the land phase of the hydrological cycle (interception, evapotranspiration, snowmelt, overland and channel flow, unsaturated and saturated zone flow). Each of the processes is modelled either by finite difference representations of the partial differential equations of mass and energy conservation or by empirical equations derived from independent experimental research. The spatial distribution of catchment properties, rainfall input and hydrological response is achieved in the horizontal direction through the representation of the catchment by an orthogonal grid network and in the vertical direction by a column of horizontal layers at each grid square.

SHETRAN-parameters

Within each model grid square, each physical characteristic is represented by one parameter value. As long as the grid square is small compared with the distances over which there is significant spatial variability in basin properties and hydrological response, this does not compromise the modelís ability to represent local variations in response. However, as grid scales increase, the local spatial variability in properties and response becomes subgrid. There are then difficulties in applying the equations of small scale physics which make up SHETRAN and evaluating their parameters, at the

grid scale (e.g. Beven, 1989). In particular, the field measurements which form the basis of parameter evaluation are most easily carried out at the point or plot scale, which may not be representative of the larger grid scales used in modelling river basins. The solution has been to use ëeffectiveí parameter values, which represent the subgrid spatial variability; to give a grid scale response. However, this is a pragmatic approach and it is recognized that the concept may not allow an accurate reproduction of the observed response in all circumstances (as shown for example by Binley et al, 1989).

The principal soil parameters and functions in SHETRAN are the soil depth, the saturated zone conductivity, the saturated values of conductivity and moisture content for the unsaturated zone and the water retention (moisture content/tension) and moisture content/conductivity relationships for the unsaturated zone. These characteristics do not vary through a simulation. The proportion of ground covered by vegetation at the grid scale (i.e. the proportion of the grid square which is not bare soil) is accounted for by a proportional index on a scale from 0 to 1. This represents the integrated cover provided by the full range of vegetation present. It is determined from field surveys and aerial photographs and can be varied in a predetermined manner through the simulation. The vegetation parameters are interception drainage and storage terms, properties affecting evapotranspiration, and root distribution, and are mostly time invariant. Overland flow resistance is quantified by the Strickler resistance coefficient (the reciprocal of the Manning coefficient). The coefficient is specified by the modeller, usually according to land use, and does not vary through the simulation. Topographic elevations are determined from appropriate maps or Digital Elevation Models. Channel characteristics are quantified in terms of the channel cross-sectional shape, elevation and Strickler resistance coefficient. All the above parameters and functions are spatially variable between grid squares (or channel links as appropriate), as are also the specified time-varying rainfall and meteorological variables determining potential evapotranspiration, and the simulated time-varying hydrological responses.

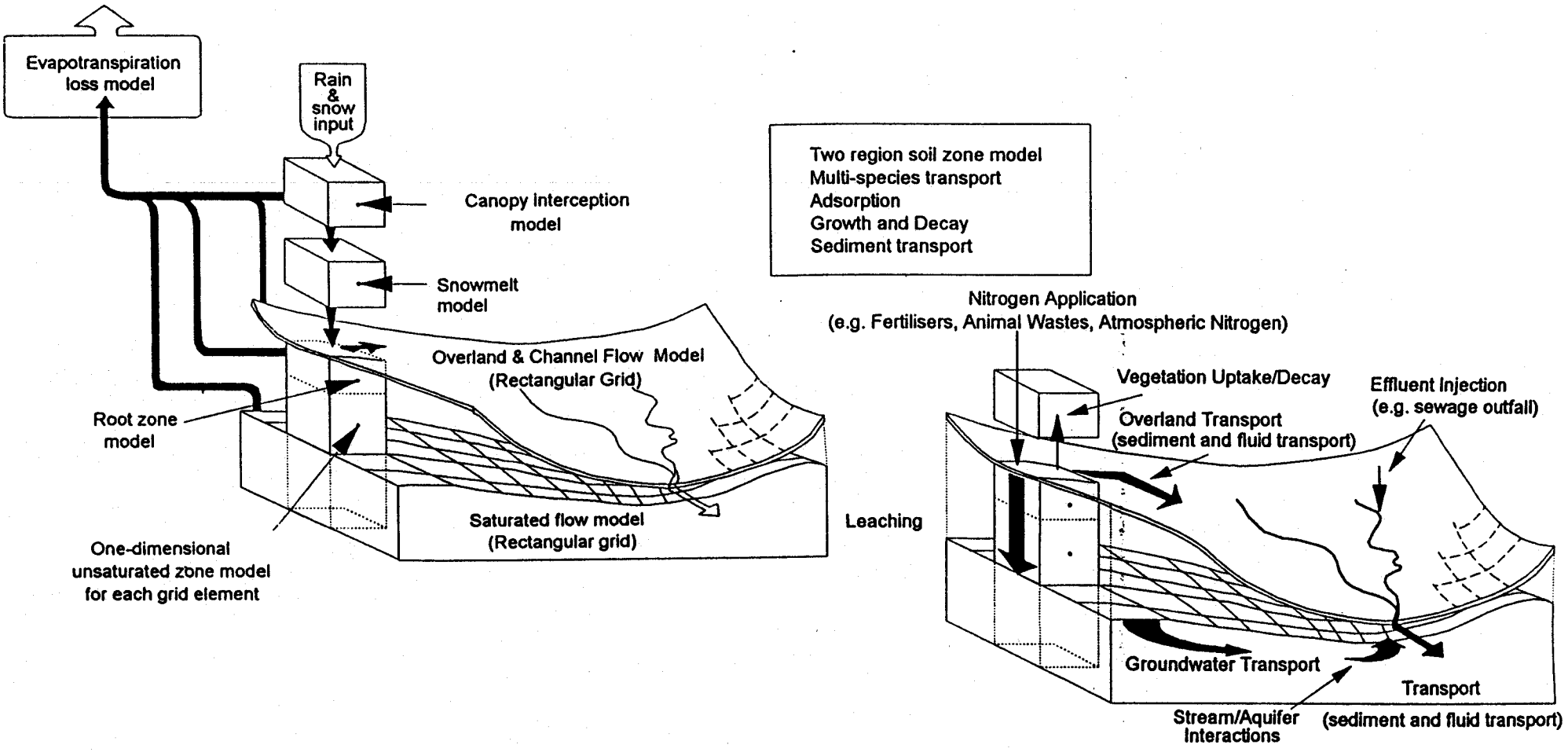

Figure 3.5.1 - Schematic of SHETRAN flow, sediment and contaminant transport modelling system

Application of SHETRAN to the Reno

Before describing the steps involved in parameterizing a SHETRAN model of the upper Reno basin it must be stated that only limited data were available on the required time scale for this work, and so only a very approximate SHETRAN model of the basin has been developed. However, the work on assessing the sensitivity of Reno basin response to different levels of rainfall information should be broadly indicative of what might be expected to prevail in reality. The size of the Reno catchment, and of the computational grid employed for SHETRAN, has also limited the length of simulation which could be performed. However, this has not posed a major problem, since the main focus of the work is the response to the historic storm which occurred in November 1990, and to possible alternative realizations of this storm which might have occurred, given the sampled rainfall information for the historic storm (Section 2.3.2.3).

It is first necessary to reach a compromise in the representation of the Reno catchment between a discretization which is as fine as the data available, and hence makes maximum use of that data, and a discretization which is computationally feasible given the processing power, core memory and disk storage capacity of the available computers, and logistically feasible given the time and manpower available for the processing of the data. The coarsest data set is the altitude data obtained from a digital terrain model supplied by Centro IDEA, which is at 400 metre resolution. The smallest multiple of this which leads to a distributed model which is feasible is 800 metres, resulting in a model with 50 grid squares in the east-west direction and 75 squares in the north-south (the upper Reno catchment is about 40 kilometres east-west and 60 kilometres north-south). The total number of computational elements in this model is 1875, and there are 281 river links in all. This catchment is displayed in Figure 3.5.2.

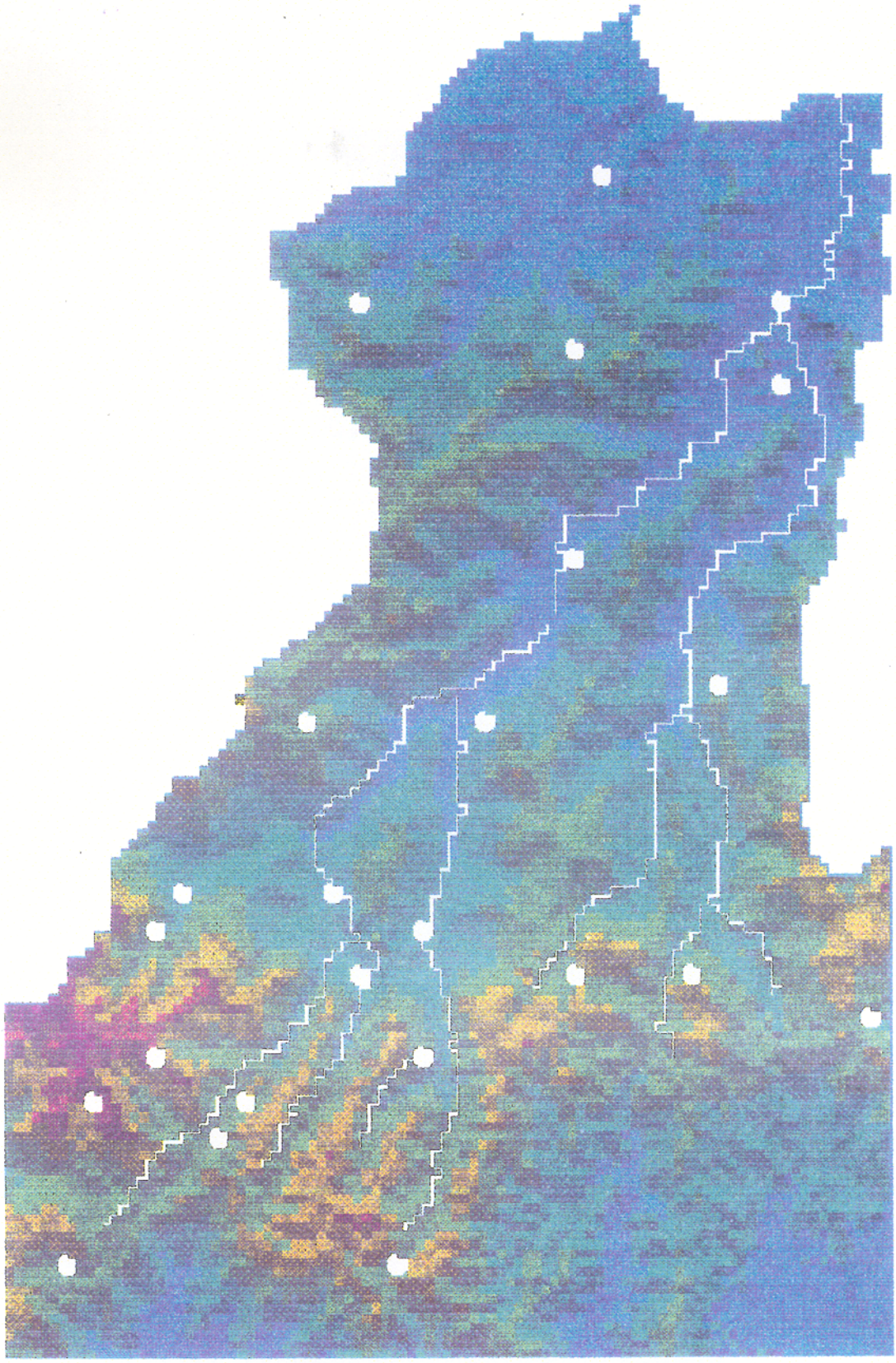

Figure 3.5.2. - A digital elevation map of the upper Reno basin (altitude range 80m - 1800m) showing the discretized river network and the positions of raingauges.

The river links and annual average rainfalls over the catchment were originally digitized optically from paper maps, and this was done to a resolution of 400 metres in line with the resolution of most of the original data. Initially, enough river branches were used to drain each of the seven sub-catchments as identified by Wendling (1993), but it was found that part of the catchment (as modelled) became water-logged, and inspection of the river map indicates that this part of the catchment indeed has a channel, and this was subsequently included.

The only information supplied as regards the size and shape of the river channel network is that it is about 20 metres wide and 2 metres deep at the top of the catchment and 100 metres wide and 3 metres deep at catchment outlets. Thus the network has been set up so that the width and depth increase in proportion to the 0.4th power of the total upstream run length. If there is a merging of two branches of the river, then the downstream elements will have upstream run lengths composed of the sum of the run lengths of the two upstream branches. The channel is everywhere assumed to have a rectangular cross-section. The alternative method of making the size of the channels proportional to the distance of each link element from its source was also tried, but lead to some difficulties with localised overland flooding where branches came together and the downstream channel was not sufficiently wide to take the combined upper fluxes.

The altitude of each channel link was initially taken to be such that the bank-top was at the same elevation as the lowest of the two adjacent land elements. However, in places this causes the river to run uphill, hence the 'lower' river link is lowered so that it is 10 metres below the "upper" one, with a subsequent modification being made to the downstream links where necessary to make the network flow everywhere downhill.

Information about the coverage of the land came from land-use data obtained from the Forest Authority of the Emilia Romagna region at a 200 metre resolution. These data indicate whether a land element is built up, pasture, woodland, or bare rock, with many subdivisions within these main classes. It was seen that most of the surface of the land was either grass or forest, hence two vegetation types were defined for the SHETRAN model. The parameters for these vegetation types were chosen based on previous experience at Newcastle.

No information on the soils is available. The catchment is assumed to be homogeneous

in this respect, and the soil parameters are based on previous experience at Newcastle. The only information on the soil depth is that the impermeable bed-rock is everywhere very close to the surface, the surface area of the land where the depth is more than 10 metres being less than 10 km2, and this only in the river plains of the lower catchment. There is also information on the bedrock to be extracted from the land-use data, as this indicates the points on the ground where the bedrock reaches the surface. With these considerations in mind, then, the depth of the bedrock below the ground is allowed to vary from 0.1 to 0.5 metres; with the shallowest soils being at the points where the bedrock is observed at the ground, and the soils increase linearly in depth with distance from the bare rock element, so that the deepest soils are located at the points most remote from anywhere the bedrock has been observed at the ground. With a basic time-step of one hour, but a restriction so that no more than 0.1mm of rain ever falls in one time step (the time step is reduced when this would otherwise occur), a SHETRAN model simulation including a large flood wave takes approximately seven hours to run.

The bulk of the effort which went into the calibration of the SHETRAN modelling system was in getting the represented shape of the land to reflect not only the average altitude of each grid square for which there is sufficient data, but also to reflect the typical gradients present between two different grid squares. Information on the altitude of the land is not always sufficient to properly characterize the gradients, and it was found that much trial and-error was needed to get this right. The main problems which arose are that, when the altitude is sampled on a grid with a large spacing, there are points on the ground which appear to lie in a hollow, and in the SHETRAN simulations these collect water instead of propagating it further down the catchment. Overall the gradient of the land are underestimated by the coarse sampling of the land altitude. Also small rivers and streams are not represented at all coarse spatial resolutions; rather, the overland flows are represented as simple overland shear flows. These have a much higher friction coefficient than flow which passes through a network of channels, again causing the simulations to occur as though the overland flow is unduly restricted. The solution of these problems is to make the Strickler coefficients slightly higher than observed and to smooth out the shape of the land slightly so that there is well defined path from all parts of the catchment to the basin outfalls.

The final SHETRAN simulation of the outflow hydrograph for the storm of 24/26

November 1990 is shown in Figure 3.5.3. The agreement is quite good but this in itself does not constitute sufficient evidence that the calibrated model provides a unique, physically based representation of the response of the upper Reno basin to rainfall. Much more data on the internal behaviour of the catchment (tributary flows, soil moisture, groundwater levels, etc) would be needed to achieve this. Nonetheless, the responses obtained from the synthetic storms should provide a useful indication of the sensitivity to the level of rainfall information for the real catchment.

3.5.1.2. Sensitivity of predicted runoff to rainfall sampling in space

The MTB model is used to generate an ensemble of storm conditioned on the storm of 24/26 November 1990, as described in Section 2.3.2.3, and these are first fed into the catchment model so that each computational element of the model receives a unique amount of rainfall as implied by the rainfall field. Of the 24 raingauges present in the catchment, subsets of 6, 12 and 18 are selected to give a uniform distribution across the basin. Then the SHETRAN model is run 4 more times with rainfall inputs "sampled" by the different sets of raingauges, i.e. the rainfall is sampled at the point in the field where a raingauge is located, and all the computational grid elements of the SHETRAN model in the vicinity of this raingauge receive the sampled amount of rainfall; the allocation of grid elements to each raingauge is done using Thiessen polygons. The temporal sampling of the rainfall is done on a 6 minute basis, and then aggregated to the hour.

The complete experiment was performed on a network of 145 workstations so, while each individual run of the model took about seven hours, the whole experiment was completed in about three nights, with 30 synthetic storms being used. For each storm event, and each level of rainfall information used, the runoff from the outfall of the basin was stored. Figure 3.5.4 shows the runoff hydrograph obtained from both the complete rainfall field input and rainfall sampled at 24 raingauges for all thirty storms. Summary statistics for the differences between the runoff obtained from the complete rainfall field and the four different levels of sampled rainfall information are given in Table 3.5.1. Figures 3.5.5 and 3.5.6 shows all five runoff scenarios for two of the storm events displayed in Figure 3.5.4. One of these (Figure 3.5.5) shows a sharp response in

the complete runoff case (marked with a star in Figure 3.5.4) which is unaccounted for on the sampled rainfall simulations, while the other (Figure 3.5.6) has been randomly selected from the ensemble. This latter figure is representative of the ensemble. The first impression gained from the results in Table 3.5.1 is that the estimation errors do not decrease in a smooth fashion with an increasing number of raingauges. Moreover the estimation errors are of quite a significant magnitude (15-20% of the true peak discharge). Clearly, the estimation errors must decrease as the number of raingauges approaches the number of computational nodes; the number of raingauges required to achieve this convergence is clearly larger than 24, but has not been investigated here.

No. of gauges	Av. diff. in time of peak		Av. diff. in magnitude of peak		Av. diff. in av. runoff volume		Av. efficiency	
	(hours)	±	(cumecs)	±	(cumecs)	±	(R^2)	±
6	2.12	1.94	-216.66	167.46	-19.07	5.13	0.86	0.03
12	3.25	2.23	-131.93	175.64	-13.20	5.73	0.79	0.07
18	2.29	2.64	-132.05	187.61	-10.20	6.32	0.78	0.05
24	4.77	2.26	-162.97	180.83	-12.18	6.20	0.81	0.04

Table 3.5.1 Sumary statistics of differences in runoffs from inputs of complete rainfall information and sampled raingauge information, averaged across thirty simulations (the ± tolerances indicate 60% confidence intervals, and positive statistics indicate that the runoff from the sampled raingauge input is bigger or later than runoff from the complete rainfall information).

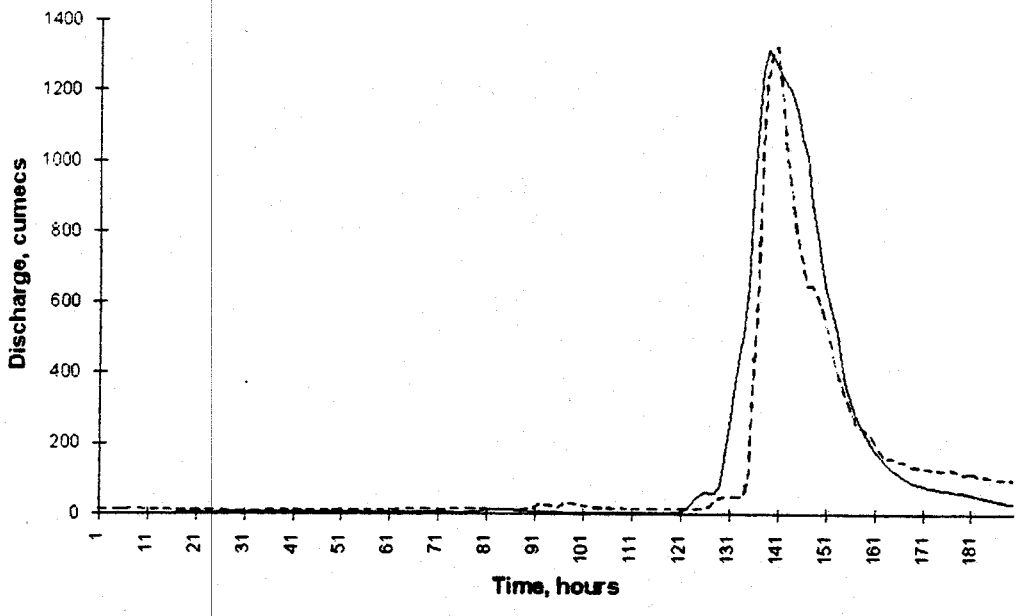

Figure 3.5.3 - Plot of observed (dashed line) and simulated (solid line) streamflow at Casalecchio for the storm of 24/26 November 1990

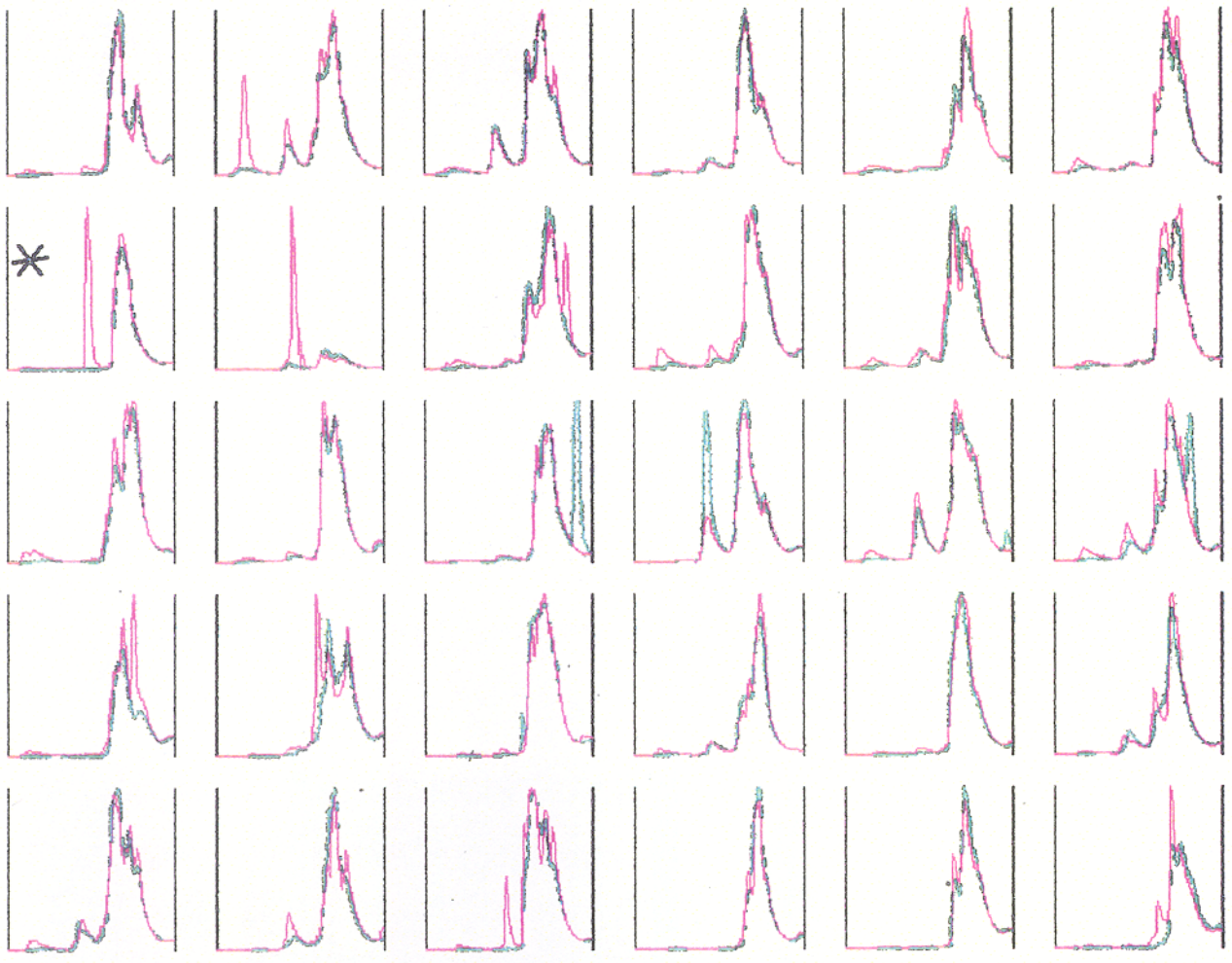

Figure 3.5.4. - Simulated storm hydrographs corresponding to the complete rainfall fields (blue) and rainfall inputs sampled by 24 raingauges (green) for the ensemble of 30 MTB storms.

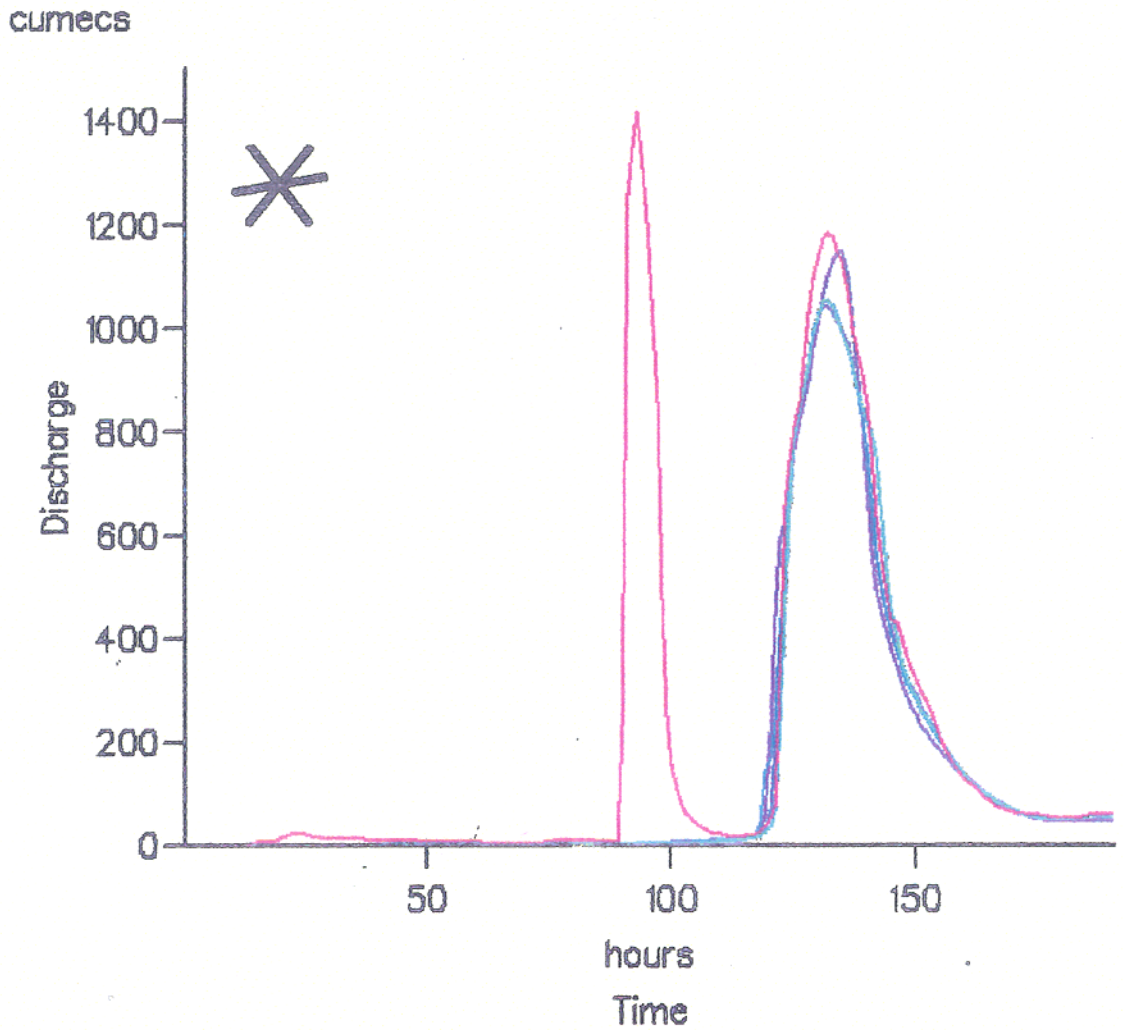

Figure 3.5.5 - Storm hydrographs corresponding to the complete rainfall field (red) and rainfall inputs sampled by 6, 12, 18 and 24 raingauges (blue-green) for the storm marked * in Figure 3.5.4

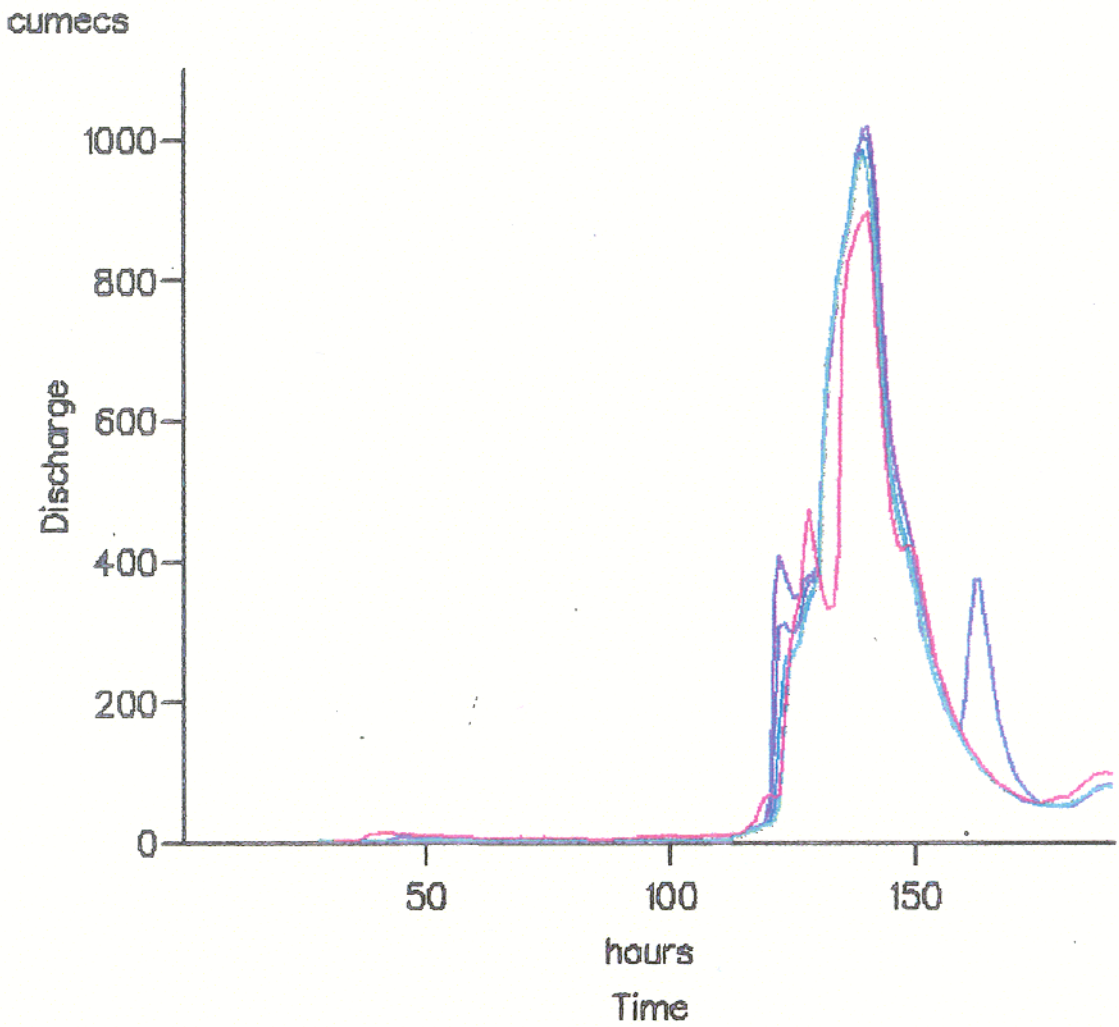

Figure 3.5.6 -Simulated storm hydrographs corresponding to the complete rainfall field (red) and rainfall inputs sampled by 6, 12, 18 and 24 raingauges (blue-green) for a 'typical' storm in Figure 3.5.4.

A close inspection of the hydrographs in Figure 3.5.4 shows that there are two occasions when sharp responses in the flow occur when no response is observed from the input sampled by the 24 raingauges, while in two further cases, the reverse occurs. If these four storms are eliminated and the statistics in Table 3.5.1 are recalculated, there is a major reduction in the magnitudes of the error with, notably of timing errors, but again no clear evidence of a reduction in estimation error with increasing numbers of raingauges. This calculations sumarised in Table 3.5.2. While errors in the range 4-8% for peak discharge are not of great concern for this set of storms, the very large errors observed for the remaining four storms are.

No. Gauges	Av. diff. in time of peak		Av. diff. in magnitude of peak		Av. diff. in av. runoff volume		Av. goodness of fit	
	(hours)	±	(%)	±	(%)	±	(R^2)	±
6	-0.42	0.98	-5	2	-9	2	0.90	0.02
12	1.27	1.83	8	8	-5	3	0.81	0.08
18	-0.76	2.36	-4	3	-5	2	0.86	0.03
24	0.96	1.37	-5	2	-8	2	0.90	0.01

Table 3.5.2. As Table 3.5.1, but with four exceptional storms removed from analysis and displaying relative differences in runoff characteristics.

Figure 3.5.7 shows a series of snapshots of the rainfall field over the basin which caused the unaccounted for response in the plot marked with the star (Figure 3.5.5), with the positions of all 24 raingauges marked by white dots. It can be seen that, by chance, all the major features of the rainfall field have fallen in between the raingauges. The case where the reverse is true (i.e. a peak in the response to the input based on 24 raingauges with none in that for the complete field) can be explained as very local intense rainfall sampled by a raingauge which is distributed over a larger area through the Thiessen polygon procedure. It may be expected that if more runs of the experiment were performed, then there would be cases where a peak was reproduced by an input based on 24 raingauges when fewer raingauges are used. This is a case for maximising the number of raingauges available, but the effect of the number of raingauges on the probability of missing such a peak flow have not been investigated here. The result is an impetus for providing an input from a rainfall radar, which provides much better spatial coverage than any raingauge network, but not with the same quantitative accuracy.

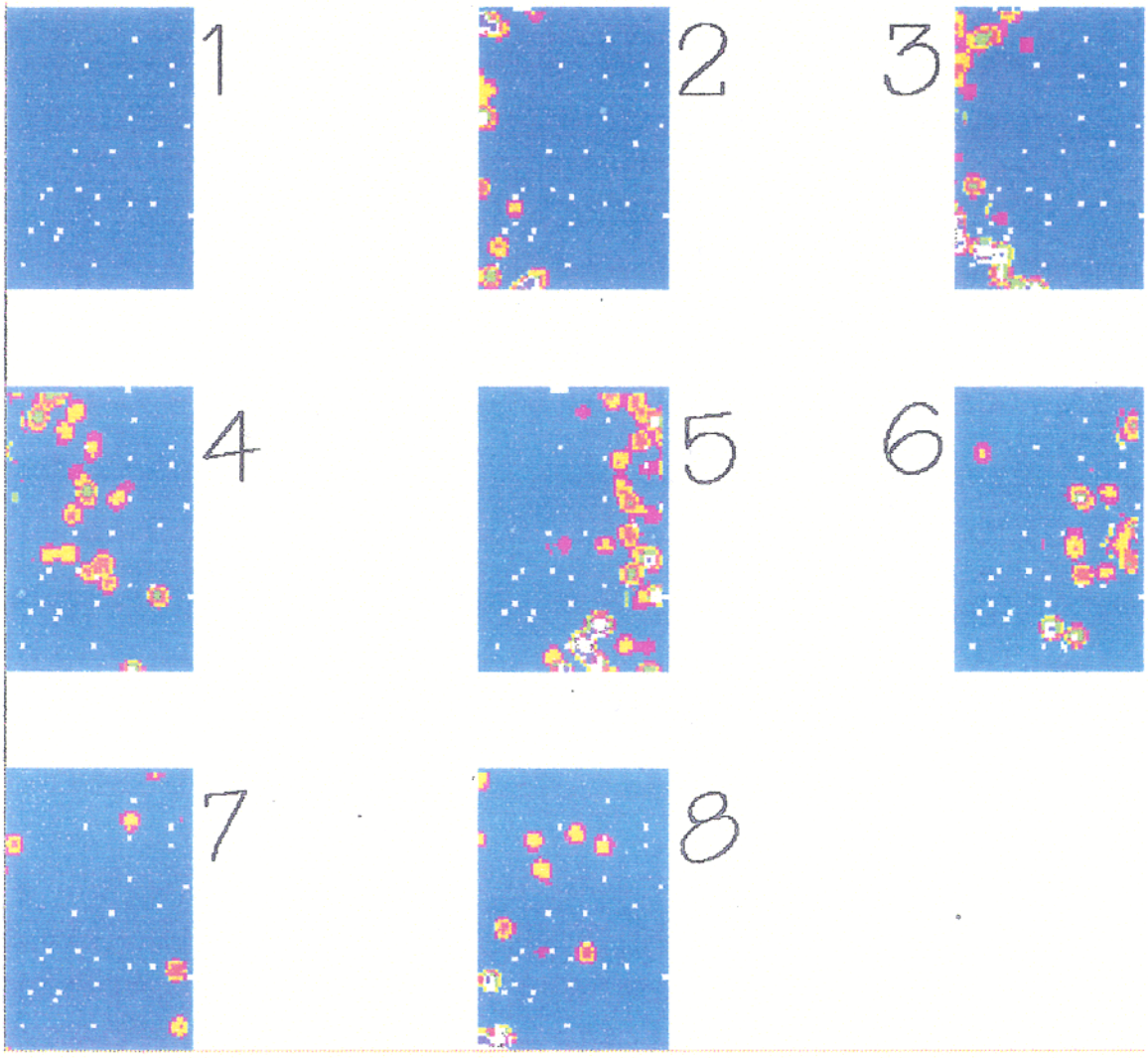

Figure 3.5.7. Sequence of spatial rainfall snapshots for the storm shown in Figure 3.5.5.

In conclusion, it may be stated that for more than 80% of the storms simulated, in general the runoff predicted from a network of 6 raingauges is sufficiently accurate for flood warning and mitigation purposes, but there is some probability that the actual runoff will contain a peak which is completely missed by hydrological simulations based on inputs from a small number of raingauges. It is expected that this probability will diminish as the number of raingauges is increased, but while the possibility remains there is a problem. The thirty simulations are conditional on the November 1990 storm, and are therefore alternative possible realizations of this storm, rather than independent realizations of other possible storms. By conditioning on the 1990 storm, it is hoped that the simulations are as realistic as possible, given the available rainfall data. However, more extensive investigations are needed of the spatial structure of rainfall storms over the Reno before definite conclusions can be drawn about the risk of failing to capture localized intense rainfall with a raingauge network. Depending on the risks involved, there may be a case for providing radar information for the purposes of real-time forecasting.

Many of the model assumptions should be borne in mind with the above conclusions. The results depend critically on the accuracy of the MTB model in reproducing the characteristics of real rainfall fields, and in reproducing with the correct frequency the extremes in the variability of the phenomenon. The results also depend on the accuracy with which the SHETRAN model reproduces the response of the catchment to extreme rainfall events. Unfortunately, it has not been possible to investigate the reliability of the SHETRAN model in this respect because data for only one major flood event were available for this work. Much more data are required to enable a more robust SHETRAN model to be derived.

3.5.2 Model Sensitivity to rainfall Information: Test on real observed data.

Spatial variability of rainfall is often considered as a major source of temporal variability in the resulting basin hydrograph (Krajewski et al., 1991, or Niemczynowicz, 1987). Since direct experimental evidence cannot be easily reached, this must be verified through a modelling approach, provided adequate data are available. A first approach, described above in section 3.5.1, has been made with

synthetic data generated over the gridded domain used by the SHE model for a small catchment in U.K. Here, a second approach will be shown over some French Mediterranean catchments based this time on real data.

The bulk of the work has been done using a semi-distributed version of TOPMODEL, but some trials will also be reported about attempts with a cruder index method.

A semi-distributed version of TOPMODEL has been applied to the Réal Collobrier experimental basin (71 km^2 in South East France with 21 recording raingauges available - see Figure 3.5.8. Since the model can be easily initialised from previous discharges (see paragraph 3.4.2 in this chapter), a series of 19 independent events has been selected using hourly time steps.

First, a set of reference results has been built under the assumption of spatial uniformity for the rainfall, but two different densities of network have been tested:

- one based on only 5 gauges, supposed to represent operational conditions (estimate called P5)

- and another one using all the 21 available gauges.(estimate called P21)

The difference between these two estimates P5 and P21 was therefore in terms of uncertainty on the estimation of the true basin average rainfall. A scatterplot (see Figure 3.5.9a) shows how those two estimates are correlated, and their distribution above a given threshold of intensity is shown in Figure 3.5.9(b).

Secondly, the 21 gauge network has been used to evaluate the rain input over the sub-basins managed by the semi-distributed model. Because of this automatic splitting into land units, performed on hydraulic assumptions, there were 20 of them, with rather large differences in area.

Consequently, they have been aggregated into a set of 9 Precipitation units with similar areas of about 8 km2 (i.e $< 3 \times 3$ km2) as can be seen in Figure 3.5.10, for which the average precipitation has been computed. Given their similarity in area and the relative homogeneïty of the network, the uncertainity on the average rainfall was also much similar for all those precipitation units.

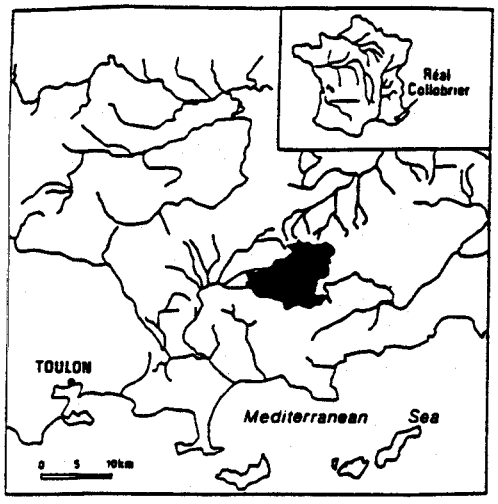

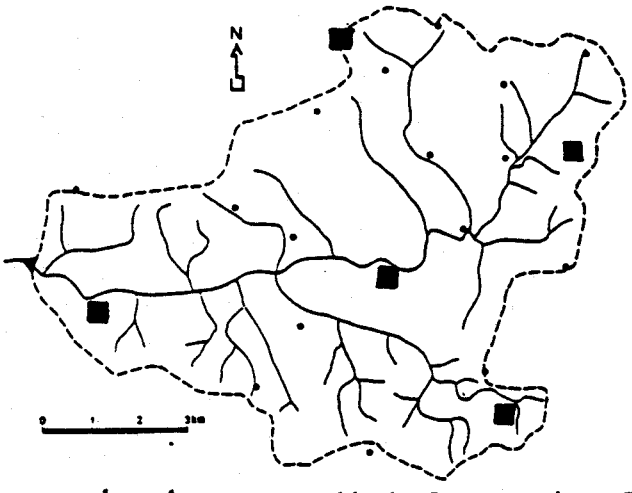

(squares show the gauges used in the 5 gauge estimate P5)

Figure 3.5.8 - Réal Collobrier catchment and Raingauge network used

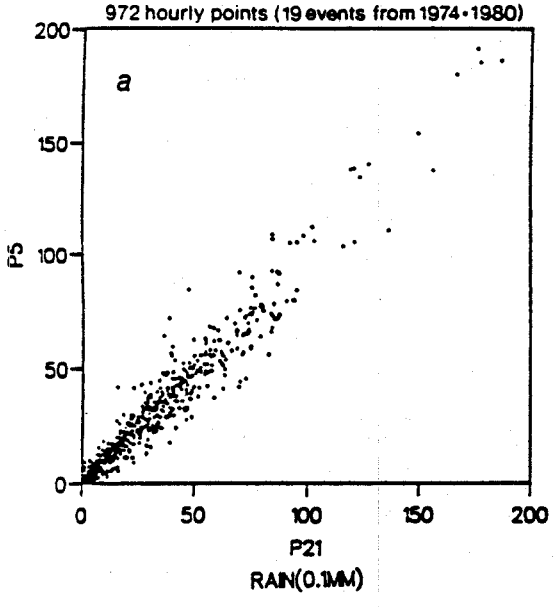

a) scatter diagram over all values

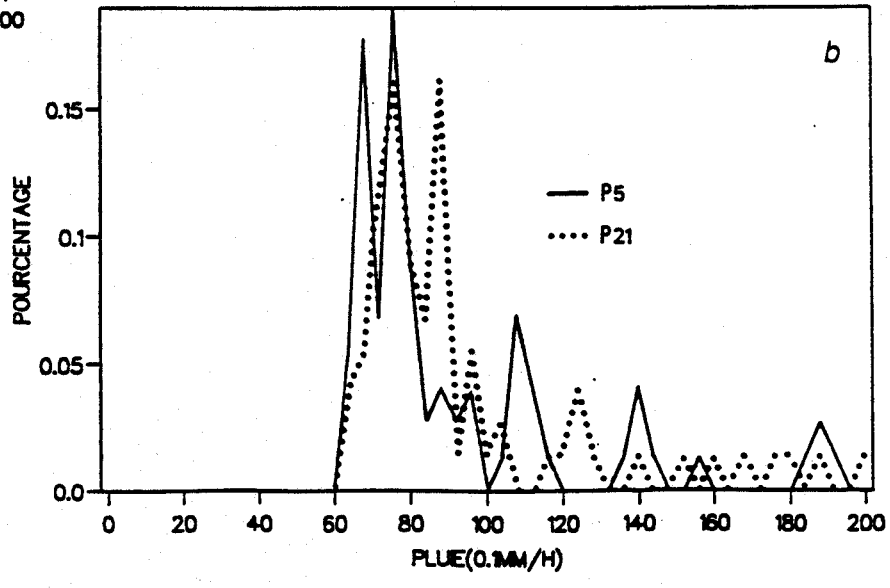

b) histograms for values above 6 mm/h

Figure 3.5.9 - Comparison between the 5 and the 21 gauge estimates P5 and P21.

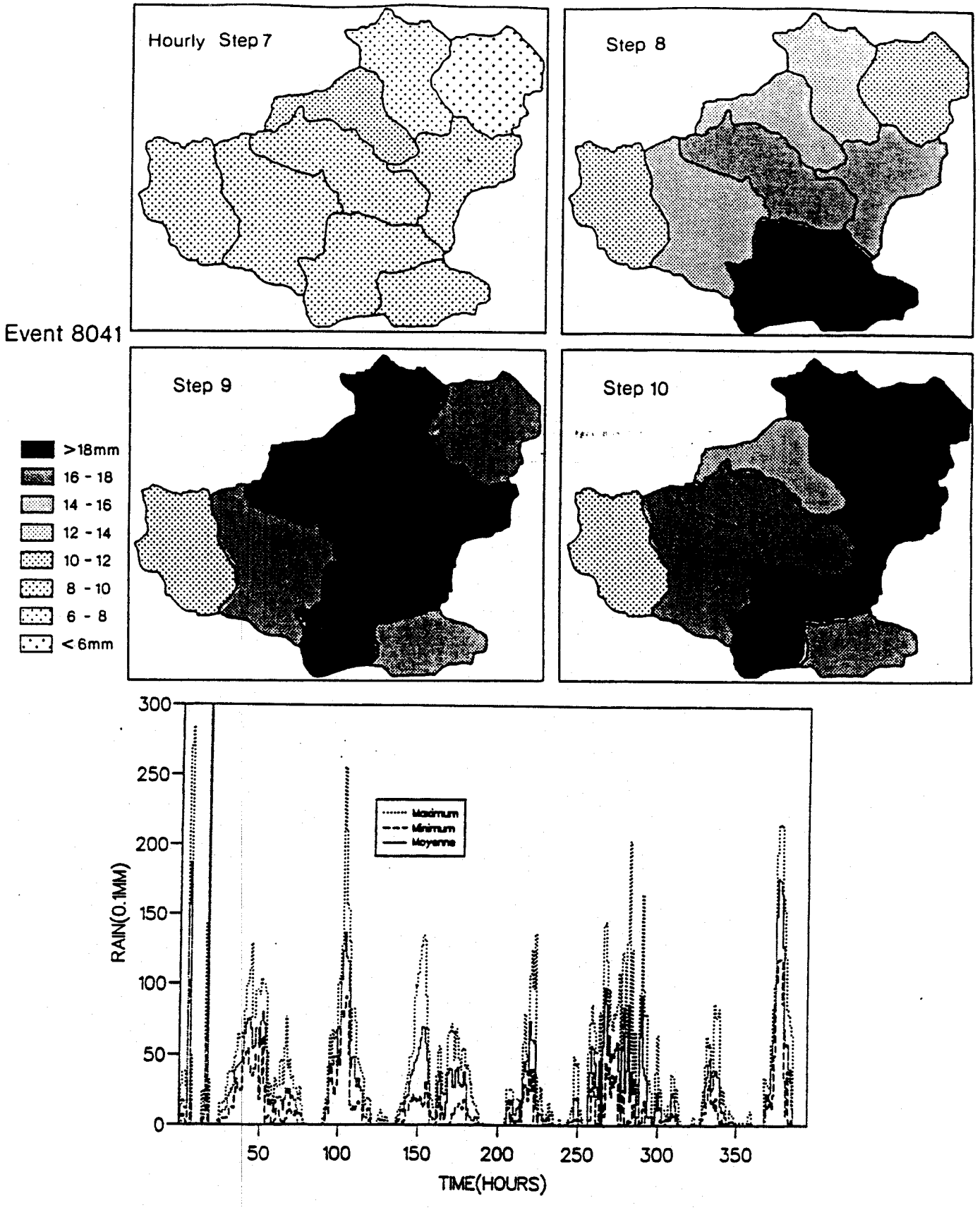

Figure 3.5.10 Temporal variability of spatially variable rainfall (averaged over precipitation units of approximately 8 Km^2)
a) Typical time evolution of the rainpattern over the precipitation units.
b) Minimum, median and maximum rainfalls computed over the 9 precipitations units for a set of rainy hours.

The test procedure has thereafter been as follows:

1) recalibration of the initial model (see paragraph 3.4.2 in this chapter) with the Uniform rainfall P5 computed from 5 gauges, but using only 9 events instead of the 21 used previously for the calibration. The decrease in the number of calibration events does not change significantly the parameters values nor the performances, (around 75% in Nash efficiency).see Figure 3.5.11(a) and (b)

2) Calibration using again a Uniform rainfall, - i.e. the basin average is input to all precipitation units -, but this time with a basin average P21 computed from up to 21 gauges. Careful comparisons between the 5 gauge and the 21 gauge estimates have shown that the volume differences hardly exceeds 3% .

   However, some sequences are systematically under- or over-estimated by one estimate (an intense cell can be detected by the 21 gauge network while not by the 5 gauge one, or one of the gauges of the 5 gauge network can be struck by an intense but local cell, that is overweighted in the averaging). Anyway, just by changing the input by this better estimate, and although it remains uniform, the performances of the model, were significantly increased, by 4 to 5 % see Figure 3.5.12 (a) and (b).

3) Before providing the semidistributed model with a spatially varying rainfall, this spatial variability has been tested, and confirmed, showing commonly a factor of 3 between simultaneous average rainfalls computed respectively over those 9 subdivisions 6 to 8 km2 wide. see Figure 3.5.10 (b).

4) Nevertheless, once this distributed rainfall is input into the model, this one responds only by small secondary peaks to such spatial variability. Such peaks are usually an order of magnitude smaller than the bulk of the hydrograph.

In this case different routing procedures have been tested, to avoid the dampening of potential effects through a too crude routing. Therefore, the isochrone routing of the river network has been combined with a calibrated hillslope transfer function, to represent the routing over the hillslope prior to the channel transfer.

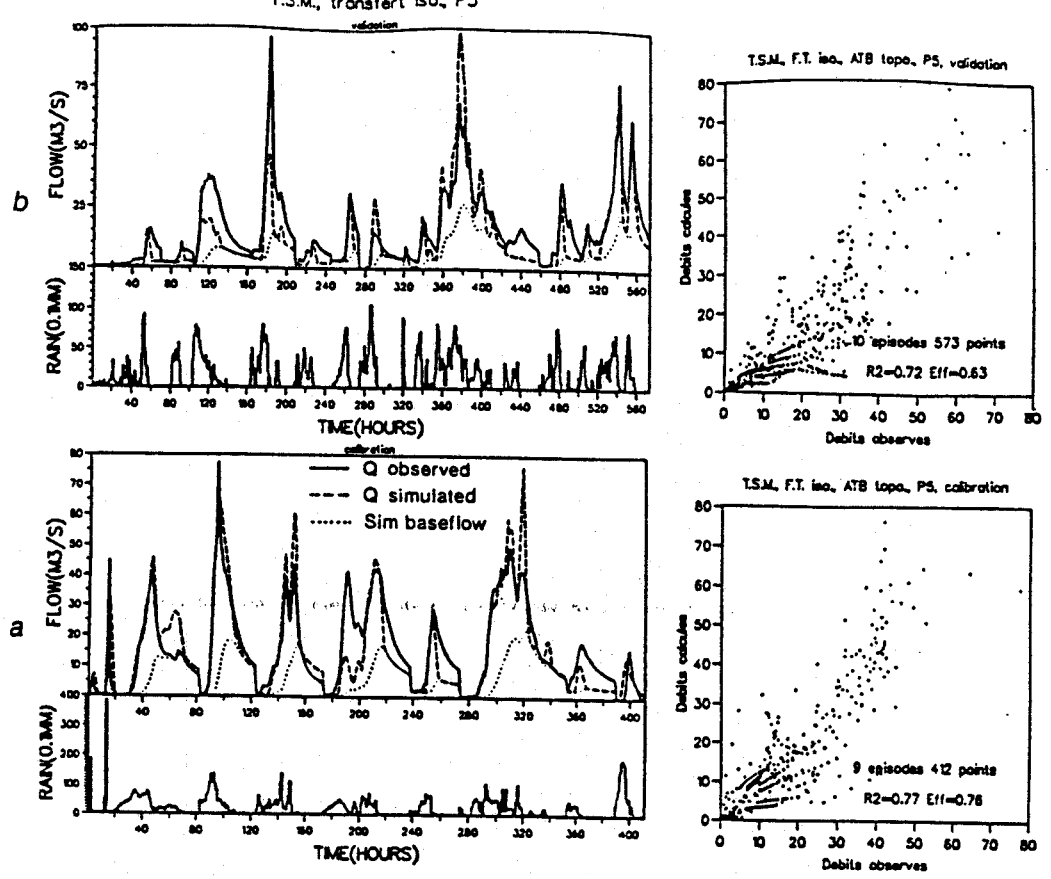

Figure 3.5.11 - Simulation results (Calibration and Validation) with uniform rainfall input using the 5 gauge estimated rainfall P5

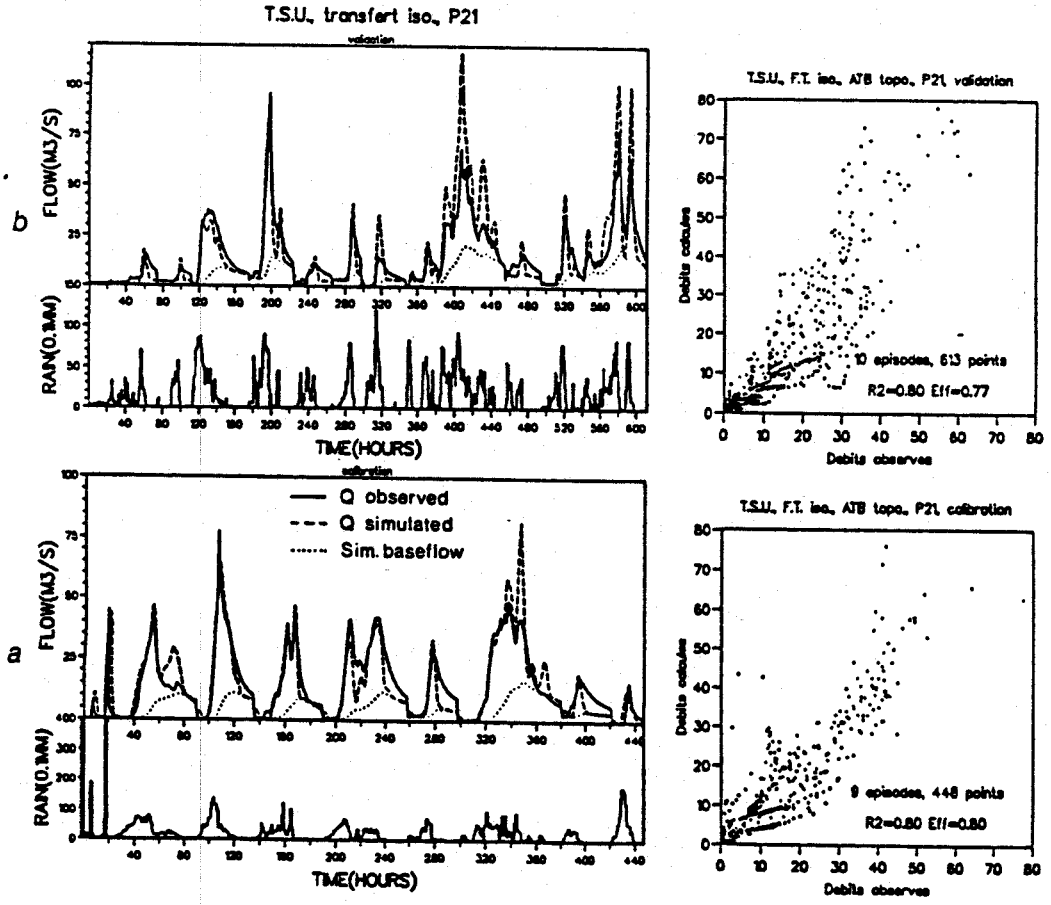

Figure 3.5.12 - Simulation results (Calibration and Validation) with uniform rainfall input using the 21 gauge estimated rainfall P21

However, although often present in the computed hydrographs, such secondary peaks are much less frequent, although sometimes present, in the observed discharges. This means that the model itself is still overreactive to the effect of spatial rainfall variability, as compared to the actual system.

An extensive discussion has considered if these results were dependent on the model or not, or on the setting up of the numerical experiment.

In fact, it seems that the spatial variability of rainfall, although effective, is not enough organised in time and space to avoid smoothing and dampening when fallin on this medium-sized rural catchment.

Said otherwise, given the time response of the catchment, a time step of half to 1 hour seems appropriate. With such time step, the rainsystem usually covers the whole of the catchment, although this rainsystem has definitely large internal space variability, even at the scale of 9 km^2 units. But this variability is not organised strongly enough in space nor time, i.e. patterns do not last long enough to avoid being homogenised by the catchment.

The fact that the model used (TOPMODEL) proves still too reactive to spatial variability may be due to its assumption of a simple averaged soil structure. In the real world, the spatial variability of the soil and landcover may contribute still further to destroy the structure of overland flow potentially imposed by the rainpattern.This explanation for this dampening effect may be followed also when considering the runoff generating mechanism:

- if the overland flow is limited to the saturated contributing areas only, themselves restricted to narrow zones around the channel network, then the possible effect of rainfall variability on quick overland flow would be restricted to those limited zones only,

- if an important part of the floodflow has transited through the soil (temporary aquifers, etc..), then it is quite obvious that the quickly time-varying patterns of the rainfall can easily be rubbed out from the resulting interflow.

Such results may hold only for such small to medium sized rural basins. In fact, they are usually subjected to a complete wetting of the catchment by the rainsystem, even if they demonstrate then a dampening capacity sufficient to rub out its internal spatial variability.

Larger catchments could be sensitive not more to the internal variability of the rainsystems, but to the fact that some parts of the catchment are rain striken while others are not.

This has been tested through a third step, by trying to introduce rainfall variability in a lumped way into the lumped models. The idea was to use, concurrently with the uniform basin averaged rainfall, an index of spatial variability over the basin.

Several indexes have been conceived and tested, working either additively or multiplicatively over the excess rainfall computed from the uniform gross rainfall.

In a nutshell, the best index consists of a factor expressing both:

- whether the intense part (-above a threshold-) of the rainsystem is concentrated in area or spread
- and if the volume above threshold departs significantly or not from the average rainfall.

This index enters in a factor that respectively increases or decreases the production of excess rainfall computed from the uniform gross rainfall, depending on whether the rainfall is more or less concentrated.

It has been observed that with hourly data, this index causes no or little increase in performances on the Réal Collobrier data (71 km^2), while causing a significant increase (up to 10% in Nash efficiency) over the Gardon d'Anduze simulations (545 km^2), where previous studies had shown that the catchment is less often concerned globally by the hourly rainfall patterns.

The transition between these two types of functionning depends on the relative size of the basin as compared to the rainsystem extension at the time-step considered. It seems to lay around a size between 50 to 500 km^2, depending on the network structure and reactivity (response time, influencing the appropriate timestep) of the basin.

Another concern comes from the network structure of the basin itself. Usually, when the basin is reasonnably elongated to allow the main river to remain dominant compared with each tributary, a lumped treatment seems sufficient. Conversely, when at some points of interest, the river originates from the merging of two or more branches rather similar in size, then these subbasins must be treated separately, since they can react very differently to the same rainsystem.

Summary

This work still leaves open the concern of rainfall variability effects, but sheds some light on the scale at which they should be looked for. The large scale pattern (something as crude as a yes/no rainfall variable), is probably more effective on runoff, and easier to get from radar imagery for example, than the detailed, chaotic, spatial variability inside the rainsystem. This last one is more difficult to monitor and very likely dampened by the catchment processes at the scales considered for rurual hydrology.

The most significant improvements have been obtained by increasing the accuracy of the estimate of the basin average rainfall. Since the crudest one was based on a density of one gauge per 14 km^2 (5 gauges for 71 km^2) which is already far beyond current operational densities, such improvements in the input are more likely expected from multisensor estimates, like radar plus raingauges.

3.6 INTERIM CONCLUSIONS

The conclusions that may be drawn from the AFORISM study, insofar as they apply to the modelling of the rainfall-runoff relationship, are relevant to three major open questions. The first one relates to the physical representativeness of the presently available conceptual models; the second one concerns the validity of using spatially averaged precipitation measures at sub-catchement scale, given a specific rain-gauge network, as input to semi-distributed rainfall-runoff conceptual models and the third one poses the problem of the future research lines aiming at improving the models physical interpretation without losing their overall simplicity of use.

From the tests executed during the study, substantiated by experimental evidence, it emerged that although TOPMODEL seems to explain the physical behaviour at the hill-slope scale, its extention at the catchment scale fails to produce a unique solution. It was proven in fact (Franchini et al., 1996), that alternative topographic index curves can produce practically the same discharge estimates, by adjusting the model parameters, but the surface and subsurface components produced by the model can be extremely different. In addition the saturated permeability parameter is scale dependent, due to the unrealistic assumption that the steady state can be reached immediately.

Therefore it was concluded that, when applied to problems at catchment scale, both the TOPMODEL and the ARNO model must be considered as reasonably good conceptual models, with parameters to be estimated from rainfall and runoff data, but where the real physical behaviour is only preserved on average.

From the study it also appeared that the routing component needed in the rainfall-runoff models is the one that poses less problems and which can be reasonably well represented by linear transfer functions derived either by the FDTF-ERHUDIT approach or as the response to a linear convective-diffusion model based upon the parabolic simplification of the De Saint Venant equations (Todini, 1996).

With respect to the second question, i.e. the use of average rainfall over the different sub-catchments when using a semi-distributed representation of the catchment, instead of a distributed modelling approach, it must be said when dealing with floods, that a complete distributed approach is not really economical, more because of data and calibration requirements than of compute time consumption.

Further studies have definitely to be conducted in this domain, but it is reasonable to assume that a catchment subdivision in units of the order of magnitude of 200-300 km^2, is at present, the best choice.

Finally, experiments conducted at UNIBO showed that the possibility exists of developing a representation of the physical processes lumped at catchment or at sub-catchment scales. Although much work is still needed in order to validate the hypotheses on the TOPKAPI parametrization, a number of points can already be reasonably established, allowing the problem, of extending the high non-linearities inherent in the unsaturated soil horizontal flow phenomena to larger scales, to be

overcome.

The first hypothesis addresses the reasonableness of lumping the horizontal flow hydraulic conveyance characteristics in the vertical dimension and relating them to the total soil moisture content.

The second is the possibility of using a unique partial differential model (the kinematic model) from the micro scale to that of the hillslope and beyond, in order to derive a non linear reservoir type model, also valid at catchment scale.

In addition, although it may well be that the present assumptions, made in order to extend the validity of the point model to larger scales, will have to be modified after verification with real world data, nevertheless it has been shown that:

1) the concentration time is an important characteristic to be preserved in the model in order to guarantee the physical meaning of the parameters;

2) a physically meaningful characteristic index must include not only the soil properties and the topography, but also the topological connection among the meshes (a well known principle in the derivation of the Geomorphological Unit Hydrograph);

3) the kinematic wave model is one of the most appropriate schemes to study the horizontal flow on the surface slopes of the catchments but also in the unsaturated zone.

Finally it is hoped that experimental work will be carried out in order to verify and validate the assumptions made. In particular the assumption of the space invariance of the specific yield, which although certainly more realistic than the steady state assumption of the TOPMODEL, should still be verified and if necessarily improved.

REFERENCES

Abbott, M.B., Bathurst, J.C., Cunge, J.A., O'Connell, P.E. and Rasmussen, J., 1986. An introduction to the European Hydrological System - Système Hydrologique Européen, 'SHE', 1. History and phylosophy of a physically-based, distributed modelling system. J. Hydrol., 87:61-77.

Benning, R.G., 1994. Towards a New Lumped Parameterization at Catchment Scale. Umpublished M. Sc. Thesis, Wagenningen Agricultural University.

Bernier, P.Y., 1985. Variable source areas and storm-flow generation: an update of the concept and a simulation effort. J. Hydrol., 79: 195-213.

Beven K.J. & Kirkby M. J., 1979. A physically based variable contributing area model of basin hydrology Hydrol. Sci. Bull., vol 24 (1), pp. 43-69

Beven, K.J., 1981. Kinematic subsurface stormflow, Water Resour. Res., Vol. 17 no. 5, pp. 1419-1424.

Beven, K.J., 1982. On subsurface stormflow: Predictions with simple kinematic theory for saturated and unsaturated flows, Water Resour. Res., Vol. 18 no. 6, pp. 1627-1633.

Beven, K.J. and P. Germann, 1982. Macropores and water flow in soils, Water Resour. Res., Vol. 18, no. 5, pp. 1311-1325.

Beven, K.J. and Wood, E.F., 1983. Catchment geomorphology and the dynamic of runoff contributing areas. J. Hydrol., 65: 139-158.

Beven, K.J., 1986. Runoff production and flood frequency in catchments of order n: an alternative approach. In: Gupta et al. (Editors) Scale problems in Hydrology, Reidel Publishing Company, Dordrecht, pp. 107-131.

Beven K.J., Wood E.F., Sivapalan M., 1988. On hydrological heterogeneity-catchment morphology and catchment response. J. Hydrol. 100, 353-375.

Beven, K.J., 1989a. Changing ideas in hydrology - The case of physically-based

models. J. Hydrol., 105: 157-172.

Beven, K.J., 1989b. Interflow. In: Morel-Seytoux (Editor), Unsaturated flow in hydrologic modeling. Theory and practice, NATO ASI, Series C, Vol. 275: 191-221, Kluwer Academic Publishers, Dordrecht.

Beven, K. and Binley, A.M., 1992. The future of Distributed Models: Model Calibration and Uncertainty Prediction. Hydrol. Processes, 6:279-298.

Binley, A., Egly, J. and Beven, K.J., 1989. A physically-based model of heterogeneous hillslopes, 1. Runoff production, 2. Effective Hydraulic Conductivities. Water Resour. Res., 25: 1219-1233.

Borah, D.K., S.N. Prasad and C.V. Alonso, 1980. Kinematic wave routing incorporating shock fitting, Water Resour. Res. Vol. 16, no. 3, pp. 529-541.

Brooks, R.H. and A.T. Corey, 1964. Hydraulic properties of porous media, Hydrol. Pap. 3, Colo. State Univ., Fort Collins.

Calder I.R., 1990. Evaporation in the Uplands J. Wiley ed. Chichester U.K. , 148 p.

Charbeneau, R.J., 1984. Kinematic models for soil moisture and solute transport, Water Resour. Res., Vol. 20, no. 6, pp. 699-706.

Chiew, F.H.S., Stewardson, McMahon, T.A., 1993. Comparison of six rainfall-runoff modelling approaches. J. Hydrol., 147: 1-36.

Christophersen, N., Neal, C., Hooper, R.P., Vogt, R.D. and Andersen, S., 1990. Modelling streamwater chemistry as a mixture of soilwater end-members - a step towards second-generation acidification models. J. Hydrol., 116:307-320.

Cordova J.R., Rodriguez-Iturbe I., 1983 Geomorphologic estimation of extreme flow probabilities , J. Hydrol., 65: 159-173.

Doorembos J., Pruitt W.O., Aboukhaled A., Damagnez J., Dastane N.G., Van Den Berg C., Rijtema p.e., Ashford O.M., Frere M.,1984. Guidelines for Predicting Crop Water Requirements - FAO - Irrigation and Drainage Paper n. 24.

Dunne, T. and Black, R.D., 1970. Partial area contributions to storm runoff in a small New England watershed. Water Resour. Res., 6: 1296-1311.

Dunne, T., 1978. Field studies of hillslope flow processes. In: Kirkby, M.J. (Editor), Hillslope hydrology, John Wiley, New York, pp. 227-293.

Durand P., Robson A., Colin N., 1993. Modelling the hydrology of submediterranean montane catchments (Mont-Lozère, France) using TOPMODEL: initial results, J. Hydrol, 139: 1-14.

Eagleson, P.S., 1970. Dynamic Hydrology, McGraw-Hill, New York.

Franchini M., Todini E., 1988. BAPL: A parabolic and backwater scheme with lateral inflow and outflow. Proc. Fifth IAHR International Symposium on Stochastic Hydraulics, Birmingham.

Franchini, M. and Pacciani, M., 1991. Comparative analysis of several conceptual rainfall-runoff models. J. Hydrol., 122:161-219.

Franchini M., Wendling J., Obled Ch, .Todini E., 1996. Physical interpretation and sensitivity analysis of the TOPMODEL, J. of Hydrol., 175.

Freeze, R.A., 1972a. Role of subsurface flow in generating surface runoff, 1. Baseflow contributions to channel flow. Water Resour. Res., 8 (6): 609-623.

Freeze, R.A., 1972b. Role of subsurface flow in generating surface runoff, 2, Upstream source areas, Water Resour. Res., 8 (6), 1272-1283.

Gresillon J.M., J.M. Neyret-Jigot, F. Lemeillour, and Ch. Obled, 1994. Colloque de Nîmes.

Henderson, F.M., R.A. Wooding, 1964. Overland flow and groundwater flow from a steady rainfall of finite duration, Journal of Geophysical Research, Vol. 69, no. 6 pp. 1531-1540.

Horton, R.E., 1933. The role of infiltration in the hydrologic cycle. Trans. Am. Geophys. Union, Vol. 14, pp. 446-460.

Hurley, D.G. and G. Pantelis, 1985. Unsaturated and saturated flow through a thin porous layer on a hillslope, Water Resour. Res., Vol. 21, no. 6, pp. 821-824.

Iorgulescu, I., Jordan, J.-P., 1994. Validation of TOPMODEL on a small Swiss catchment. J. Hydrol, 159: 255-273.

Iorgulescu, I., Mouillère, D. and Musy, A., 1994. Investigation of stormflow generation mechanisms in a small Swiss catchment using environmental tracing. EGS General Assembly, Grenoble april 1994. Abstracted in Annalae Geophysicae, Vol.12 p.C343.

Jordan, J.-P., 1992. Identification et modélisation des processus de génération des crues.(in French, with English abstract), Ph. D. thesis, Swiss Institute of Technology, Lausanne.

Jordan, J.-P., Iorgulescu, I., 1992. Problèmes d'échelle dans les relations pluie-débit d'un petit bassin versant. In: Carbonnel, J.P. et al.: Rencontres Hydrologiques Franco-Roumaines. UNESCO, Paris, pp 355-362.

Jordan, J.-P., 1994a. Spatial and temporal variability of stormflow generation processes on a Swiss catchment. J.Hydrol, 153: 357-382.

Jordan, J.-P., 1994b. Bassin de recherche et modélisation des processus de formation des crues, proposition d'une approche couplée. La houille Blanche, no3-1994, p15-22.

Kelliher F.M., .Witehead D., and Pollock D.S. , 1992. Rainfall interception by trees and slash in a young Pinus radiata D.Don stand, J. of Hydrol., 131, pp. 187-204

Keulegan, G.H., 1945. Spatially varied discharge over a sloping plane. Amer. Geophys. Union Trans. Part 6, pp. 956-959.

Kirkby, M.J. and Chorley, R.J., 1967. Throughflow, overland flow and erosion. Int. Assoc. Sci. Hydrology Bull., 10, no.3: 5-21.

Krajewski F. W., Lakshmi V., Georgakakos K. P., & Subhash C. J., 1991. "A Monte Carlo study of rainfall sampling effect on a distributed catchment model" Water

Ressour. Res., Vol. 27, n°1, pp. 119-128

Lighthill, F.R.S. and G.B. Whitham, 1955. On kinematic waves, I, Flood measurements in long rivers. Proc. Royal Soc. of Londen, A, 229, pp. 281-316.

Moore, R.J., and Clarke, R.T., 1981 A Distribution Function Approach to Rainfall-Runoff Modelling, Water Resources. 17, no. 5, pp. 1367-1382.

Moore R.J., 1985. The probability-distributed principle and runoff production at point and basin scales, Hydrological Sciences Journal, Vol. 30, no. 2, pp. 273-297.

Naden, P.S., 1992. Spatial variability in flood estimation for large catchments: the exploitation of channel network structure. J. Hydrological Sciences, 37,1,2:53-71.

Nash, J.E. 1958 The form of the instantaneous unit hydrograph, IUGG General Assembly of Toronto, Vol. III, Publ. N. 45 - IAHS, Gentbrugge, pp. 114-121.

Nash, J.E. and Sutcliffe, J.V., 1970. River flow forecasting through conceptual models. Part 1 - a discussion of principles. J. Hydrol., 10: 282-290.

Niemczynowicz J., 1987. "Storm tracking using raingauge data", J. of Hydrol., 93, pp. 135-152.

O'Connell, P.E., 1991. A Historical Perspective. In: Recent Advances in the Modeling of Hydrologic Systems, ed. Bowles, D.S. et O'Connell, P.E., NATO ASI Series, 667p.

Obled Ch., 1989. Reflexions on Rainfall Information Requirements for Operational Rainfall-Runoff Modelling. Internat. Symp., Univ. of Salford(UK), Aug. 1989, published by I.D. Cluckie and C.G. Collier (1991) in " Hydrological Applications of Weather Radar", Ellis Horwood ed., pp. 469-482

Obled Ch. and Wendling J., 1991. Development of TOPMODEL: applications to Mediterranean catchments. Role of rainfall spatial variability and further simplifications for operational use. Technical Report TR n°89 CRES Center for Research on Environmental Systems - University of Lancaster 300p.

Ogunkoya, O.O. and Jenkins, A., 1993. Analysis of storm hydrograph and flow

pathways using a three-component hydrograph separation model. J. Hydrol., 142: 71-88.

Philip J.R., 1957. The theory of infiltration 1-7. Soil Sci., Vols. 83, 84 and 85.

Quinn, P., Beven, K.J., Chevallier, P. and Planchon, O., 1991. The prediction of hillslope flow paths for distributed hydrological modelling using terrain models. Hydrological Processes, 5: 59-79.

Quinn, P., Beven, K.J., Morris, D. and Moore, R., 1991. The use of Digital Terrain Data in Modelling the Response of Hillslopes and Headwaters, Internal technical report, University of Lancaster.

Rutter, A.J., Kershaw, K.A., Robins, P.C. E Marton, A.J., 1971; A predictive model of rainfall interception in forests. I:Derivation of the model from observations in a plantation of Corsican Pine , Agric. Met., 9, 367p.

Rutter , A.J., Marton, A.J. E Robins, P.C. , 1975; A predictive model of rainfall interception in forests. II:Generalisation of the model and comparison with observations in some coniferous and hardwood stands , J. Appl. Ecol. 12, 367p.

Shuttleworth , W.J. 1979 Evaporation, Institute of Hydrology report n. 56.Wallingford.

Sivapalan M., K. Beven, E.F. Wood, 1987. On Hydrologic Similartiy. 2. A Scaled Model of Storm Runoff Production, Water Resour. Res., Vol.23, n.12 2266-2278.

Sloan, G.P., I.D. Moore, 1984. Modelling subsurface stormflow on steeply sloping forested watersheds, Water Resour. Res., Vol. 20, no. 12, pp. 1815-1822.

Sorooshian, S. and Gupta, V.K., 1983. Automatic calibration of conceptual rainfall-runoff models: The question of parameter observability and uniqueness. Water Resour. Res., 19: 260-268

Sorooshian, S., Gupta, V.K. and Fulton, J.L., 1983. Evaluation of maximum likelihood estimation techniques for conceptual rainfall-runoff models: Influence of calibration data variability and length on model credibility. Water Resour. Res. 19: 251-259.

Stagnitti, F., M.B. Parlange, T.S. Steenhuis and J.-Y. Parlange, 1986. Drainage from a uniform soil layer on a hillslope, Water Resour. Res., Vol. 22, no. 5, pp. 631-634.

Steenhuis, T.S., J.-Y. Parlange, M.B. Parlange and F. Stagnetti, 1988. A simple model for flow on hillslopes, Agric. Water Manage., 14, pp. 153-168.

Stephenson, D. and M.E. Meadows, 1986. Kinematic Hydrology and Modeling, Developments in Water Science 26, Elsevier, Amsterdam.

Tarantola, A., 1987. Inverse problem theory. 613 pp. Elsevier Science Publishers, Amsterdam, The Netherlands.

Todini E., Bossi A., 1986. PAB (Parabolic And Backwater) an unconditionally stable flood routing scheme particularly suited for real time forecasting and control, J. of Hydraulic Res. Vol.24, n.5 pp.405-424.

Todini, E., 1988. Rainfall-runoff modeling- Past, present and future. J. Hydrol., 100: 341-352.

Todini, E. 1995 New Trends in Modelling Soil Processes from Hillslope to GCM Scales, in H.R. Oliver and S.A. Oliver (Eds.) "The Role of Water and the Hydrological Cycle in Global Change", Springer.

Todini, E., 1996. The ARNO Rainfall-Runoff Model. Journal of Hydrology, n. 175.

Van Genuchten, M.Th., 1980. A closed-form for predicting the hydraulic conductivity of unsaturated soils, Soil Sci. Soc. Am. J. no. 44, pp. 892-898.

Wendling, J., 1992. Modélisation pluie débit: comparison d'approaches conceptualles/physicodéterministes, globales/semi-distributées. Essai de prise en compte de la variablité spatiale des pluies. (Application au bassin versnat du Réal Collobrier). Institut National Polytechnique de Grenoble.

WMO 1975, "Intercomparison of Conceptual Models used in Operational Hydrological Forecasting"; OHR n. 7; WMO n. 429.

Wood F.E, Sivapalan M., Beven K., Band L., 1988. "Effects of Spatial Variability and scale with implications to Hydrologic modeling", Journal of Hydrology, n.102.

Woolhiser, D.A. and J.A. Ligget, 1967. Unsteady one-dimensional flow over a plane - The rising hydrograph. Water Resour. Res., Vol., 3 no. 3, pp. 753-771.

Zhao , R.J. 1977 Flood forecasting method for humid regions of China, East China College of Hydraulic Engineering, Nanjing, China.

Zhao , R.J., 1984, Watershed Hydrological Modelling, Water Resources and Electric Power Press, Beijing.

4. RAINFALL-RUNOFF MODELLING: OPERATIONAL USE

4.1 INTRODUCTION

The use of rainfall runoff models in an operational context differs markedly from the way they are seen in the research environment in which these models were developed. Todini (1988) classifies rainfall runoff models in three categories: research models, engineering purpose models and operational models.

Operational models are those that will not be used by the scientists, engineers nor the highly skilled personnel that developed the models and the associated computer programs. Therefore it is essential that a variety of error traps, complexity controls and problem solving routines be added to the experimental code in order to convert what might be consider by the designers to be a simple computer program, into a highly reliable, understandable and friendly operational tool.

In addition, operational flood forecasting requires a real-time data acquisition system (rainfall, water levels, air temperature etc.) the nature of which may heavily condition the type of models to be used. There may also be a need to calculate initial soil moisture conditions, which may be simple for continuous type models, but quite complex for event based ones. Calibration is another problem to be addressed. When first establishing an operational real time flood forecasting system, the real-time data acquisition system is usually not yet established, so the initial calibration depends on the availability of historical data, which is frequently based on a different measurement network and time base than the one under development.

Experience shows that at least three calibrations of a model is needed before releasing it as an "operational" real time flood forecasting system: the first is generally based upon the historical data; the second is based upon the data collected after the first year of operation (taking into account the fact that during the first year the system is under test and several data acquired in real time may be missing or corrupt); the final calibration will be done after at least two or three years of operation.

Even when using highly reliable data acquisition systems, one must anticipate that a given percentage of data will be lost for a number of reasons, for example as a consequence of

the failure of a reporting station due to lack of power, lightning or just bad transmission. Telephone cable transmissions are in general less efficient than radio transmissions due to the time taken by their communication protocol; this increases the probability of failure so one should allow for a 10% failure rate in telephone communications and a 2% failure rate in radio links. In any case an automatic procedure for checking and reconstructing missing data is a must in any operational real time flood forecasting system.

A description of the studies carried out within the frame of AFORISM by the different groups in order to convert a simple program into an operational tool is given in the sequel.

4.2 REAL-TIME REQUIREMENTS: MODEL SELECTION, MODEL CALIBRATION AND INITIAL CONDITIONS

4.2.1 Model selection: continuous versus event-based models

The choice of the rainfall-runoff model to be used in real time flood forecasting systems basically depends on the nature of the problem, on the end user needs and on the structure of the available data acquisition system.

With respect to the nature of the problem, as a minimum requirement the rainfall runoff model must essentially contain two basic components: a water production function and a transfer function. The water production function gives the amount of surface runoff to be successively routed, along the slopes and along the drainage system to the outlet, by means of the routing component. Unfortunately most of the problems encountered in practice are not so simple: a groundwater component is generally required as well as a snow accumulation and melting component. Routing can also be performed with a unique transfer function for the whole basin (this is generally true for small basins) or several sub-catchments must be combined in what is known in the literature as a semi-distributed conceptual model. Although a model was finally selected for the Reno river case study (Chapter 7), it was not the purpose of AFORISM to suggest a specific model as the best possible choice, but rather to point out problems that may be encountered when using the different types of models.

If an automatic data acquisition system is available which acquires data at fixed time intervals which are sufficiently short when compared to the rainfall-runoff process dynamics (30' - 1h - 3h), then a continuous model may be used which obviates the need for the estimation of the initial soil conditions. Alternatively an event type model can be implemented, provided that a procedure for establishing the initial soil moisture conditions is also available.

The reason for this constraint is due to the large amount of water that can be stored in the soil when compared to the rain totals: a rain total of 300 mm over a catchment is a quantity that may produce a large flood, fortunately the soil moisture storage may account for values ranging from 50 to 350 mm. Therefore, when the soil is mostly dry a large portion of rain will infiltrate in the soil and the flood at the outlet of the catchment will be markedly reduced; when the soil is mostly wet the rain will rapidly reach the drainage network and a larger flood will be observed.

As a consequence the selection of models should be made according to the following rules: whenever possible use a continuous soil moisture accounting model, given the automatic estimation of the initial soil moisture conditions; alternatively use an event type model, provided that a reliable technique to establish the initial soil moisture conditions is incorporated into the system.

4.2.2 Model simplification

This section presents the work of INPG-LTHE with regard to the second part of the modelling process, i.e. the development of the production function part. In Unit Hydrograph (UH) terminology, the transfer function or UH performs the routing of water, while the soil moisture accounting part of the model is performed by a loss or production function.

In the exploratory work of the INPG-LTHE presented in Section 3.4.2, it has been shown that a model based on the variable contributing area concept such as TOPMODEL was acceptable for Mediterranean catchments, and that a lumped version captured most of the model efficiency. Fully distributed approaches have not shown better performance than simpler lumped ones. This was clear not only on the test basin, but also in other

partners' test cases (SHE on the Mentue basin) or in the literature (Loague and Freeze, 1985).

Starting from the semi-distributed version of TOPMODEL made available to INPG-LTHE by Lancaster University, and from the modified lumped versions developed in Obled and Wendling (1991), a simplified version, called TOPSIMPL, has been derived that tries to fit most data situations encountered in operational works and to stick to minimum requirements currently requested in operational applications (namely a lumped model structure, operating per event, with minimum data inputs).

First, it has been seen (Sections 3.4.2 and 3.4.3), that the derivation of the actual topographic index distribution curve provided only part of the solution since the model was not very sensitive to the one specific to the basin. In fact, this topographic index should be combined with a soil transmissivity pattern which is generally unknown. Numerical effects caused by the size of the DTM still bring the physical meaning further away. So it has been accepted that all these effects could be conceptualised by assuming the topographic index is distributed as a two-parameter Gamma function of fixed origin fitted by calibration. Furthermore, as only its tail part was commonly used, a one parameter exponential curve is even optionally proposed.

Second, when running the model per event, there is no need for a detailed evapotranspiration routine since the water has not to be withdrawn deep within the soil. So, an interception loss is considered, that has been taken as a constant parameter (range 0.1 to 0.5 mm/h) which in fact holds both for evaporation losses or for some bias in precipitation measurement.

According to the developments and interpretations of the transfer functions, the routing of overland flow is performed either by an externally provided transfer function (typically identified by the FDTF-ERUHDIT approach), or by a calibrated Gamma function. The baseflow is either pooled with overland flow or routed according to a set of isochrones.

This complete modelling "chain" (FDTF-ERUHDIT + TOPSIMPL) has been applied "operationally" to our research data sets (Gardons and Réal-Collobrier) but also to two new test basins (the Paillon and the Sieve in Italy), in the following sequence:

(a) identification of the transfer function (and of likely excess rainfall series) by the FDTF=ERUHDIT approach

(b) fitting of simplified TOPMODEL as a loss function in connection with these previous transfer function and excess rainfalls.

It seems that a user with little experience can now perform a reasonably good fitting and testing exercise within three to six months depending on the data quality problems encountered (Imhoff, 1993; Roux, 1993) . This simplified version, TOPSIMPL 1.0 has been programmed for PCs in a menu driven user friendly package under Windows. It has been circulated first for test among some partners, and has now been distributed to about 20 interested correspondents, although the treatment of the Digital Terrain Model is not yet fully completed.

4.2.3 Model Calibration

As with any other model, rainfall runoff models require calibration to be adapted to a specific catchment. Calibration involves a major effort in order to prepare the data required at the space and time scales used in the model. Special attention has to be paid to the time discretization interval which must be chosen at least two or three times smaller than the time to peak, a catchment characteristic time, in order to correctly reproduce the physical behaviour of the processes. In very small catchments a sampling interval of 15 minutes is needed, while for larger catchments (>200 km^2) 1^h is generally a good choice, for very large catchments (>10,000 km^2) also 3^h - 6^h can be chosen, although it is generally more convenient to divide the catchment into sub-catchments, to allow for a better representation of the spatial variability, and then use smaller time sampling intervals (1^h). When dealing with historical data it is essential to carefully verify their validity prior to the calibration phase and to reconstruct missing data.

Apart from data preparation, another issue often discussed by modelers is the way in which calibration should be approached: by physical considerations and trial and error or by automatic optimization techniques. This is an unresolved problem, although each modeler has a different opinion.

For simple and small catchments where data are very well measured, automatic calibration, particularly if guided by physiscal constraints, may be extremely helpful. Unfortunately in larger catchments, when the number of sub-catchments contributing to a gauging station is large, a problem of non-observability occurs, which prevents indiscriminate use of automatic calibration techniques. In addition, output runoff data may be heavily modified by upstream reservoir operations, which would introduce serious inconsistencies, which would result into very poor calibrations.

4.2.3.1 Continuous type models

When dealing with continuous type models, it is necessary to calibrate the models in such a way that the succession of high and low flows is correctly reproduced, together with the overall water balance. The advantage of this type of model lies generally in the better stability of performances moving from a calibration to an operational period, and is partly due to preservation of the overall water balance.

In general only the water production function really needs calibration: the transfer function can easily be determined, following a kinematic or a parabolic flow scheme, using parameters such as diffusivity and convectivity to which a physical meaning can be easily provided (Todini and Bossi, 1986 , Franchini and Pacciani, 1991).

Experience in calibrating rainfall-runoff models can lead to the calibration of large complex catchments in three to six months (including data acquisition, data validation and missing data reconstruction) with explained variances which are in the range of 95% to 98%.

4.2.3.2 Event type models

When a single catchment is considered, there is first a diagnostic phase that can be performed on event data only (event being understood in the wide sense, i.e. rainfall periods separated by long recessions). On these events, a first part will consist in studying the characteristics of the transfers at the basin scale, and a second one will

consider the loss model or production function. Then, a second phase will consider real-time implementation purposes, and address choices like running in event mode or continuous mode, adapting model parameters, initialisation or residuals. These last aspects will be considered later in the report (see Section 4.3), while this Subsection will concentrate on the initial diagnostic phase or identification, and then the time-invariance of the transfer function.

Identifying the transfer function of a basin

Results obtained by the INPG-LTHE research group through several studies within or outside AFORISM led to a strategy for implementing the operational modelling of a given medium-sized watershed. Obviously, this strategy at the scale of a lumped catchment must combine with the splitting into elementary catchments when a large hydrographic system like the Reno or the Arno river system river in Italy, or the upper Garonne in France is to be managed (see conclusions and guidelines in Section 4.4).

Developments will be discussed on an improved transfer function identification approach. It had been partially developed before the project in co-operation with the "Division Technique Générale" of "Electricité de France" (EDF-DTG) (Rodriguez, 1989; Sempere et al., 1992) but has been extensively tested in the frame of the AFORISM project.

It takes up with the assumptions of the Unit Hydrograph model, but has proved to be a powerful tool, both exploratory and operational. The project has allowed finalisation of the FDTF-ERUHDIT method, which has been published in detail in the mean time (Duband et al., 1993). A package developed by EDF-DTG for PCs has been made available to several partners allowing the test both on real data and on synthetically generated data (Nalbantis et al., 1994). Apart from its operational use later on to provide an identified UH for the basins at hand (see Subsection 4.2.3 on TOPSIMPL), the method has also been used for exploratory analysis, where its independence from any a priori imposed loss model proves a guarantee for more objective conclusions. Its main lines are summarised first.

The input rainfalls and output discharges of a multi-event data set are the known data, while the associated excess rainfall and the transfer function ordinates are the two sets of

unknowns in the problem. The method is two-step alternating and iterative: starting from a guess for one set of unknowns, the second one is identified. Then this first identified set is kept fixed while identifying the other one. Then the process is iterated, i.e. the first set is reconsidered, then the second, alternatively until convergence is reached. At this stage the two identified unknown sets, i.e. the deconvoluted excess rainfalls and the identified ordinates of the transfer function, combine at best to approach the observed discharge series. Usually, the gross input rainfalls are used as a first guess for excess rainfalls, They are also used at every iteration step as upper limits in constraints for the excess rainfall values. A more detailed presentation of the method may be found in the references cited above.

This method has been applied to the Rio Alenquer data set (provided by ISA-DER) on which it has allowed to address the problem of the uncertainty on discharge data and its influence on identified transfer function. The main source of uncertainty here was the rating curve relating stage and discharge. Depending on the assumptions selected for extrapolating the rating curve, the higher discharges estimates may be significantly modified, while the average or low ones are unchanged. This situation of uncertainty in the large discharges is common in many basins, but still more in Mediterranean catchments where flood discharges are several orders of magnitude larger than the average flows. This uncertainty induced significant changes on the modelling capacity (e.g. on the transfer function) and on the results (Lardet, 1990).

During the Project, another approach with the same aims as the FDTF-ERUHDIT method (i.e. to identify both transfer function and excess rainfall series from rainfall and discharge series) has been tested. Based on works by De Laine (1970), recently updated by Turner et al. (1989), it relies on the z-Transform of the multi-event discharge series, and on their factorisation. Common terms found in all events are attributed to the transfer function, while terms specific to each separate event are assumed to originate from the excess rainfall input series. In spite of some results consistent with those of the FDTF-ERUHDIT (see figure 4.2.1), the required polynomial root selection algorithm proved too sensitive to data uncertainty to be included as an acceptable identification option (Gouy, 1991).

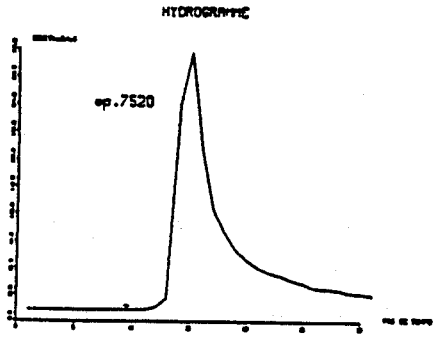

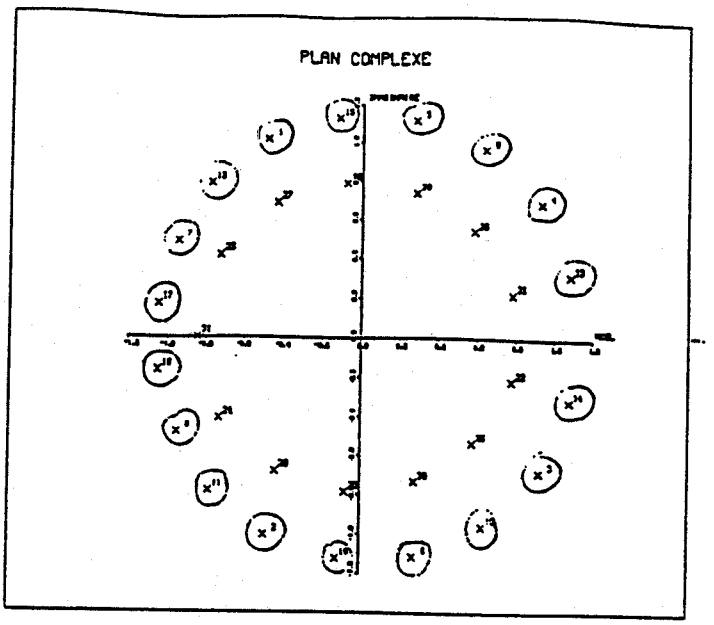

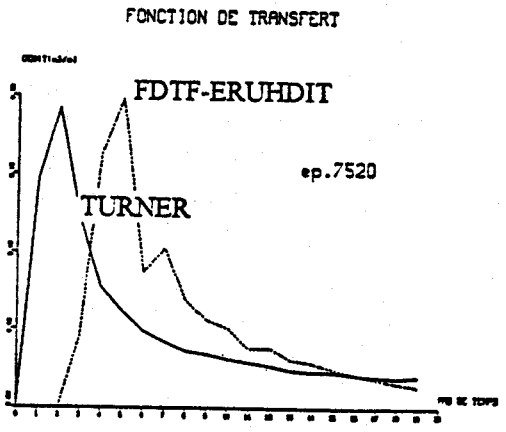

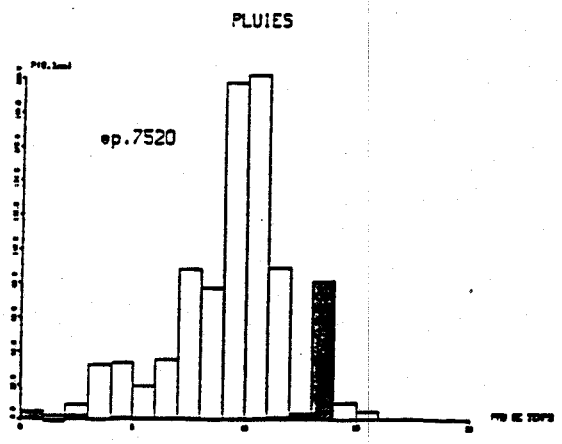

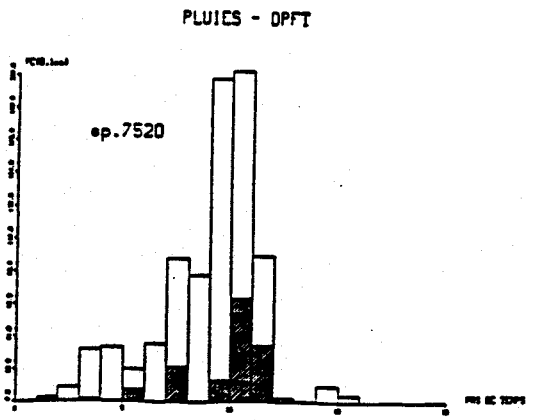

Figure 4.2.1a Successful example of comparison between Transfer Functions identified:
- by the FDTF-ERUHDIT approach on a multi-event data set
- by the Z-transfer method on separate event, from discharge serie only

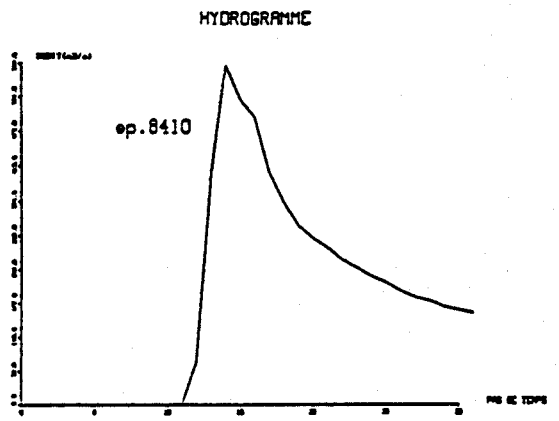

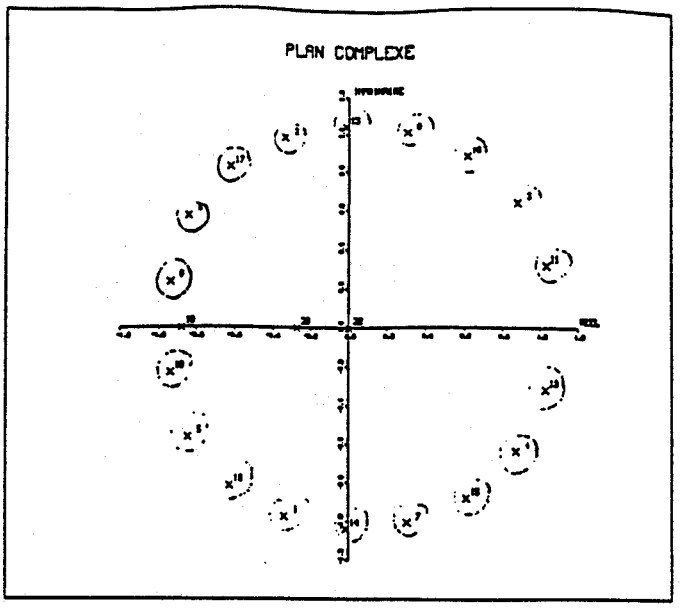

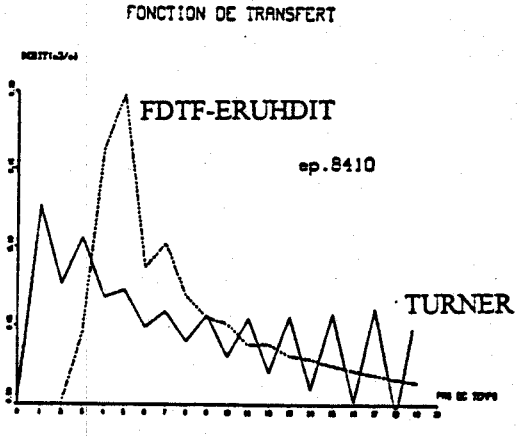

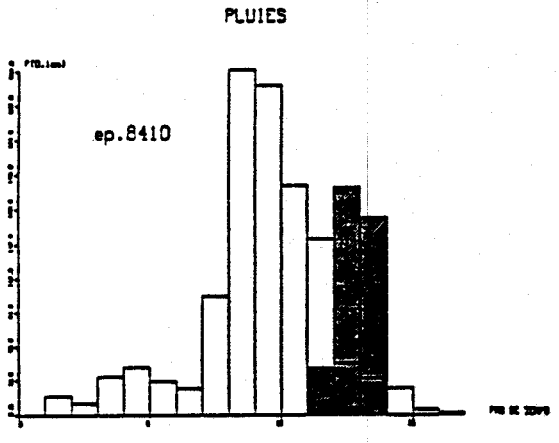

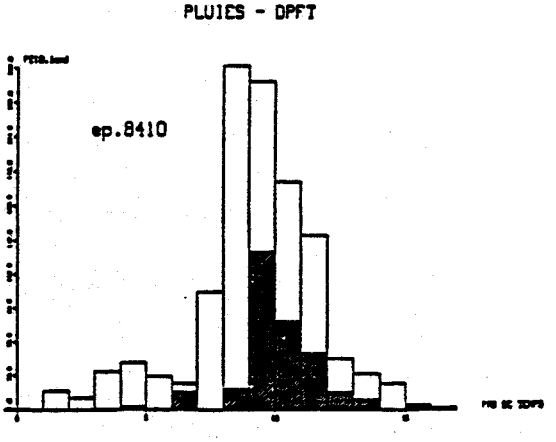

Figure 4.2.1b Failing example of comparison between Transfer Functions identified:
- by the FDTF-ERUHDIT approach on a multi-event data set
- by the Z-transfer method on separate event, from discharge serie only

The consequence is that it seems worthwhile to recommend the use of the FDTF-ERUHDIT methodology in the initial step, in order to identify ordinate by ordinate an average transfer function over the available set of events. This usually allows for detection of inconsistencies in the data set (some floods may be removed accordingly), as well as general shape of the UH, which may well depart from "classical" shapes.

Invariance of the transfer function

An important step in the diagnostic check of the modelling of a basin is to consider the stability of the transfer function as derived above, which is rather critical in lumped modelling. This point was also studied by the INPG-LTHE group and will be illustrated on two different sample cases: the Réal Collobrier (France), and the Sieve (Italy) catchments.

The first test case involves the whole Réal Collobrier catchment (71 km^2) and two of its subcatchments of approximately 9 km^2 each: Les Maurets and Valescure. A partitioning of the 30 available events has been performed to maximise the difference between the identified transfer function of one sample from the others. Several criteria have been used to stratify the data (see Figure 4.2.2). It appears that the best criteria for splitting the initial sample are the following:

(a) the initial discharge in the river, and

(b) the global runoff coefficient of the event, with the following effects (summarised in Figure 4.2.2).

Events with low runoff coefficients (<.2 and averaging.06 on the Maurets) coincide with small initial discharges and show a quick and peaky transfer function. Events with high runoff coefficients (>.2 and .27 on average) coincide with sustained initial discharges and show a long and smooth transfer function.

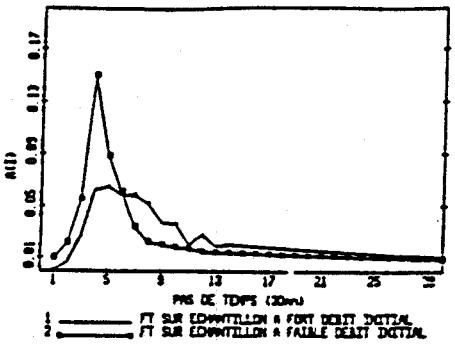

a) according to initial pre-event discharge

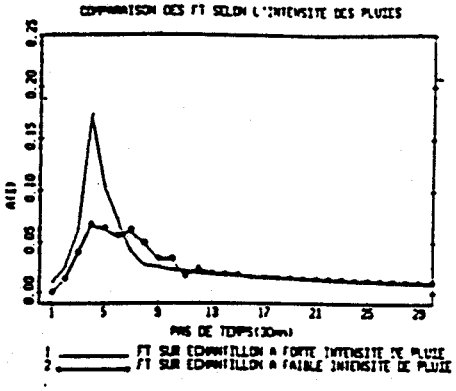

b) according to event maximum rain intensity

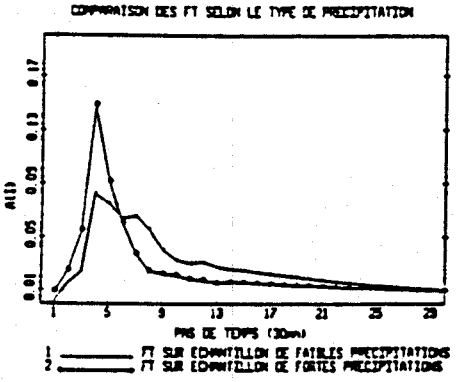

c) according to event rainfall total

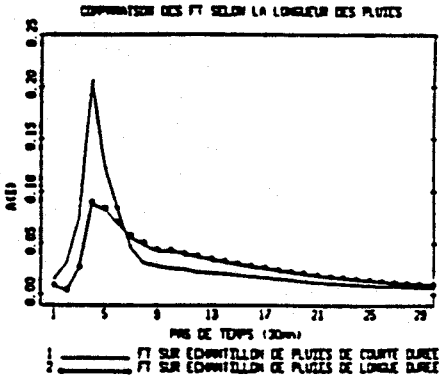

d) according to event rain duration

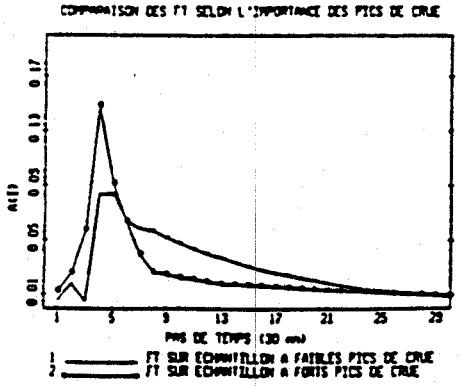

e) according to event maximum discharge

Figure 4.2.2 Stratification of events on the Real Collobrier data set and respective Transfer Functions for each group

This has been interpreted in terms of expanding runoff generating (source) areas, i.e.:

(1) Events with a small initial discharge have a small percentage of antecedent saturated areas, essentially localised close to the river. If an event occurs, then the existing source areas respond quickly to the river network, while the expansion of contributing areas, even if the increase is relatively large, remain limited in absolute terms. The distance for water to travel as overland flow remains proportionally limited as compared to the quicker travel in the channels. Accordingly, the small percentage of saturated area limits the overall coefficient, while the initial discharge is known to be a good index of the initial percentage of saturated area.

(2) Conversely, when initial discharge is large, this means a rather large development of initially saturated areas, and therefore a potential for large runoff coefficient. But this also means increased travel time as overland flow over a very rough soil, and therefore a dampening in the response function. This may look contradictory from an Hortonian viewpoint, where the increase in initial wetness or runoff coefficient is essentially interpreted as an increase in water depth and therefore in travel speed of overland flow, thus causing an acceleration in the response function.

If these observations appear to be contradictory in the Hortonian framework, they can be interpreted very consistently assuming contributing areas extension as the dominant process. From this viewpoint, there is an increase in the distance to the channel which explains a dampened response at the outlet. In the literature, it is commonly accepted that average channel flow is in the range of a few m/s, while hillslope flow is in the range of a few cm/s, i.e. two orders of magnitude smaller. Therefore there is competition between increase in channel speed (and channel extension), and contributing area extension on hillslopes. The overall result in terms of travel time to the outlet may therefore depend on the particular shape and geomorphology of each catchment (See also guidelines in the conclusions in Section 4.4).

The second test case involved the Sieve catchment, (840 km^2). A partitioning into three classes has been performed, based this time on peak discharges (50 to 150 m^3/s, 150 to 300 m^3/s, and larger than 300 m^3/s). This splitting is again reasonably consistent with a ranking by runoff coefficients.

Figure 4.2.3 shows the evolution of each transfer function along the iteration within the FDTF-ERUHDIT approach. Effects that are similar to those of Réal-Collobrier case are detected, showing a transfer function less peaky and delayed by almost 2 hours when moving from the first to the second group. But the third group shows a recovering in response time, which becomes even shorter than in the first group. This is probably due to the competition between channel and hillslope processes, and therefore, extensive studies of the saturated zones and rainfall spatial distribution are needed to understand this in detail.

Conclusions about this transfer function approach are:

(1) In spite of the wide range of observed peak discharges, an average invariant transfer function may usually be selected, and this seems to hold still better for large catchments than small ones, probably because the various influences are smoothed by integration into the resulting transfer function. Given other possible sources of error, it still remains a good operational tool for forecasting within the range of currently encountered floods (ten years return period and probably up to 100 years).

(2) This apparent invariance is, however, likely to result from counteracting influences (Gresillon et al., 1994). Some variability is definitely present, and this requires a specific checking on every catchment to be processed. As long as the available sample of events allows partitioning in subsets of around ten events, the FDTF-ERUHDIT method allows for easy exploratory analysis, before an eventually unique transfer function is selected for operational use.

Note that in large basins, the competition between hillslope and channel processes may also include the dynamics and localisation of rainfall patterns. Nevertheless, strong stiffening of transfer functions (as sometimes suggested by some design flood methods) have not been encountered in our test cases, as long as the rain event was reasonably spread over the basin considered.

In practice, only one transfer function will usually be retained for use, but the results of analyses outlined above will weight our confidence as to its time invariance and uniqueness. In a few cases, trials have also been performed to introduce some variability into the shape of this transfer function, indexed by the discharge values.

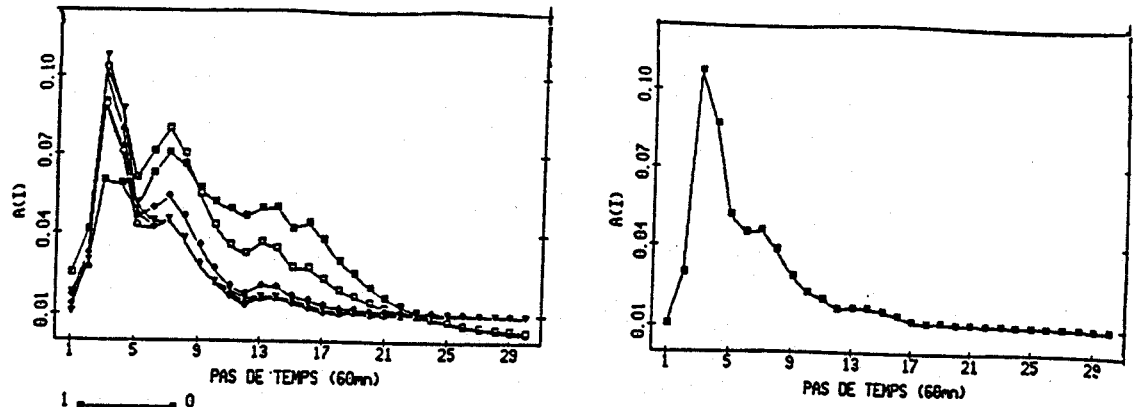

a) for discharges < 150 m^3/s

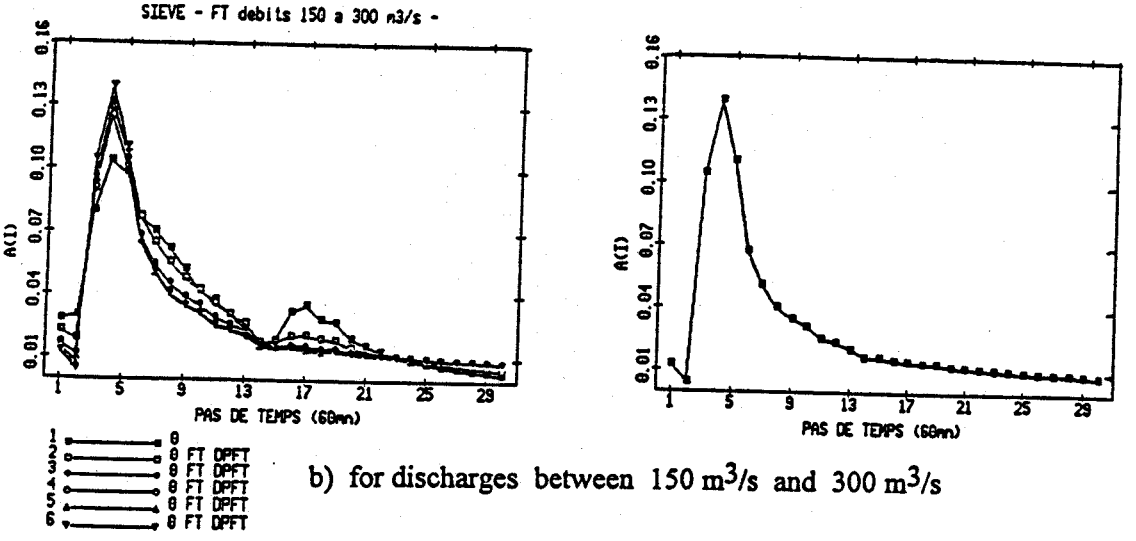

b) for discharges between 150 m^3/s and 300 m^3/s

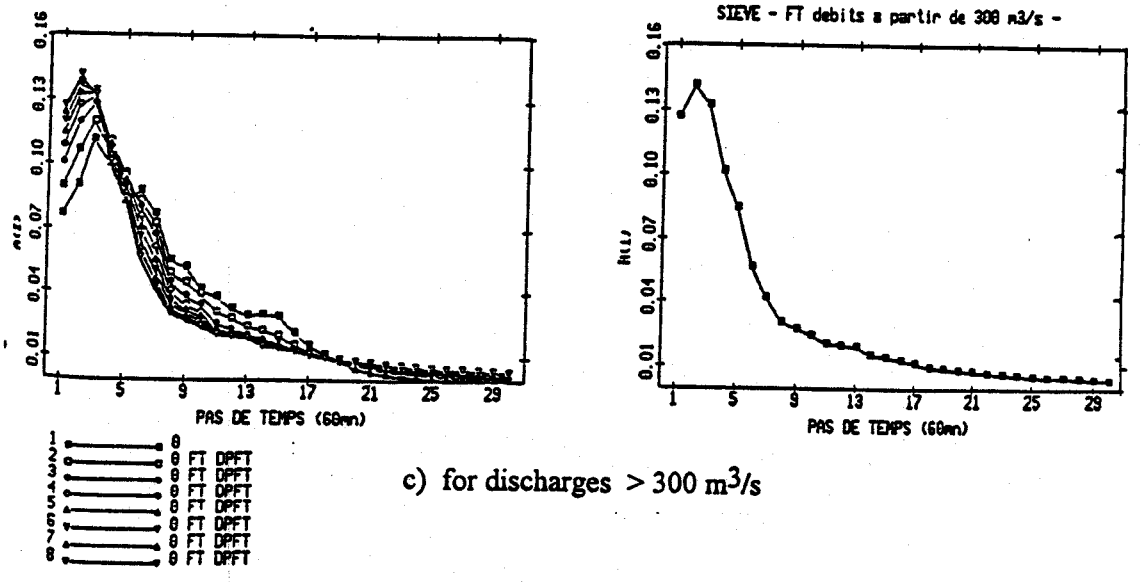

c) for discharges > 300 m^3/s

Figure 4.2.3 Stratification of events on the SIEVE data set according to maximum discharges and respective Transfer Functions for each group

Normally, once the exploratory analyses have been performed, more refined identifications of the transfer function may be undertaken, including for example a more systematic removal of the baseflow (than that made by the FDTF-ERUHDIT method itself), and the fitting of an ARMAX transfer function (the orders of which are guided by the shape obtained in the very first diagnostic step).

At the level of the individual basin it is time then to proceed to the next step of this first phase, i.e. to deal with the water accounting model or production function. In this treatment one may favour either an Hortonian approach, assuming the runoff generation is controlled by the infiltration capacity, or on a Dunne (or Hewlett) approach, where runoff generation is rather controlled by contributing areas saturated from below. The decision usually depends on the soil types and uses. Bare soils, with intensive farming or growing urbanisation, are likely to follow the Hortonian scheme, although vegetated soils in natural catchment are more likely to develop contributing areas. This choice should rely on experimental evidence, since recent experiments, some performed within this projects (see chapter 3) have demonstrated that even Mediterranean basins may follow the second scheme.

The second step of this first diagnostic phase will consist in calibrating a lumped loss model, the routing of the water being performed by the identified transfer function. A detailed example will be given in Subsection 4.2.3.3 in which a simplified version of TOPMODEL is calibrated. Once this first diagnostic and calibration phase is complete, then the second phase dealing with operational implementation and running in real time may be considered.

4.2.3.3 Calibration of rainfall-runoff models on sparse data

A methodology was developed by NTUA-DWRHME within the AFORISM project to tackle the problems in the identification and use of rainfall-runoff models on the basis of sparse data (Nalbantis, 1994a, b). These problems are posed by gauging networks that are comprised of mainly non-recording devices e.g. where a gauge is sampled on a daily basis. Such networks may be inappropriate for the identification of rainfall-runoff models to be used in flood forecasting. This is the case in steep headwater basins, especially in

the Mediterranean zone, with drainage areas ranging from several tens to several hundreds of km^2. Short response times of these basins (up to a few hours) require the use of time steps for discretisation of the hydrologic data that range from a fraction of an hour to a few hours. Therefore, recording devices are necessary to provide the appropriate data. However, during the design phase or even in the very early stages of operation of a flood forecasting system, a common situation in regard to data availability for many catchments consists of the following:

- a rather dense network of non-recording devices has been providing data for a long period (e.g., 20 or 30 years or more) on a daily basis in the most usual case,
- very few recording devices have been operating for short discontinuous periods in most cases related to specific hydrologic studies, and
- a proper network of recording devices is planned to be installed as a part of a flood forecasting system.

In the initial phase of the system implementation, the modeler of the basin faces two alternatives:

- use only pieces of continuous charts to extract information for some historical flood events and then follow an event-based modelling approach,
- use the charts in combination with the long series of daily data in the hope to embody all available information in a single model that can be operated either as event-based or as continuous-time.

It is the latter approach that was investigated within the AFORISM project.

The methodology developed here refers to the calibration of lumped conceptual rainfall-runoff models that are widely used internationally for flood forecasting. These models were used within a context that complies with the Unit-Hydrograph theory, i.e. they comprise two parts. The first part is the production function which involves all hydrologic processes that can be considered at the point or hillslope scale and yields the runoff volume or effective rainfall. The second part is the transfer function that encompasses all transfer processes within the catchment and is assumed to be linear. The FDTF-ERUHDIT method was used to simultaneously identify the Unit Hydrograph and

the effective rainfall series (Duband et al., 1990; Duband et al., 1993; Nalbantis et al., 1994). A brief description of the method is given in Section 4.2.2.

The methodology developed involves the following identification steps:

(a) The model selected is calibrated over a long continuous-time data set that is available on a daily time basis.

(b) The transfer function is identified on a time step suitable for the dynamics of the basin (herein called short time step); for this, the FDTF-ERUHDIT method is applied to the multi-event data set that is available on a short time step.

(c) Based on the above identified parameters, a complete model that operates on the short time step is constructed; this new model is called the derived model; its production function parameters are derived from those of the daily model while the parameters of its transfer function are the only ones which are directly identified (as described in b).

Two series of computer experiments were designed to evaluate the methodology proposed. The first series comprise tests on real-world data from the Evinos catchment (884 km^2) in West Sterea Hellas, Greece (Fig. 4.2.4).

The data sets used were:

- an eight-year series of daily data for rainfall and runoff,
- a two-year continuous record of hourly rainfall and runoff,
- an event-based data set for 20 flood events, and
- an eight-year series of monthly potential evapotranspiration.

Two well-known rainfall-runoff models were selected as production functions: the version of SACRAMENTO model adopted by the U.S. National Weather Service known as the Soil Moisture Accounting routine of the U.S. National Weather Service River Forecast Service or SMA-NWSRFS (Burnash et al., 1973), and the TANK model (Sugawara, 1976; Sugawara et al., 1983).

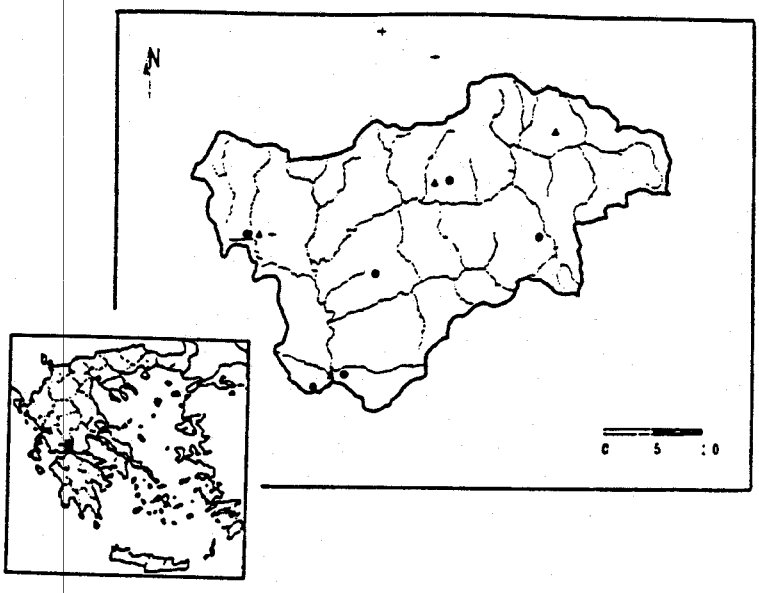

Figure 4.2.4 The Envinos River Basin at Poros Righaniou in Western Greece. The non-recording rain gauges are shown by circles, the recording ones in crosses and the temperature gauges in triangles.

The second series of tests was performed on synthetic data (Nalbantis, 1994b). A simplified version of TOPMODEL (Beven and Kirkby, 1979; Beven, 1986) with three parameters was used. It is very similar to that used by the French research group (see Section 4.2.4). A 20-year series of observed areal rainfall playing the role of the "true" rainfall series was introduced into the model to produce the "true" series of discharge. Errors were added to the rainfall to reproduce the uncertainty related to the areal rainfall estimation. A white noise applied on the true values in a multiplicative manner was used (described by Nalbantis et al., 1994). Its standard deviation in % represents the amount of error in the rainfall. Also, errors in the model parameters were considered to reproduce parameter estimation errors.

To evaluate the derived model which is the main output of the methodology proposed, two modes of operation of this model were considered:

- a continuous-time operation for a whole wet period, and
- an event-based operation for a set of flood events.

In the second case a new method for model initialisation was proposed and tested. It involves initialising the derived model through the daily model which is in all cases available as a by-product of the whole identification process. More details about this are given in Section 4.2.2. The reference case in all tests with the two operation modes was a continuous-time model that is directly identified on an hourly time step. It is reminded that in all test cases the model structure remains the same (e.g., that of the SMA-NWSRFS model).

The extensive series of tests on the methodological aspects described above allowed one to gain experience on the specific models and identification methods used. First, the identification of transfer function of the Evinos catchment (see Fig. 4.2.5) through the FDTF-ERUHDIT method showed that:

- a small secondary peak of the transfer function appears at the ninth time step while the main peak occurred at the sixth time step (Fig. 4.2.5(a)); this may be well due to errors in the data especially in the discharge as it has been verified through computer experiments on synthetic data (Nalbantis, 1987; Nalbantis et al., 1994),

- to achieve convergence, some of the events chosen had to be removed from the calibration set, this is a common problem when data contain significant errors,

- the discharge in the recession limbs of the observed hydrographs were underestimated as was observed in previous applications (see Figures. 4.2.5(b) and 4.2.6).

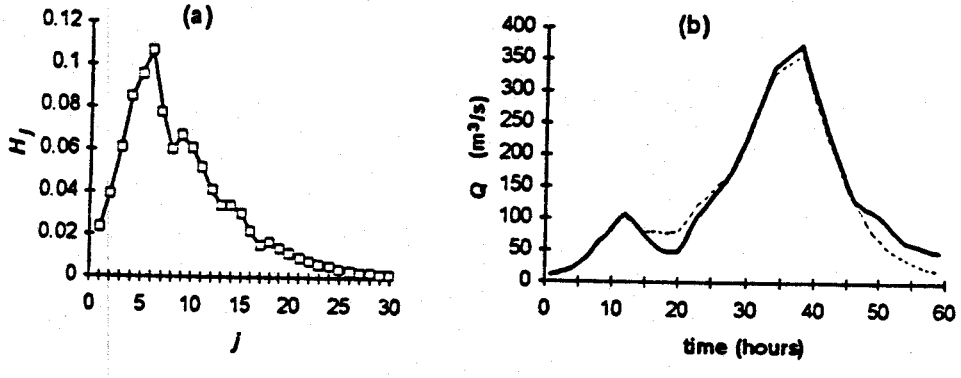

Figure 4.2.5 Transfer function identification through the FDTF-ERUHDIT method: (a) the transfer function identified, and (b) observed (solid line) versus simulated hydrograph (dashed line) for the event of 22-10-1974.

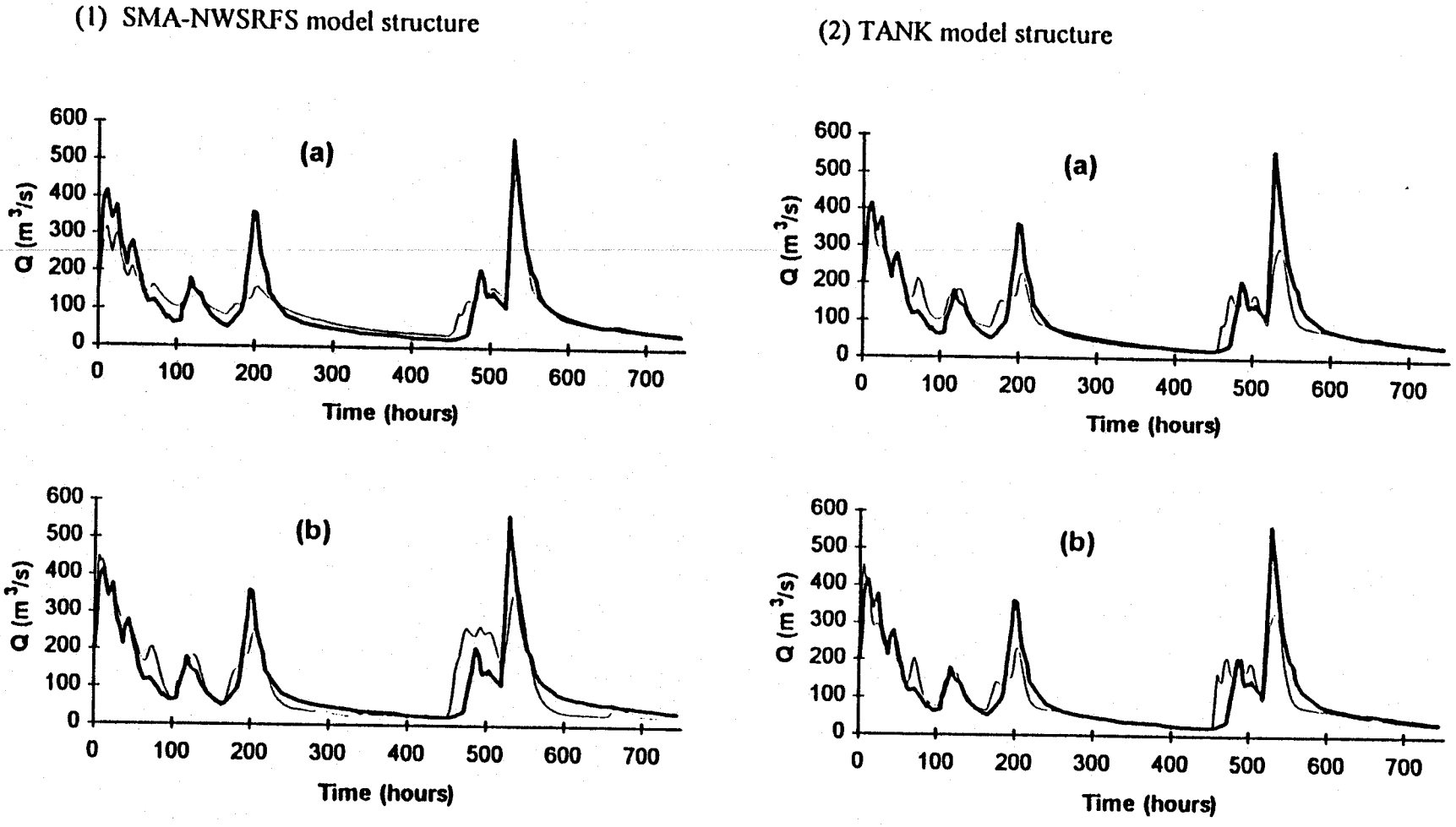

Figure 4.2.6 Continuous-time simulation with: (a) the reference and (b) the derived model and a period of one month (December 1980). The observed hydrograph is shown in bold solid line while the simulated one is in hairline.

In the calibration of the models SACRAMENTO and TANK, a semi-automatic method was followed through the use of the optimisation routines proposed by the builders of these models (Burnash et al., 1973 for the SACRAMENTO model; Sugawara, 1979 for the TANK model). It was found that for the TANK model the version with two extra subtanks adjacent to the upper tank was necessary to account for the long dry spells and the high evapotranspiration demand encountered in the test basin.

The main conclusions drawn from the study may be summarised as follows:

(1) Inappropriate historical hydrologic data may constitute a significant limiting factor in the identification of rainfall-runoff models to be used for flood forecasting. Such situations commonly appear in the design phase or even the early stages of operation of flood forecasting systems. They are characterised by the existence of large amounts of daily observations while continuous records are limited to some significant flood events. It is however known that in most small and medium-sized basins with small response times, small time steps in the order of an hour are necessary. Within the AFORISM project it was realised that a methodology for model identification that takes advantage of the daily data may be very useful.

(2) The methodology proposed involves three steps. First, the model selected is calibrated on a daily basis. Second, the transfer function of the model is identified through the FDTF-ERUHDIT method on the final sub-daily time step without supposing any production function. Finally, a new model, called the "derived" model, is created based on the parameters previously identified.

(3) The end product of the method, i.e. the derived model, was found to perform satisfactorily both as a continuous-time and as event-based. In the latter case, it can be effectively initialised through the daily model. In most cases, it exhibits performances that are lower by only 10 to 20% as compared to that of a continuous-time model that would ideally be directly identified on the final time step (see Figures 4.2.6 and 4.2.7).

(1) SMA-NWSRFS model structure

(2) TANK model structure

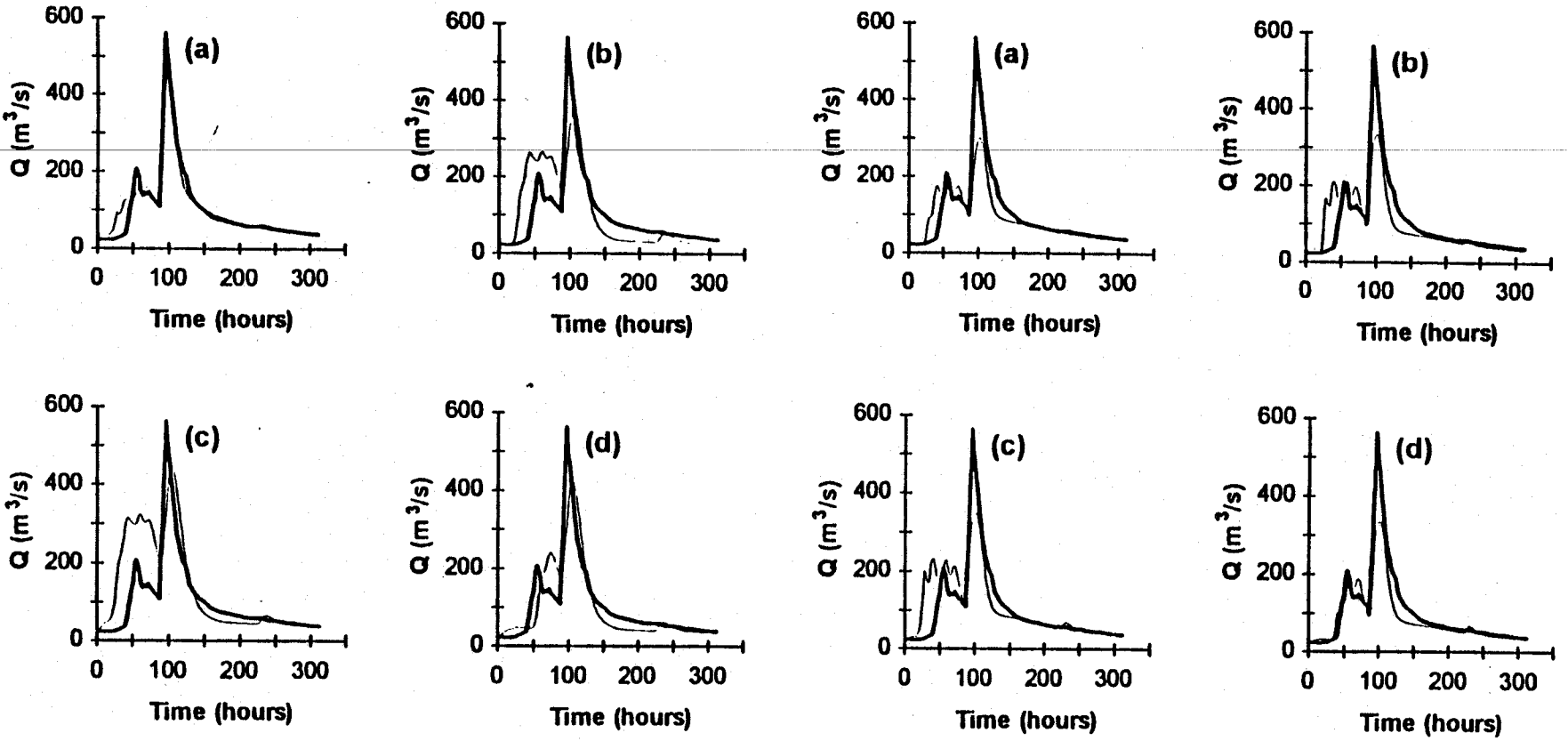

Figure 4.2.7 Comparison of various simulation schemes: (a) continuous-time reference model, (b) continuous-time derived model, (c) event-based derived model initialised via the daily model, and (d) as in (c) with tuning of some parameters. The observed hydrographs are shown in bold solid lines while the simulated ones are in hairlines.

(4) The transferability of the values of the state variables from the daily to the derived model has been verified. However, some problems were encountered in the prediction, by the daily model, of some of the state variables of the upper soil zone for the model structures of SACRAMENTO and TANK. On the contrary, predictions were very accurate for TOPMODEL. This due to the fact that the former two models are overparameterised and the number of state variables in them is rather large compared to TOPMODEL.

(5) The TANK model proved better adapted to the methodology proposed than the SACRAMENTO model. This result is specific to the context of this methodology. A strict intercomparison of the two models has been given by Franchini and Pacciani (1991).

(6) Tests on synthetic data showed that predictions, through the daily model, of the values of the state variables for TOPMODEL are extremely accurate for errors in the estimation of the areal rainfall with a standard deviation up to 50%. These errors are represented by a white noise applied on the true rainfall in a multiplicative way.

(7) The performance of the proposed scheme (derived model initialised through the daily model) for models SACRAMENTO and TANK can be very much improved through (a) tuning of those state variables (one or two) of the upper zone that are poorly predicted by the daily model, (b) residual treatment. In both cases good performances were obtained that are practically equal to a directly identified continuous-time model. But these aspects will be discussed sections 4.2.4 (for tuning of initial values of state variables) and 4.3.1 (for residual treatment).

4.2.4 Initial Conditions

As previously mentioned, operational real-time flood forecasting can be performed in two alternative ways: (a) using continuous-time models, and (b) using event-based models. Continuous type models do not present the initial conditions problem in that the model itself updates all the water storages (soil moisture storage, ground water storage, snowpack) by continuously accounting for the water budget.

Model initialisation through continuous-time run on a daily basis

A methodology for model identification based on sparse data was described in Section 4.2.3.3. It was developed within the AFORISM project by NTUA-DWRHME (Nalbantis, 1994a, b). The end product of the identification process is a lumped rainfall-runoff model called the derived model. Two modes of operation of this model were implemented and tested. In the first mode the model is run in continuous time i.e. from the beginning to the end of the wet period. In the second mode, an event-based approach is followed, e.g., the model is run only in flood periods. In the latter case a new method for model initialisation was proposed and tested. It involves the continuous-time run of the model on a daily basis. From this model run, the values of the basin state variables are extracted for the end of the day before the first rise of the flood discharge. These state predictions are then used to initialise the derived model which is operated on a short time step (e.g. one hour).

Both operation modes (continuous-time and event-based) were applied to a number of tests cases. The reference case was the continuous-time model that is directly identified as a whole, based on a continuous-time data set. Two series of tests were performed as described in section 4.2.3.3.

The main conclusions drawn from the study are:

(1) Model implementation for real-time use is much simpler for continuous-time modelling than for the event-based approach. This is due to the fact that continuous-time modelling involves no procedures for model initialisation, neither does it need the implementation of criteria for model activation (e.g. water level thresholds).

(2) Continuous-time modelling may sometimes be unfeasible. This is the case of a flood forecasting system that is dormant during dry periods for a number of reasons (e.g. economic).

(3) An efficient method for model initialisation relies in the continuous-time run of the model on a daily basis and the prediction through this daily model of the values of the state variables that are necessary for model initialisation. Prediction of state

variables through daily models was very accurate for all model structures tested. However, poor predictions were obtained for the values of some state variables mostly related to the upper soil zone for the SACRAMENTO and the TANK model structure. This is due to the fact that these two models are overparameterised and some parameters are only related to the fast response of the basin which is considerably dampened in the time step of the identification (i.e. one day). Contrary to this, for TOPMODEL high accuracy rates were obtained in the prediction of state variables thus proving the superiority of this model relative to earlier conceptual models.

(4) It appeared that the performance of the proposed scheme (derived model initialised through the daily model) for models SACRAMENTO and TANK can be very much improved through tuning of those state variables (one or two) of the upper zone that are not well predicted by the daily model. The tuning process aims at optimising the model performance in the whole test period. This may prove difficult in real-time where one will have to wait for the system to be sufficiently excited before activating the tuning process.

4.2.5 Intercomparison of models: application of the TOPMODEL and the ARNO model on the real world case of the Sieve catchment

The description of the two models is given in Section 3.3. In that section, the degree of dominance of the soil-level water balance component with respect to the transfer component has been carefully delineated. In order to proceed with a comparison of the two models, it seemed opportune to use the same transfer component for both, thereby focusing attention only on the soil-water balance component. The transfer component of the ARNO model was adopted; that is, for transferring to the outlet of the basin a double application of the parabolic unit hydrograph, obtained from an analytical solution of the diffusive-convective flow equation, under the boundary condition of an impulse (time) input uniformly distributed (in space) over the basin. The first convolution represents the transfer along the hillslopes, and the second is that along the drainage network.

A unified procedure was also used to calculate the potential evapotranspiration demand. This procedure, developed for the ARNO model, is based on hourly temperature and a

compensation factor which depends on temperature, altitude and the maximum number of hours of sunlight per day, taking into account the latitude. This procedure reproduces monthly total potential evapotranspiration demand equivalent to that obtained by the Thornthwaite method. Details of this algorithm may be found in the Section 3.3.

The watershed used for the intercomparison of the two models is that of the Sieve River, a tributary of the ARNO River (Fig. 4.2.8), closed at the Fornacina gauge station. In this figure, the basin is further divided into four sub-basins to better characterise the geomorphologic features of the terrain; some of the main quantities relative to the various sub-basins are shown in Table 4.2.1. The rain gauges considered and their effective areas, obtained using Thiessen polygons, are shown in Figure 4.2.9, while Figure 4.2.10 shows the thermometric stations. The period taken into consideration runs from December 1, 1959 to March 31, 1960.

Section outlet	Hillslopes lengths	Reach lengths	Area	Average altitude	Outlet altitude
	km	km	km^2	m	m
SI04 Fornacina	6.0	13.0	157.	517.	92.
SI03 Dicomano	7.5	20.0	300.	532.	180.
SI02 Borgo S.Lorenzo	9.8	11.0	215.	425.	190.
SI01 Bilancino	5.7	14.0	150.	468.	230.

Table 4.2.1 - Outlets of the four sub-basins of the Sieve catchment.

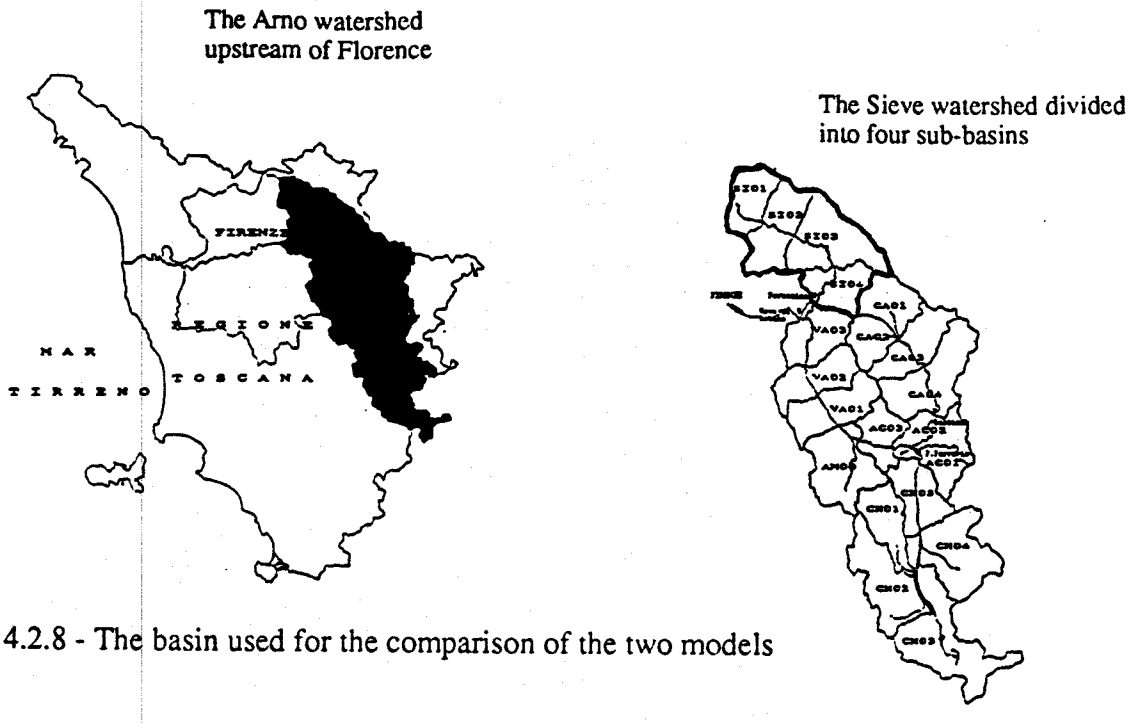

Fig. 4.2.8 - The basin used for the comparison of the two models

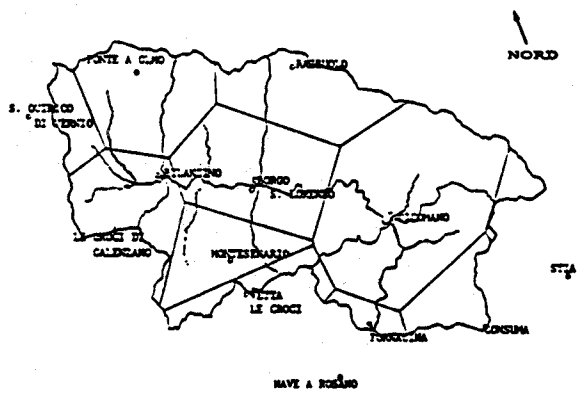

Figure 4.2.9 - Distribution of the rain gauges

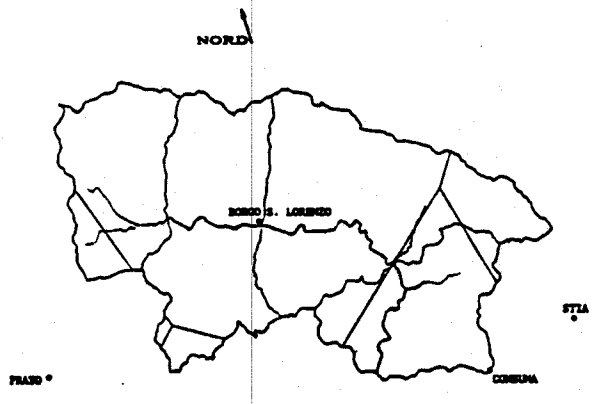

Figure 4.2.10 - Distribution of the temperature stations

The calibration of the models was carried out on the basis of a trial search procedure. A description of the parameters which characterise the soil-moisture balance component of the two models is given in Tables 4.2.2. and 4.2.3.

W_m	Average storage capacity over the entire watershed
b	Shape coefficient of the spatial distribution curve of the storage capacity
D_s	Maximum drainage fraction, corresponding to the threshold value of the moisture content
Dmax	Maximum drainage value
W_s	Threshold value of moisture content used in calculating drainage
c	Shape coefficient of the drainage curve
W_i	Threshold value of moisture content used in calculating deep infiltration
α	Proportion of (W_0-W_i), used in calculating deep infiltration
B	Base flow
Imp	Percentage of impervious surface.

Table 4.2.2 - Parameters of the soil-moisture balance module of the ARNO model

K_0	Saturated hydraulic conductivity at the soil level;
f	Decay factor of the hydraulic conductivity with depth
SRmax	Canopy interception capacity

Table 4.2.3 - Parameters of the soil-moisture balance module of TOPMODEL

As a general rule, the calibration of the two models was performed using the data for the month of December 1959 and then verified over the remaining three months. In this way it was possible to verify that the calibration achieved was not a simple numerical combination, but rather the result of a consistent evaluation of the parameters.

Judgement of the effectiveness of the calibration achieved was essentially based on a criterion of visual comparison between computed and observed discharges, also aided by the estimate of the explained variance (EV), the determination coefficient (DC), and the correlation coefficient (CC) evaluated on the basis of the following formulas:

$$EV = 1 - \frac{\sum_i (\varepsilon_i - \mu_\varepsilon)^2}{\sum_i (Q_{ob_i} - \mu_{ob})^2}; \qquad DC = 1 - \frac{\sum_i \varepsilon_i^2}{\sum_i (Q_{ob_i} - \mu_{ob})^2}; \qquad CC = \sqrt{DC}$$

ε = Error = $Q_{ob} - Q_s$; Q_{ob} = Observed discharges;

Q_S = Simulated discharges; μ_{ob} = Mean of the observed discharges;

μ_ε = Mean of the error.

The results of the calibrations are gathered in Figures 4.2.11 and 4.2.12; the observed series are represented by a continuous line, while the dashed line represents the series simulated by the models. Finally, Table 4.2.4 shows the EV, DC, and CC values for each model, calculated with reference both to the month of December (calibration month) and to the three months (January, February, and March) representing the validation (simulation) period.

The results of the two models are almost of the same quality, or rather, at least as far as this specific case is concerned, the ARNO model produces slightly better results in terms of validation. This does not, however, create a hierarchy of validity among the various models since, by virtue of the diverse formulations which distinguish them, they may be found to be more or less suited to the specific case being studied.

Model	Calibration			Validation		
	EV	DC	CC	EV	DC	CC
ARNO	0.888	0.880	0.938	0.853	0.851	0.923
TOPMODEL	0.914	0.912	0.955	0.852	0.846	0.920

Table4.2.4 Sieve Basin. Calibration period: December 1959; Validation period: January, February, March, 1960. Intercomparison between ARNO and TOPMODEL..

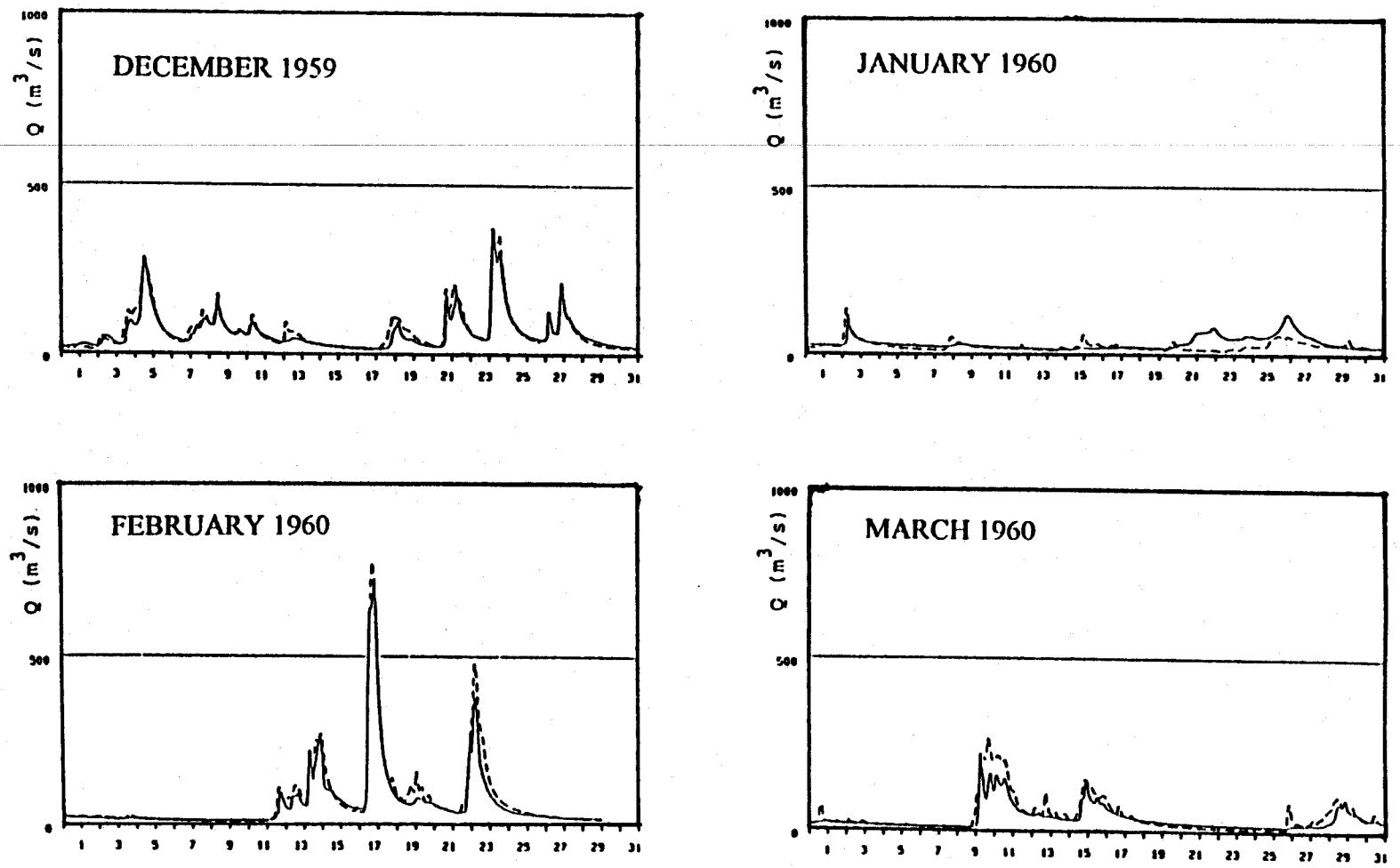

Figure 4.2.11 Sieve basin; ARNO model. Observed (solid line) and simulated (dashed line) discharges. Calibration period: December 1959; Validation (January, February, March 1960).

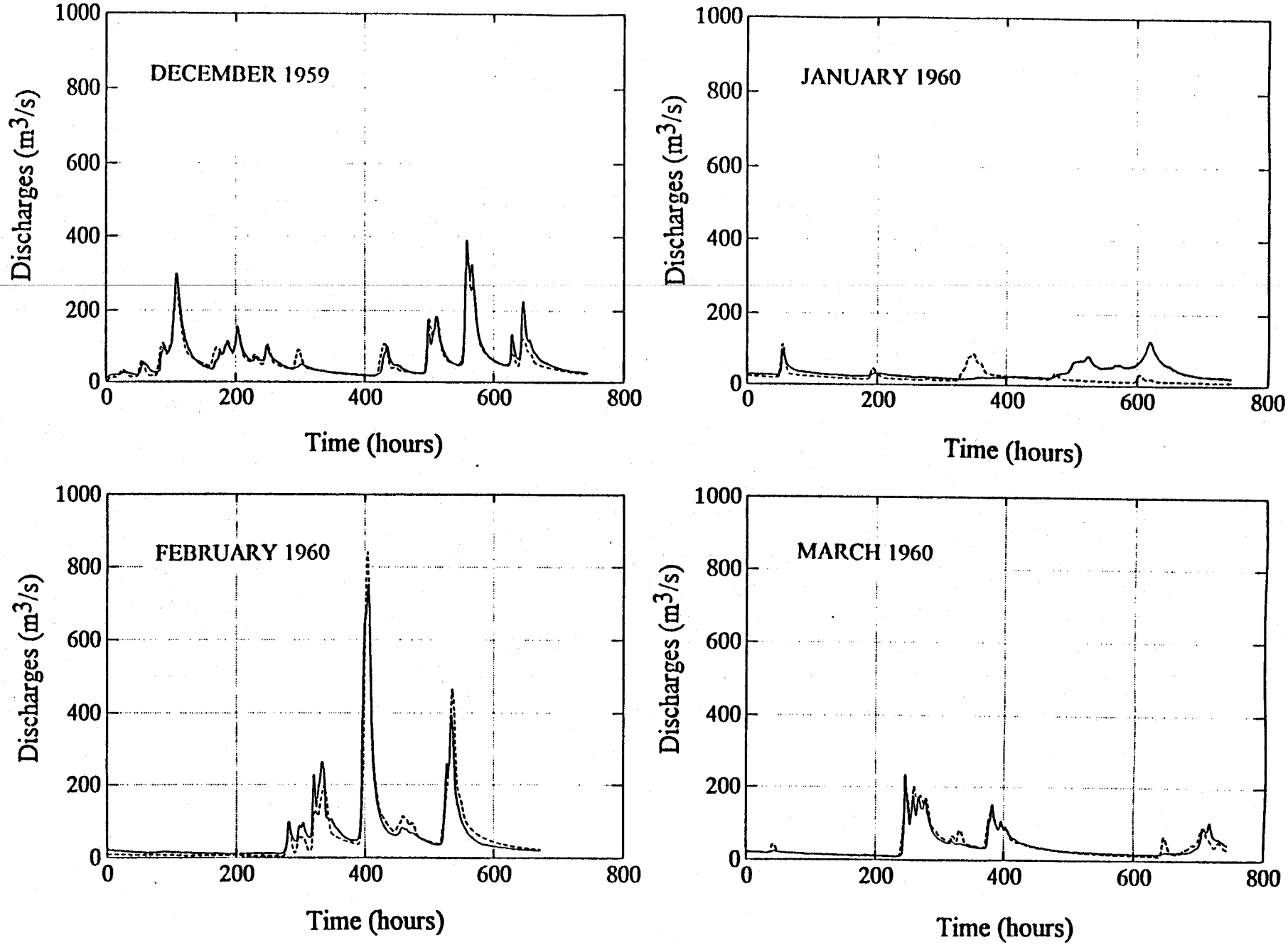

Figure 4.2.12 Sieve basin; TOPMODEL. Observed (solid line) and simulated (dashed line) discharges. Calibration period: December 1959; Validation (January, February, March 1960).

The main conclusion that may be drawn from the intercomparison of the two models based on the statistical criteria is that both the models produce results which have a similar quality level. The calibration of the ARNO model appears slightly more complex due to its relatively large number of parameters. By contrast TOPMODEL does not give a correct representation of the unsaturated zone and, in turn, of the depletion phase during the long periods without rainfall. Furthermore, TOPMODEL performs slightly worse in the validation phase. For this reason and because the ARNO model is part of an automatic real time operational system (the European Flood Forecasting Operational Real Time System - EFFORTS) in the operational part of the study, the latter has been used to perform the simulation in the frame of the forecasting system prototype.

4.3 ADAPTIVE IMPLEMENTATION FOR REAL-TIME USE

In rainfall-runoff modelling there are basically three known procedures for adjusting forecasts on the basis of real-time acquired observations.

The first procedure is to correct the observed input to the model, given its large uncertainty (for instance areal precipitation) and re-run the model until there is a reasonable match between model output and observed runoff (Bergstrom (1976). Although several objections may be raised to this method, its rationale is to modify the state variables (the different water storages present in the model such as soil moisture storage content, groundwater content, etc.) in order to meet the observed output. Given its very limited validity, which is restricted to reservoir type models, this method was not tested within the frame of AFORISM and will not be discussed further in this report.

The second procedure is to modify the parameters of the model by means of a real time re-calibration approach. This can be performed either limiting it to the transfer function relevant to the routing component of the model, or or by re-calibrating in real time all the model parameters, as proposed by Georgakakos for the SACRAMENTO model, by means of an Extended Kalman Filter (Georgakakos, 1986).

The third procedure, assumes the output of the model as an *a priori* estimate, and without modifying the model parameters and state variables, combines it with the observed values

in order to obtain the *a posteriori* final estimate. This approach can be viewed as a stochastic treatment of model residuals; it is this third method that will be developed here.

4.3.1 Adapting parameters vs residual treatment

4.3.1.1 Stochastic treatment of residuals

This paragraph describes the stochastic model used for the real time treatment of model residuals in flood forecasting applications where a continuous model is used. Following the results of the WMO Intercomparison of Real Time Flood Forecasting Models (1992), the real time update of model parameters was not taken into consideration, not only because of its computational requirements such as complex non-linear Kalman Filters, but chiefly because it may lead to highly unstable estimates.

The technique adopted here is based upon the interpretation of the "deterministic" simulation model results as *a priori* estimates of the actually measured discharges, adjusting them *a posteriori,* given the new observations. What this means is that a well-tried, physically based model is used to perform the non-linear transformation of precipitation to runoff, yielding not only current estimates of the flow, but in addition future forecasts. The Kalman Filter is then used in the form in which it was designed, as a linear interpolator, not a non-linear extrapolator. The predicted and measured flows are then compared and the measured flows are extended into the future using the physical model. An additional advantage of this approach is to compare concurrent values, overcoming one of the disadvantages of the Kalman Filter, which is that it typically compares values lagged one or more time-intervals apart.

At each time step during the calibration phase, the model output is compared with the observed flow and instead of modelling their differences, (the residuals) a linear Kalman Filter is used to filter out the residual variance which is assumed to be the uncertainty associated with the model output.

The adopted scheme is represented in Figure 4.3.1, where Q_d is the rainfall runoff model output which is here taken as the *a priori* estimate, Q_o is the observed discharge and Q_{ds} represents their final combination.

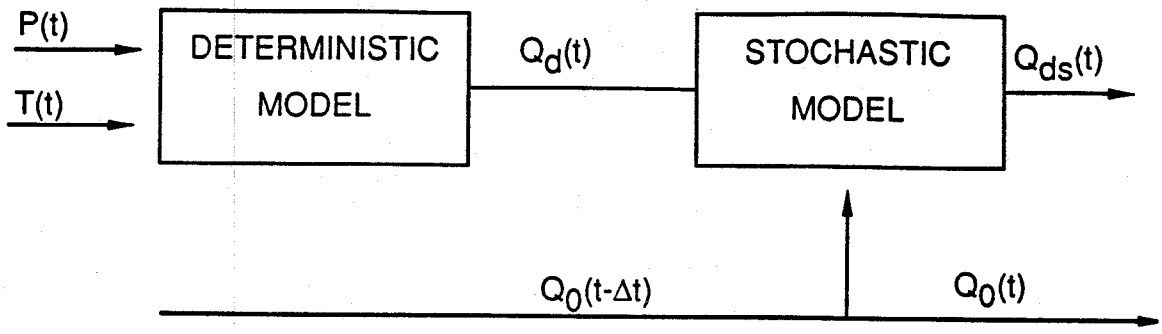

Figure 4.3.1 - Real time updating model

The advantage of the proposed scheme emerges from the fact that beyond the last measurement in time one can generate, by means of the rainfall-runoff forecasting model, a trace of future flows. This trace is then used in the Kalman Filter (KF) to reconstruct the future "observations" after filtering out the "measurement errors", which in this case correspond to the residuals (the differences between observed and simulated flows.

The main difference of this approach from the more conventional modelling of residuals can be explained as follows. When modelling the residuals in unconventional approach, after the last measurement, the KF only performs successive extrapolations and therefore the results will chiefly depend upon the stochastic model adopted. On the other hand, considering the rainfall-runoff model output as a noise corrupted measurement (in other words an *a priori* estimate) of the observations, at each time step an extrapolation phase is followed by a correction phase, thus improving the overall performance of the filter.

On the face of it, because the adopted approach requires the simultaneous estimation of state and parameter vectors, conventional treatment results in a non-linear estimation problem. The standard response is to use extended filters (EKF - Extended Kalman Filter) in which the state vector is extended to the parameters of the model. This not only poses considerable difficulties connected with both the size of the problem that results and its non-linearity but also leads to estimates affected by systematic error.

By contrast, the configuration of the algorithm used for the implementation and the calibration of the multivariate KF required for the problem of producing forecasts of

flows in real time, is based on two linear, interactive KFs, one in the space of the state vector and one in the space of the parameters. This algorithm has been called MISP (Mutually Interactive State Parameter estimation), which has been demonstrated to produce consistent real time parameter estimates. A description of the basic KF and of the MISP algorithm is provided in section 4.3.1.2.

4.3.1.2. The MISP Algorithm for Real-Time Flow Forecasting.

The Kalman filter

Before addressing the subject of the MISP it is worth making a few brief remarks on the basic equations of the Kalman filter.

The formulation in terms of state vector of a linear dynamic system discretised over time is represented by the following vectorial equations:

$$\begin{cases} \mathbf{x}_t = \Phi_{t|t-1}\mathbf{x}_{t-1} + \mathbf{v}_t \\ \mathbf{z}_t = \mathbf{H}_t\mathbf{x}_t + \Gamma_t\mathbf{w}_t \end{cases}$$

The first of the two equations is known as a dynamic system equation, while the second equation represents the measuring system.

The vector $\mathbf{x}_t$ of dimensions (n, 1) is the vector which contains all the quantities required, and possibly also sufficient, to describe the state of the system and it is known accordingly as the state vector. The matrix $\Phi_{t/t-1}$ of dimensions (n, n) is the transition matrix which describes the dynamic evolution of the state vector between the state at step t - 1 and the state at step t.

The vector $\mathbf{z}_t$ of dimensions (m, 1), with $m \leq n$, is the measurements vector which contains the quantities measured at step t.

The matrices Γ_t and H_t, their respective dimensions being (n, mw) and (m, n), are generally dimensional conversion matrices, while the vectors $\mathbf{w}_t$ and $\mathbf{v}_t$, dimensions (mw, 1) and (m, 1), represent respectively the errors due to the schematisation of the model and the measurement errors.

The optimality of the Kalman filter is generally demonstrated only in the case of multinormal distributions of w_t and v_t. In the case of different distribution of the errors sub optimal filters are generated. In any case the following assumptions must apply:

$$E\{w_t\} = \overline{w}$$

$$E\{v_t\} = \overline{v}$$

$$E\left\{(w_t - \overline{w})(w_k - \overline{w})^T\right\} = Q\,\delta_{t,k}$$

$$E\left\{(v_t - \overline{v})(v_k - \overline{v})^T\right\} = R\,\delta_{t,k}$$

$$E\left\{(w_t - \overline{w})(v_k - \overline{w})^T\right\} = E\left\{(v_t - \overline{v})(w_k - \overline{w})^T\right\} = 0 \quad \forall\, k$$

where $\delta_{t,\,k}$ is the Kroneker delta defined as:

$$\delta_{t,\,k} = 1 \quad \text{for } t = k$$

$$\delta_{t,\,k} = 0 \quad \text{for } t \neq k$$

As previously mentioned, because they are so well known, only brief mention will be made here of the equations required for Kalman filter calculation cycle, i.e. for the transition from minimal variance evaluation of the state at step t to the minimal variance calculation at step t + 1.

Table 4.3.1 shows the equations required to accomplish this calculation cycle:

$$\begin{aligned}
v_t &= z_t - H_t\,\hat{x}_{t|t-1} - \overline{v}_{t-1} \\
K_t &= P_{t|t-1} H_t^T \left(H_t\,P_{t|t-1}\,H_t^T + R_{t|t}\right)^{-1} \\
\hat{x}_{t|t} &= \hat{x}_{t|t-1} + K_t\,v_t \\
P_{t|t} &= \left(I - K_t\,H_t\right) P_{t|t-1} \\
\hat{x}_{t+1|t} &= \Phi_{t+1|t}\,\hat{x}_{t|t} + \Gamma_{t+1}\,\overline{w}_t \\
P_{t+1|t} &= \Phi_{t+1|t}\,P_{t|t}\,\Phi_{t+1|t}^T + \Gamma_{t+1}\,Q_{t|t}\,\Gamma_{t+1}^T
\end{aligned}$$

TABLE 4.3.1 - Sequence of equations in a Kalman filter calculation cycle

In it:

$\hat{\mathbf{x}}_{t+1|t}$ and $\mathbf{P}_{t+1|t}$ represent respectively the estimation of the state vector and of the state error co-variance matrix at step t+1, given all the measurements up to step t;

$\hat{\mathbf{x}}_{t|t}$ and $\mathbf{P}_{t|t}$ represent respectively estimation of the state vector and of the state error co-variance matrix at step t, given all the measurements up to step t;

ν_t is the innovation of the filter, the actual residual of the model;

$\mathbf{K}_t$ is the gain of the filter, and i.e. the weight matrix which permits a minimum variance estimation of $\hat{\mathbf{x}}_{t|t}$.

If the matrices $\Phi_{t-1}, \mathbf{H}_t, \Gamma_t, \overline{\mathbf{w}}, \overline{\mathbf{v}}, \mathbf{Q}, \mathbf{R}$ are presumed to be known a priori, then the optimality of the filter implies:

$$\mathbf{E}\{\nu_t\} = 0$$

$$\mathbf{E}\{\nu_t, \nu_{t-k}^T\} = \mathbf{C}_k = \left(\mathbf{H}_t^T \mathbf{P}_{t|t-1} \mathbf{H}_t + \mathbf{R}\right) \delta_{t,k}$$

In practice, while the matrices $\mathbf{H}_t$ and Γ_t are usually known, neither the parameters matrix $\Phi_{t|t-1}$ nor the error statistics $\overline{\mathbf{w}}, \overline{\mathbf{v}}, \mathbf{Q}, \mathbf{R}$ are known.

Following various authors it is possible, albeit not in all cases, to calculate the error statistics by setting a posteriori the above-mentioned conditions on the filter innovation.

In this way a posteriori estimates are obtained for $\overline{\mathbf{w}}, \overline{\mathbf{v}}$,$\mathbf{Q}$ and $\mathbf{R}$ which, on the basis of the structure of the assumed model, allow optimal estimates of the state vector to be obtained.

Specifically, for the ARMAX models (auto-regressive moving average models with exogenous variables), which represent a wide range of transfer function models in which the inputs are affected by errors of measurement and which are therefore well suited to the study of time series, it is possible to calculate completely the matrix $\mathbf{R}$ and a sub-matrix of $\mathbf{Q}$ with rank equal to the rank of $\mathbf{R}$, while doubts remain as to the possibility of evaluating at the same time $\overline{\mathbf{w}}$ and $\overline{\mathbf{v}}$, though this is a limitation of little importance.

Nevertheless, the most crucial problem remains the simultaneous estimation of the state vector and the model's parameters, a problem which, by its very nature, is not linear.

Estimation of parameters

For the sake of simplicity, let's endeavour in a scalar case to highlight the parameter estimation problem. Suppose the system to be defined by:

$$x_t = \varphi x_{t-1} + w_t$$
$$z_t = x_t + v_t$$

with the following assumptions:

$$E\{x_t\} = E\{w_t\} = E\{v_t\} = E\{z_t\} = 0$$
$$E\{x_t v_{t-k}\} = \{v_t v_{t-k}\} = E\{w_t w_{t-k}\} = 0 \qquad \forall k \neq 0$$
$$E\{x_t w_{t-k}\} = 0 \qquad \forall k$$
$$E\{z_t^2\} = \sigma_z^2 = E\{x_t^2\} + E\{v_t^2\} = \sigma_x^2 + \sigma_v^2$$

Substituting for x_t taken from the system dynamic equation in the measurement equation, we get:

$$z_t = \varphi z_{t-1} + v_t - \varphi v_{t-1} + w_t = \varphi z_{t-1} + \eta_t$$

which shows that, in a scalar case too, the exogenous variable z_{t-1} is correlated with the error η_t, thus violating the regression assumptions.

To see the effect that this correlation has on the calculation of the parameter φ it is sufficient to evaluate the probability limit of:

$$\hat{\varphi} = \sum z_{t-1} z_t \,/\, \sum z_{t-1}^2 \xrightarrow{p} E\{z_{t-1} z_t\} \,/\, E\{z_{t-1}^2\} =$$
$$= E\{(x_{t-1} + v_{t-1})(\varphi x_{t-1} + w_t + v_t)\} \,/\, E\{z_{t-1}^2\} =$$
$$= \varphi \sigma_x^2 / \sigma_z^2 = \varphi(1 - \sigma_v^2 / \sigma_z^2)$$

In other words we obtain an inconsistent calculation except in the case of a null variance in the measurement error v.

Consequently, in using the Kalman filters for ARMAX models where the matrix **R**, measurement error variance, may not be considered null, inconsistent estimates of the parameters are obtained, if performed using traditional methods.

To get round this problem many authors propose the use of instrumental variables defined as variables closely related with the state variables x_t, yet totally independent of the measurement errors v_t.

In the case of the above example, if x_t^* is the instrumental variable such that $E\{x_t^* v_{t-k}\} = 0 \quad \forall k$, the probability limit of the estimate of φ becomes:

$$\varphi = \sum x_{t-1}^* z_t \Big/ \sum x_{t-1}^* z_{t-1} \xrightarrow{p} E\{x_{t-1}^* z_t\} \Big/ E\{x_{t-1}^* z_{t-1}\} =$$

$$= E\{x_{t-1}^* (\varphi x_{t-1}^* + v_t + w_t)\} \Big/ E\{x_{t-1}^* (x_{t-1}^* + v_{t-1})\} = \varphi$$

when, as hypothesis, $E\{x_{t-1}^* v_{t-1}\} = 0$.

A recursive algorithm for the estimate using instrumental variables has been proposed by Young (1974), while Mehra (1974) has suggested the use of the Kalman filter to calculate the instrumental variables. It should in fact be borne in mind that the efficiency of an instrumental variable algorithm improves as the correlation between the instrumental variable x_t^* and the state vector x_t^* increases. Accordingly it is clear that the variable $x_{t|t}$ can be used as instrumental variable since, for the optimality of the filter, it is the best linear estimate of x_t, (unbiased and with minimal variance) and, again for the optimality of the filter, it is also totally independent of the measurement errors v_t.

It is on the basis of these considerations that the MISP has been developed; the MISP not only permits the parameters to be calculated but also takes account of the disturbing effect that this estimation has on the optimality of the filter.

The MISP Algorithm

If, in order to estimate the parameters, the estimations of the state vector provided by the filter, i.e. $\hat{x}_{t|t}$, are used as observations instead of the actual measurements, it is possible to express the relation connecting the estimation of the state vector at step t with the estimation at step t-1 according to the following relation which can be derived from the expressions in Table 4.3.1:

$$\hat{\mathbf{x}}_{t|t} = \Phi_{t|t-1}\hat{\mathbf{x}}_{t-1|t-1} + \Gamma_t\overline{\mathbf{w}}_t + \mathbf{K}_t\nu_t$$

which, multiplied by $\mathbf{H}_t$ to link up with the dimensions of the measuring system, becomes:

$$\mathbf{H}_t\hat{\mathbf{x}}_{t|t} = \mathbf{H}_t\Phi_{t|t-1}\hat{\mathbf{x}}_{t-1|t-1} + \mathbf{H}_t\Gamma_t\overline{\mathbf{w}}_t + \mathbf{H}_t\mathbf{K}_t\nu_t$$

The j component of the vector $\Phi_{t|t-1}\hat{\mathbf{x}}_{t-1|t-1}$ can be expressed as a function of the parameters θ once $\Phi_{t|t-1}$ has been defined as follows:

$$\Phi_{t|t-1} = \begin{bmatrix} \Phi^T_{1,t|t-1} \\ \cdot \\ \cdot \\ \cdot \\ \Phi^T_{n,t|t-1} \end{bmatrix} = \begin{bmatrix} \mathbf{a}^T_{1,t} + \theta^T_{t+1}\mathbf{B}^T_{1,t} \\ \cdot \\ \cdot \\ \cdot \\ \mathbf{a}^T_{n,t} + \theta^T_{t+1}\mathbf{B}^T_{n,t} \end{bmatrix}$$

i.e., row by row, $\Phi^T_{j,t|t-1} = \mathbf{a}^T_{j,t} + \theta^T_{t+1}\mathbf{B}^T_{j,t}$ where θ_{t+1} is the vector of size (p, 1) which contains all the parameters of the model, $\mathbf{a}_{j,t}$ is a vector (n, 1) with constant coefficients, and $\mathbf{B}_{j,t}$ is a matrix (n, p) which allows the transition of the parameters of size p to the space of the state vector of size n.

The product $\mathbf{H}_t\Phi_{t-1}\hat{\mathbf{x}}_{t-1|t-1}$ can be projected in the space of the parameters once the following matrices $\mathbf{A}_t$ (n, n) and $\mathbf{F}_t$ (n, p) have been considered:

$$\mathbf{A}_t = \begin{bmatrix} \mathbf{a}^T_{1,t} \\ \cdot \\ \cdot \\ \cdot \\ \mathbf{a}^T_{n,t} \end{bmatrix} \qquad \mathbf{F}_t = \begin{bmatrix} \hat{\mathbf{x}}^T_{t-1|t-1}\mathbf{B}_{1,t} \\ \cdot \\ \cdot \\ \cdot \\ \hat{\mathbf{x}}^T_{t-1|t-1}\mathbf{B}_{n,t} \end{bmatrix}$$

where in fact $\mathbf{H}_t\Phi_{t|t-1}\hat{\mathbf{x}}_{t-1|t-1} = \mathbf{H}_t\left(\mathbf{A}_{t-1}\hat{\mathbf{x}}_{t-1|t-1} + \mathbf{F}_t\theta_t\right)$

Next, replacing the following expressions:

$$\mathbf{z}_t^* = \mathbf{H}_t\left(\hat{\mathbf{x}}_{t|t} - \mathbf{A}_{t-1}\hat{\mathbf{x}}_{t-1|t-1}\right)$$
$$\mathbf{H}_t^* = \mathbf{H}_t\mathbf{F}_t$$
$$\mathbf{v}_t^* = \mathbf{H}_t\left(\mathbf{K}_t\mathbf{v}_t + \Gamma_t\overline{\mathbf{w}}\right)$$

it is possible to set up a new model on the dynamics of the parameters, expressed by the following relations:

$$\theta_t = \theta_{t-1} + \mathbf{w}_t^*$$
$$\mathbf{z}_t^* = \mathbf{H}_t^*\theta_t + \mathbf{v}_t^*$$

where the first relation expresses the dynamic evolution of the parameters ($\mathbf{w}_t^* = 0$ in the event of steadiness in the link, and therefore constant parameters), while the second relation represents the particular measuring system chosen. The structure of this filter is virtually known. Its matrix Φ is equal to the identity matrix, while noise on the dynamics of the parameters will either be null or will have mean and variance characteristics which we may assume a priori ($\overline{\mathbf{w}}_t^*$ and $\mathbf{Q}^*$).

Calculation of the statistical characteristics of the measurement errors is also immediate since the quantities in question can in practice be obtained on the basis of the first filter in the space of the state vector:

$$\overline{\mathbf{v}}_t^* = \mathbf{E}\left\{\mathbf{v}_t^*\right\} = \mathbf{H}_t\Gamma_t\overline{\mathbf{w}}_t$$
$$\mathbf{R}_t = \mathbf{E}\left\{\left(\mathbf{v}_t^* - \overline{\mathbf{v}}^*\right)\left(\mathbf{v}_t^* - \overline{\mathbf{v}}^*\right)^{\mathrm{T}}\right\} = \mathbf{H}_t\mathbf{K}_t\mathbf{C}_0\mathbf{K}_t^{\mathrm{T}}\mathbf{H}_t^{\mathrm{T}}$$

Therefore, since all the characteristics of this new filter are known, it is possible to use, in the space of the parameters, an algorithm similar to the one shown in Table 4.3.1 for the consistent and minimal variance estimation of the parameters themselves.

It should however be said that the optimality of the estimation process, as with all methods based on instrumental variables, is reached after a series of runs through the

historical data, since the quality of the instrumental variables increases as the model residue becomes less and less correlated:

States:

$$
\begin{aligned}
\nu_t &= z_t - H_t\,\hat{x}_{t|t-1} - \bar{v}_{t-1} \\
\bar{v}_t &= \bar{v}_{t-1} + \nu_t / t \\
R_{t|t} &= R_{t|t-1} + \left(\nu_t \nu_t^T - C^{\circ}_{t|t-1}\right)/t \\
C^{\circ}_{t|t} &= H_t\,P_{t|t-1}\,H_t^T + R_{t|t} \\
K_t &= P_{t|t-1} H_t^T \left(C^{\circ}_{t|t}\right)^{-1} \\
\hat{x}_{t|t} &= \hat{x}_{t|t-1} + K_t\,\nu_t \\
P_{t|t} &= P_{t|t-1} - K_t\,C^{\circ}_{t|t}\,K_t^T \\
\bar{w}_t &= \bar{w}_{t-1} - \left(\Gamma_t^T\Gamma_t\right)^{-1}\Gamma_t^T K_t\,\nu_t/t \\
Q_{t|t} &= Q_{t|t-1} + \left[\left(\Gamma_t^T\Gamma_t\right)^{-1}\Gamma_t^T K_t\left(\nu_t\nu_t^T - C^{\circ}_{t|t-1}\right)K_t^T\Gamma_t\left(\Gamma_t^T\Gamma_t\right)^{-1}\right]/t
\end{aligned}
$$

Parameters:

$$
\begin{aligned}
\nu^*_t &= H_t\,K_t\,\nu_t \\
R^*_t &= H_t\,K_t\,C^{\circ}_{t|t}\,K_t^T\,H_t^T \\
C^{\circ *}_t &= H^*_t\,P^*_{t|t-1}\,H^{*T}_t + R^*_{t|t} \\
K^*_t &= P^*_{t|t-1}\,H^{*T}_t\left(C^{\circ *}_t\right)^{-1} \\
\hat{\theta}_{t+1|t} &= \hat{\theta}_{t|t-1} + K^*_t\,\nu^*_t + \Gamma^*_{t+1}\,\bar{w}^* \\
P^*_{t+1|t} &= P^*_{t|t-1} - K^*_t\,C^{\circ *}_t\,K^{*T}_t + \Gamma^*_{t+1}\,Q^*\,\Gamma^*_{t+1} \\
\hat{x}_{t+1|t} &= \Phi_{t+1|t}\,\hat{x}_{t|t} + \Gamma_{t+1}\,\bar{w}_t \\
P_{t+1|t} &= \Phi_{t+1|t}\,P_{t|t}\,\Phi^T_{t+1|t} + \Gamma_{t+1}\,Q_{t|t}\,\Gamma^T_{t+1}
\end{aligned}
$$

TABLE 4.3.2 - Sequence of equations in MISP estimation cycle

At the same time as the estimation of the unknown parameters of the matrix Φ it is possible to calculate, with the provisions mentioned above, the error statistics $\overline{\mathbf{w}}, \overline{\mathbf{v}}, \mathbf{Q}, \mathbf{R}$.

Table 4.3.2 show the algorithm implemented in MISP which allows for all the combined estimations to be made, and which, on the basis of an a posteriori estimation of the innovation variance matrix, also takes into account the increase of variance in the model generated by the variance of the parameter estimation errors.

4.3.1.3. Initialising Event-based models in Real-Time

In Section 4.2.3.3 a methodology was described that tackles problems of the identification and use of rainfall-runoff models based on sparse data. It was developed within the AFORISM project by NTUA-DWRHME (Nalbantis, 1994a, b). It applies to small and medium-sized basins (up to several hundreds km^2) with small response times (less than 24 hours) and gauging networks that comprise mainly non-recording devices. Hence, historical data sets consist of long series of daily observations and data for some flood events on the proper small time step (e.g. one hour). The methodology proposed there involves three steps. First, the model selected is identified on a daily time basis. Second, the transfer function of the model is estimated on the final short time step. Finally, a new model, called "derived" model is built that operates on a short time step. It can be used either as continuous-time or as event-based (see Section 4.2.3.3).

In the case of the event-based approach the problem of model initialisation appears. This is discussed in more detail in Section 4.2.1. The key idea is to run the model selected on a daily basis and transfer the values of its state variables to the short time step models i.e the derived model which is activated only in flood periods. This transfer is perfectly possible for a wide range of models. In the tests described in section 4.2.3.3, very accurate predictions of state variables were obtained for a simplified version of TOPMODEL (Beven and Kirkby, 1979; Beven, 1986) and also for most state variables of models SACRAMENTO (Burnash et al., 1973) and TANK (Sugawara, 1976; Sugawara et al., 1983). However, in the last two models some states of the upper soil zone (one or two) were inadequately predicted. This was effectively corrected through tuning of these initial states.

The tuning procedure described in Section 4.2.3.3 may be difficult to implement in real time since: (a) the forecaster has to wait for the natural system to be sufficiently excited by the input rainfall, (b) the amount of information in the first phase of the flood is in any case small, and (c) identification problems are likely to arise in regard to interdependence of the variables to be adapted. This is the reason why a second approach was examined that involves residual treatment.

A scheme was implemented that encompasses the following steps: (a) At each time t, a hydrologic model based forecast is calculated based on rainfall forecasts and a chosen hydrologic model which in this case was the derived model initialised through a daily model, (b) the residuals of this model from the previous flood are treated to yield parameters of an autoregressive-moving-average (ARMA) model called error model, (c) a prediction error forecast is calculated through the error model which is then added to the hydrologic-model-based forecast described in (a) to obtain the final forecast.

This scheme was implemented for the Evinos catchment and for two different model structures, the SACRAMENTO model and the TANK model. Autoregressive models of orders one, two and three were fitted to the residuals with the aid of the Recursive Least Squares Linear Sampling (RLSLS) algorithm. This is an adaptive identification algorithm (Delleur and Obled, 1985) that allows efficient identification in real time through parameter updating. Problems of instability encountered during the initial phase of the flood events which were tested, which led to not updating parameters during flood events and to retain the parameters from the previous event each time.

The whole scheme was also implemented with a continuous-time hydrologic model that is directly identified on a long continuous data set (i.e. the reference true continuous-time model) The Evinos catchment (884 km^2) in Western Greece was used as a test basin. An example of the results obtained is given in Figure 4.3.2.

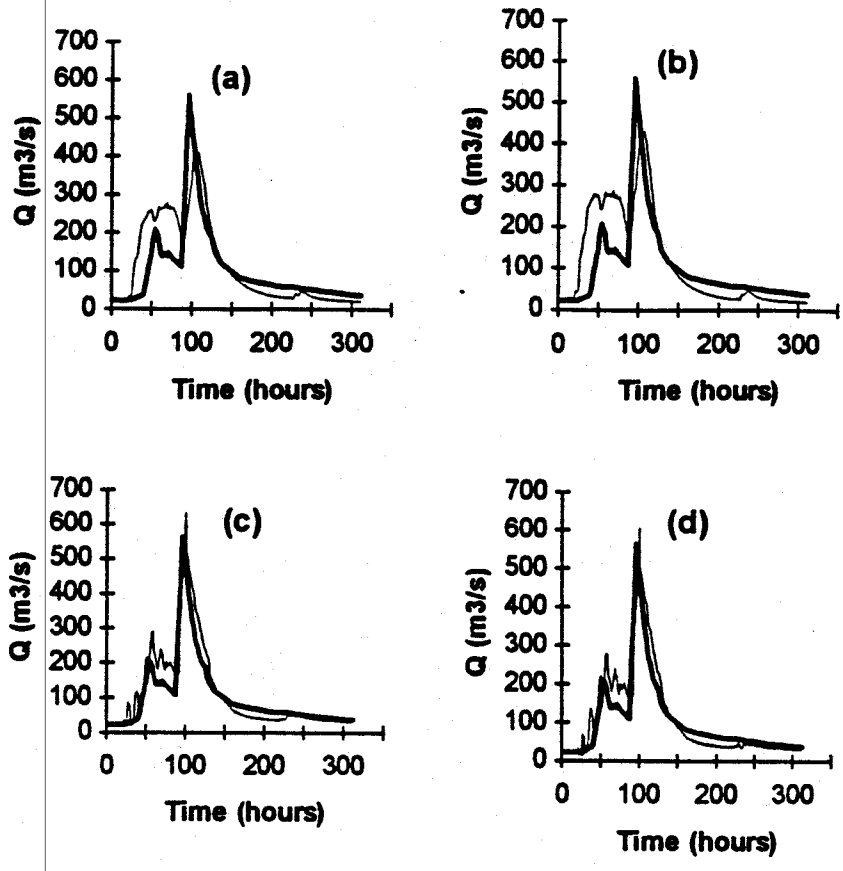

Figure 4.3.2. Effect of residual treatment applied on the TANK model: (a) continuous-time reference model, (b) event-based derived model initialised via the daily model, (c) as in (a) with residual treatment and (d) as in (b) with residual treatment. The lead time is four hours. The observed hydrographs are shown in bold solid lines while the simulated ones are in hairlines.

It appeared that:

(a) an autoregressive model of order two is sufficient to model the residuals,

(b) very high lag-one autocorrelation coefficients (> 0.95) are encountered in the treatment of residuals,

(c) this is extremely useful in correcting the hydrologic-model-based forecast for low lead times (up to four hours),

(d) the derived model initialised through a daily one performs equally to a true continuous-time model when both are subject to residual treatment; the latter result is valid for lead times up to six hours but degrades thereafter.

4.3.2 Missing data handling

The continuous type models that run in continuous mode need to possess the capablity for verification and the reconstruction of missing data. An operational method, taking advantage of space-time lag-one correlation is here presented in some detail, which enables the automatic reconstruction of missing data. (The method, originally developed on the Fuchun River project (E. Todini & Partners, 1992) was used on the Reno river for the real-time reconstruction of missing rainfall, runoff and temperature data).

A multivariate process is assumed to be defined (or approximated) by the lag-one model expressed by equation (4.1), which implies space-time dependence:

$$x_t = \Phi x_{t-1} + \varepsilon_t \tag{4.1}$$

where: x_t is the state vector with the value in the different stations at time t;

Φ is the state transition matrix from time interval t-1 to interval t ;

ε_t is the vector of residuals of the proposed model.

In order to set up a Kalman Filter, which will allow for the reconstruction of missing data, one must find an estimate for the matrix Φ as well as for the variance covariance matrix of residuals V_ε.

From equation (4.1), the residuals ε_t can be expressed as:

$$\varepsilon_t = x_t - \Phi x_{t-1} \tag{4.2}$$

and the problem of estimating the matrix Φ can be formulated as the following constrained quadratic programming problem in order to obtain an unbiased minimum variance estimator:

$$\begin{cases} \text{Min. Trace}\{V_\varepsilon\} \\ \text{s.t.} \quad \mu_\varepsilon = 0 \end{cases} \tag{4.3}$$

i.e. by minimising the trace of the variance covariance matrix of residuals V_ε, while imposing to zero their means μ_ε (given by equations (4.4) and (4.5) respectively):

$$V_\varepsilon = E\left\{(x_t - \Phi x_{t-1})(x_t - \Phi x_{t-1})^T\right\} = V_0 + \Phi V_0 \Phi^T - V_1 \Phi^T - \Phi V_1^T \quad (4.4)$$

$$\mu_\varepsilon = \mu_x - \Phi \mu_x \quad (4.5)$$

where: V_0 is the lag 0 variance-covariance matrix of observations at the different measurement stations.

V_1 is the lag 1 variance-covariance matrix of observations at the different measurement stations.

The constrained quadratic programming problem defined by equation (4.3) can be easily transformed into an unconstrained one by minimizing the Lagrangian function obtained by introducing the constraints into the objective function using a vector of Lagrange multipliers λ:

$$L(\Phi,\lambda) = \text{Trace}\left\{V_0 + \Phi V_0 \Phi^T - V_1 \Phi^T - \Phi V_1^T\right\} - \lambda^T(\mu_x - \Phi \mu_x) \quad (4.6)$$

By imposing the necessary conditions for an extreme, thus equating to zero the derivatives of the Lagrangian function with respect to the elements of matrix Φ and vector λ:

$$\begin{aligned} \frac{\partial L(\Phi,\lambda)}{\partial \Phi} &= \Phi V_0 - V_1 + \lambda \mu_x^T = 0 \\ \frac{\partial L(\Phi,\lambda)}{\partial \lambda} &= \Phi \mu_x - \mu_x \quad = 0 \end{aligned} \quad (4.7)$$

the problem can be further converted into the solution of a system of linear equations:

$$\begin{cases} \Phi V_0 + \lambda \mu_x^T & = V_1 \\ \Phi \mu_x & = \mu_x \end{cases} \quad (4.8)$$

From the first of equations (4.8) one obtains:

$$\Phi = \left(V_1 - \lambda \mu_x^T\right) V_0^{-1} \quad (4.9)$$

Substituting for Φ into the second of equations (4.8), gives:

$$\left(V_1 - \lambda \mu_x^T\right) V_0^{-1} \mu_x = \mu_x \tag{4.10}$$

from which one can derive the value of λ :

$$\lambda = \frac{V_1 V_0^{-1} - I}{\mu_x^T V_0^{-1} \mu_x} \mu_x \tag{4.11}$$

that can be substituted back into equation (4.9) to give:

$$\Phi = \left[V_1 - \left(V_1 V_0^{-1} - I\right) \frac{\mu_x \mu_x^T}{\mu_x^T V_0^{-1} \mu_x} \right] V_0^{-1} \tag{4.12}$$

which allows for the estimation of matrix Φ once the elements of vector μ_x and matrices V_0 and V_1 are estimated by means of equations (4.13), (4.14) and (4.15) respectively:

$$\mu_{x_i} = \frac{1}{n} \sum_{k=1}^{n} x_{i,k} \tag{4.13}$$

$$V_o(i,j) = \frac{1}{n} \sum_{k=1}^{n} \left(x_{i,k} - \mu_{x_i}\right)\left(x_{j,k} - \mu_{x_j}\right) \tag{4.14}$$

$$V_1(i,j) = \frac{1}{n} \sum_{k=1}^{n} \left(x_{i,k} - \mu_{x_i}\right)\left(x_{j,k-1} - \mu_{x_j}\right) \tag{4.15}$$

The estimate of Φ given by equation (4.12), if μ_x is not equal to zero, differs from the classical estimate that one obtains when dealing with zero mean processes and which is given by equation (4.16):

$$\Phi = V_1 V_0^{-1} \tag{16}$$

The estimator given by equation (4.12) is required by the fact that expression (4.16) fails to produce physically meaningful results in the case of rainfall time series where long dry spells are followed by rainfall events and where the overall mean is non null.

Once the matrix Φ has been estimated one can formulate a Kalman Filter which expression is given by equation (4.17):

$$\begin{cases} x_t = \Phi\, x_{t-1} + \varepsilon_t \\ C_t z_t = C_t (H\, x_t + v_t) \end{cases} \tag{4.17}$$

with the following definition of the noise terms ε and v:

$$\begin{cases} E\{\varepsilon\} = \mu_\varepsilon = 0 \\ E\left\{(\varepsilon - \mu_\varepsilon)(\varepsilon - \mu_\varepsilon)^T\right\} = V_\varepsilon = V_0 + \Phi\, V_0\, \Phi^T - V_1\, \Phi^T - \Phi\, V_1^T \end{cases}$$

$$\begin{cases} E\{v\} = \mu_v = 0 \\ E\left\{(v - \mu_v)(v - \mu_v)^T\right\} = V_v = R \end{cases} \tag{4.18}$$

where: R is the variance covariance matrix of measurement errors that must be provided.

As one can see, the measurement equation of the Kalman Filter has been slightly modified by the introduction of the matrix C_t for a question of dimensionality of the problem.

At time t, if the data are available in all the stations, the matrix C_t is an identity matrix, while if a number of stations do not report at time t the corresponding rows in matrix C_t will be eliminated.

The application of the Kalman Filtering equations then gives the algorithm described by equations (4.19), (4.20) and (4.21):

Extrapolation

$$\boxed{\begin{aligned} \hat{X}_{t|t-1} &= \Phi\, \hat{X}_{t-1|t-1} \\ P_{t|t-1} &= \Phi\, P_{t-1|t-1}\, \Phi^T + v_\varepsilon \end{aligned}} \tag{4.19}$$

Measurement and estimation

$$\boxed{\begin{aligned} v_t &= C_t\left(z_t - H\, \hat{X}_{t|t-1}\right) \\ K_t &= P_{t|t-1}\, H^T C_t^T \left[C_t\left(H\, P_{t|t-1}\, H^T + R\right) C_t^T\right]^{-1} \end{aligned}} \tag{4.20}$$

Correction

$$\boxed{\begin{aligned}\hat{X}_{t|t} &= \hat{X}_{t|t-1} + K_t\, v_t \\ P_{t|t} &= (I - K_t\, C_t\, H)\, P_{t|t-1}\end{aligned}} \qquad (4.21)$$

The application of this methodology to different hydro-meteorological measurements requires a different definition of variable x_t.

In the case of rainfall or discharges x_t will be respectively the total rain rate and the average discharge in the sampling interval.

In the case of temperature, in order to eliminate the strong daily cyclicity and to approximately stationarise the time series, x_t will be defined as

$$x_t = T_t - T_{t-n\Delta t} \qquad (4.22)$$

i.e. the difference between the sampled temperature at time t and that of n increments of time before (being n the ratio between the number of seconds in one day and the number of seconds in one sampling interval).

A number of examples of application of the proposed methodology to the Fuchun river catchment (Figure 4.3.3), for which the methodology was developed, are reported in the sequel. Figures 4.3.4, 4.3.5, 4.3.6 show the comparison between the actual precipitation measurements and their reconstruction obtained by means of the Kalman Filter in the hypothesis of a completely non available record for each of the three stations.

Figures 4.3.7, 4.3.8, 4.3.9 show the comparison between the actual discharge measurements and their reconstruction obtained by means of the Kalman Filter in the hypothesis of a completely non available record for each of the three stations.

Figures 4.3.10, 4.3.11, 4.3.12 show the comparison between the actual temperature measurements and their reconstruction obtained by means of the Kalman Filter in the hypothesis of a completely non available record for each of the three stations.

Examples of application of the methodology to the Reno river are reported in Figures 7.8 and 7.9 (Chapter 7).

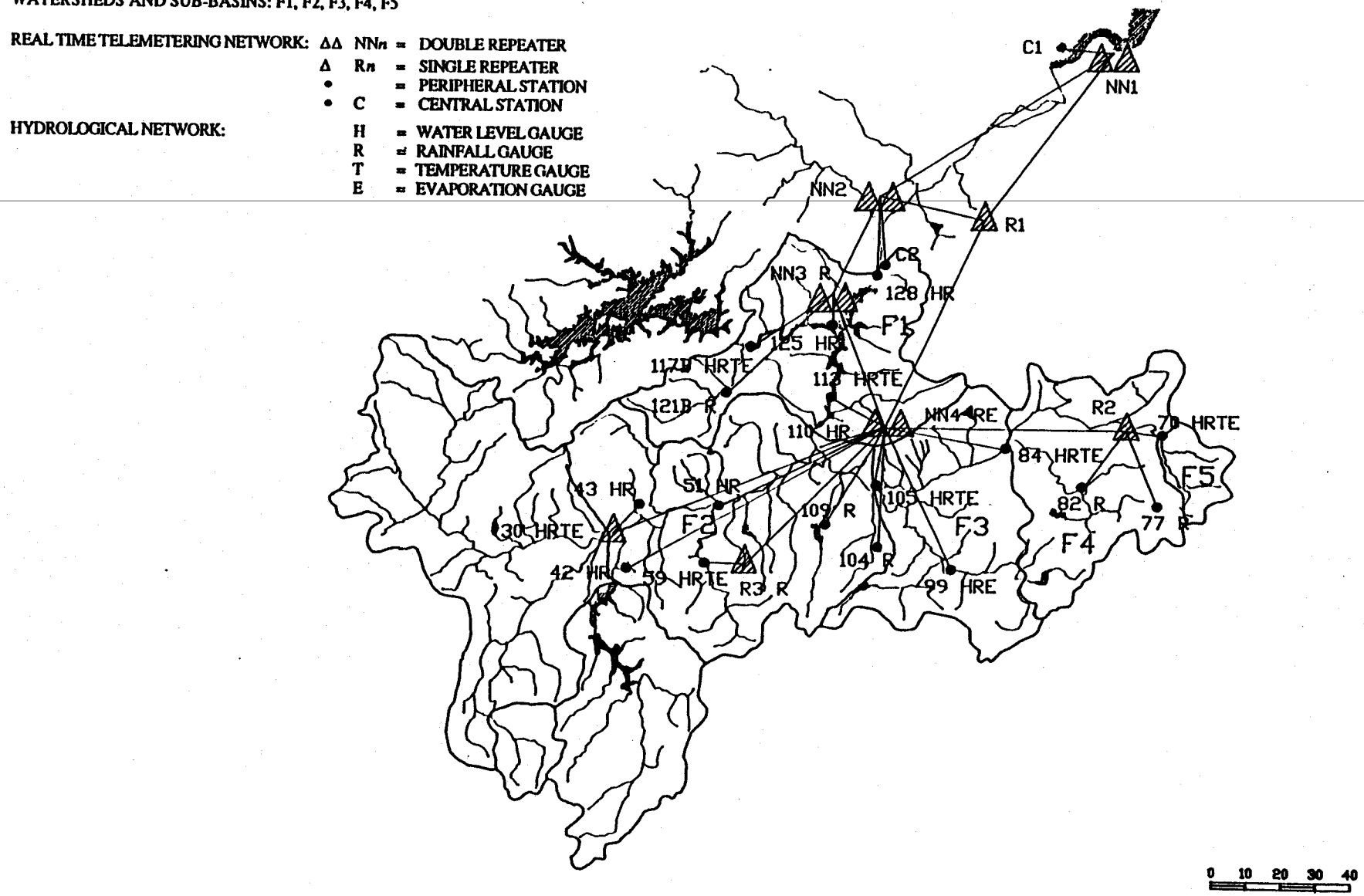

Figure 4.3.3 - The Fuchun catchment and the hydro-meteorological network.

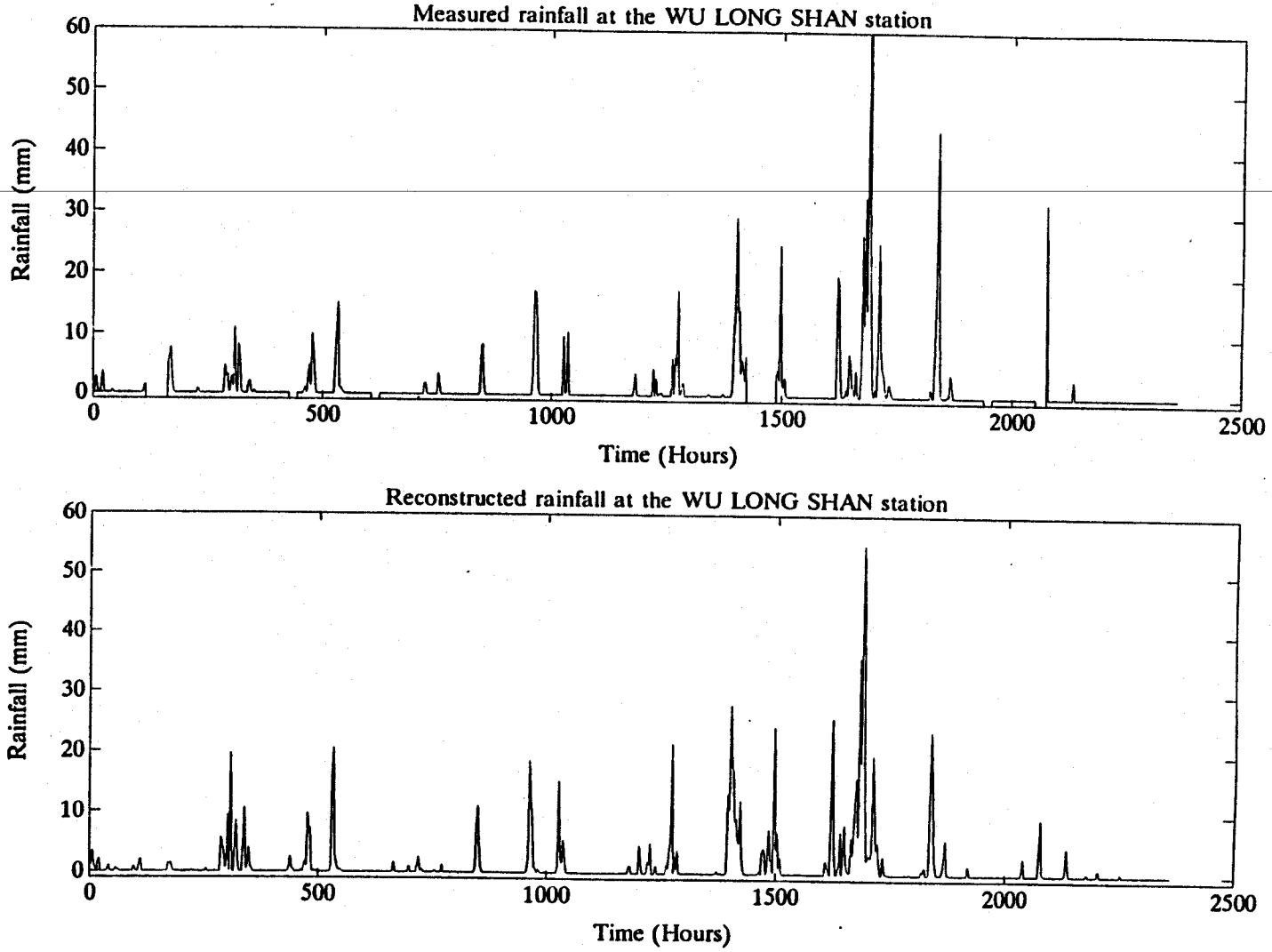

Figure 4.3.4 Reconstruction of precipitation data at Wu Long Shan assuming that the measurements were not available for the entire period

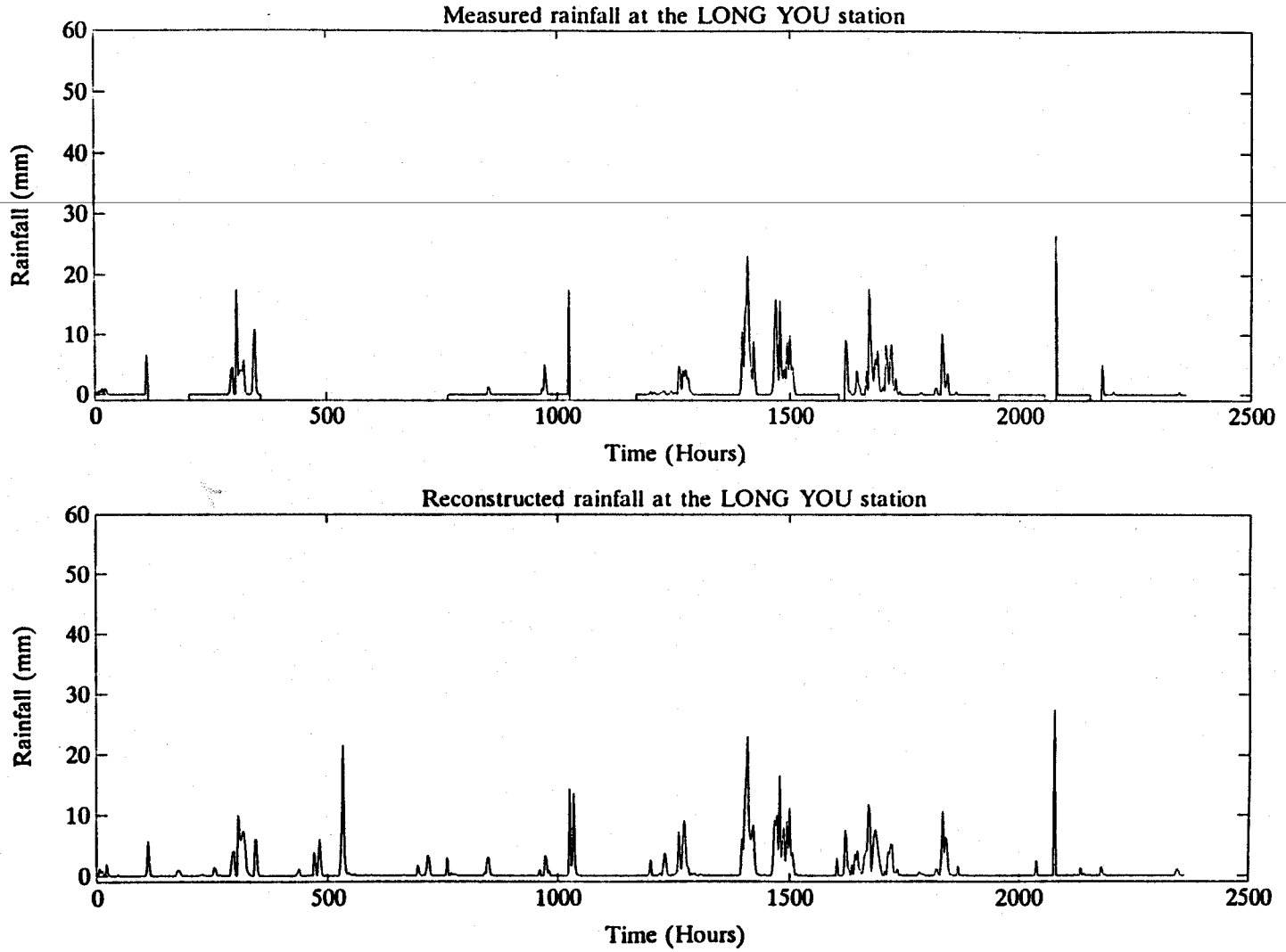

Figure 4.3.5 Reconstruction of precipitation data at Long You assuming that the measurements were not available for the entire period

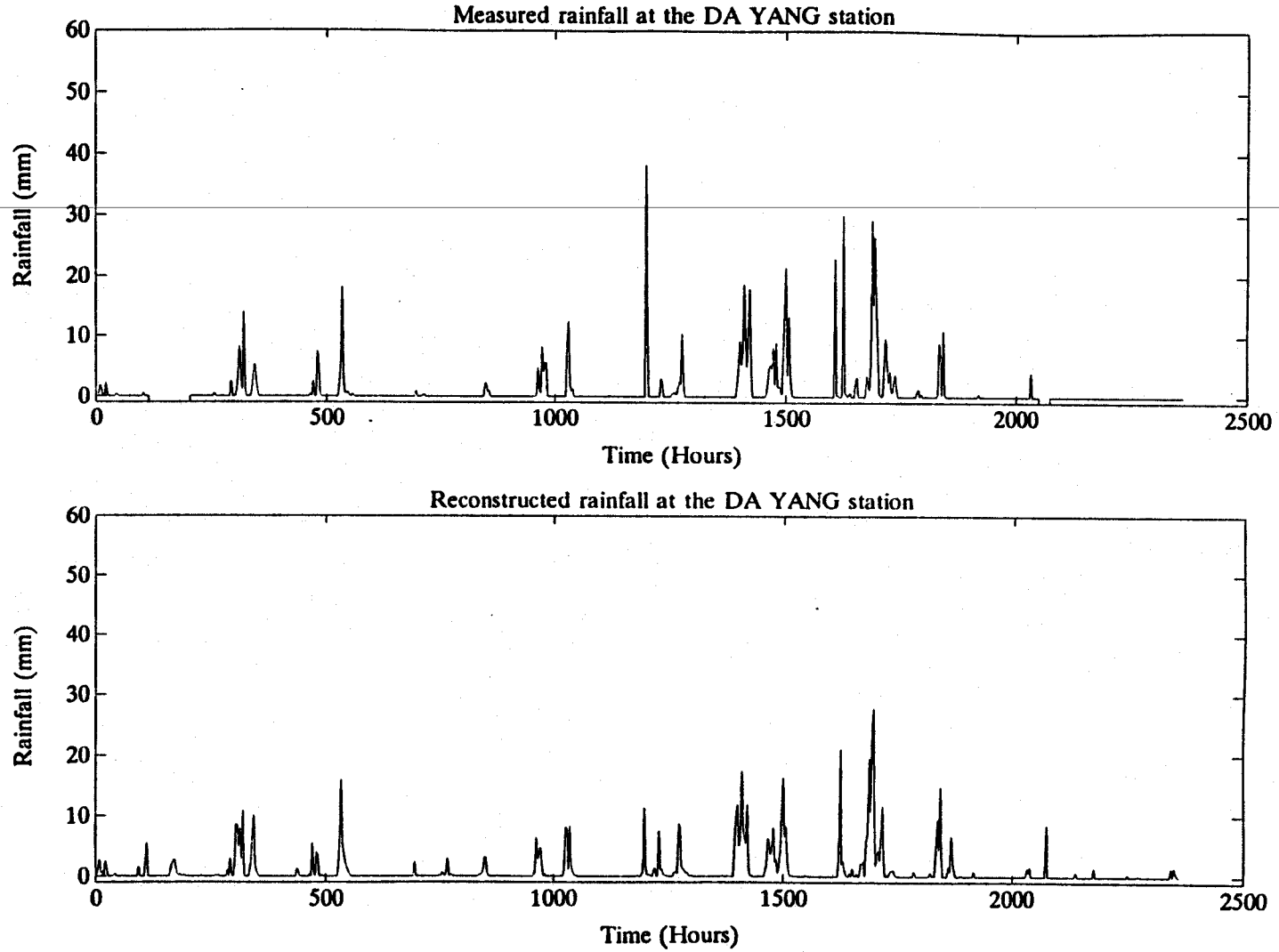

Figure 4.3.6 Reconstruction of precipitation data at Da Yang assuming that the measurements were not available for the entire period

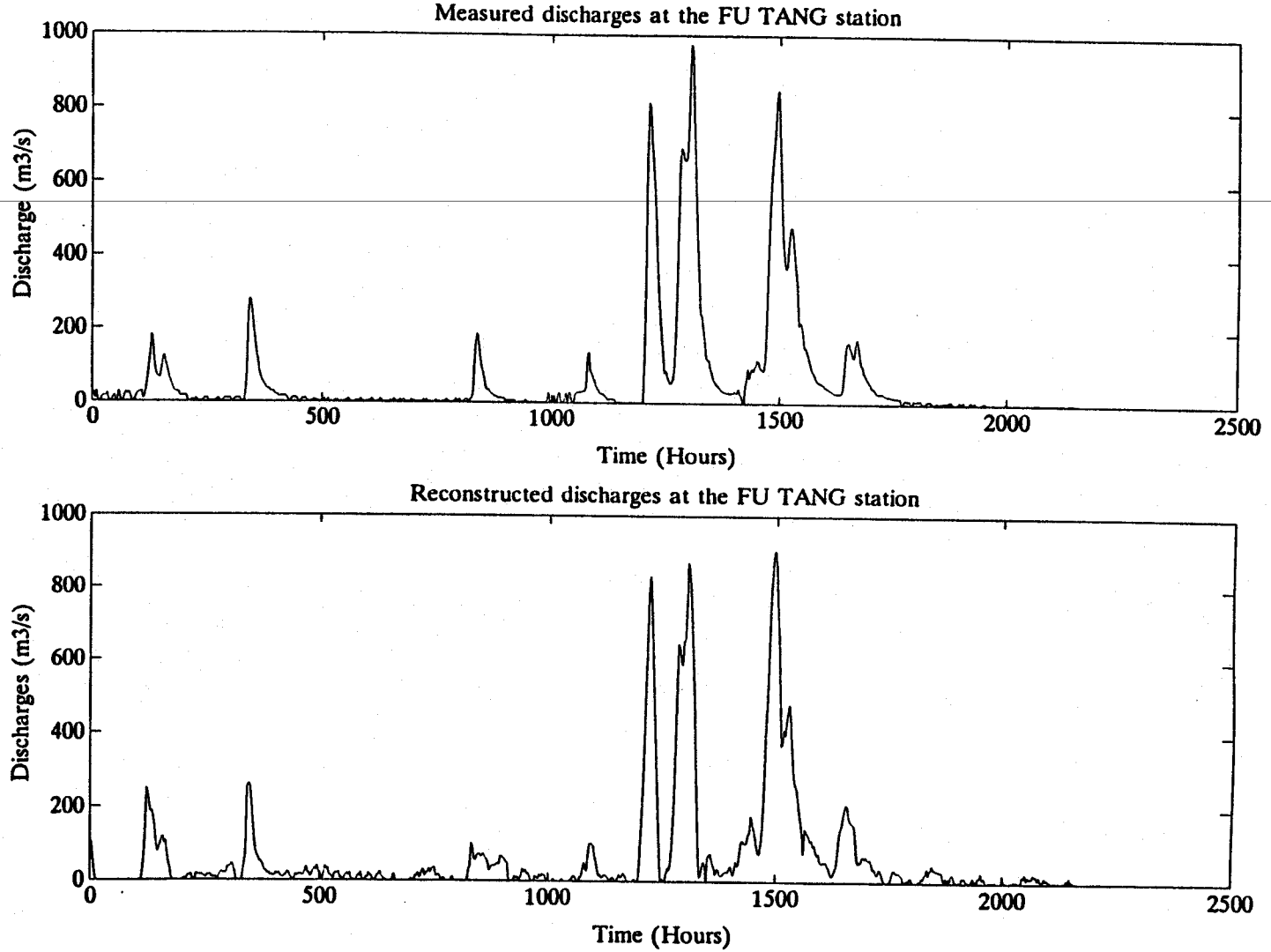

Figure 4.3.7 Reconstruction of discharge data at Fu Tang assuming that the measurements were not available for the entire period

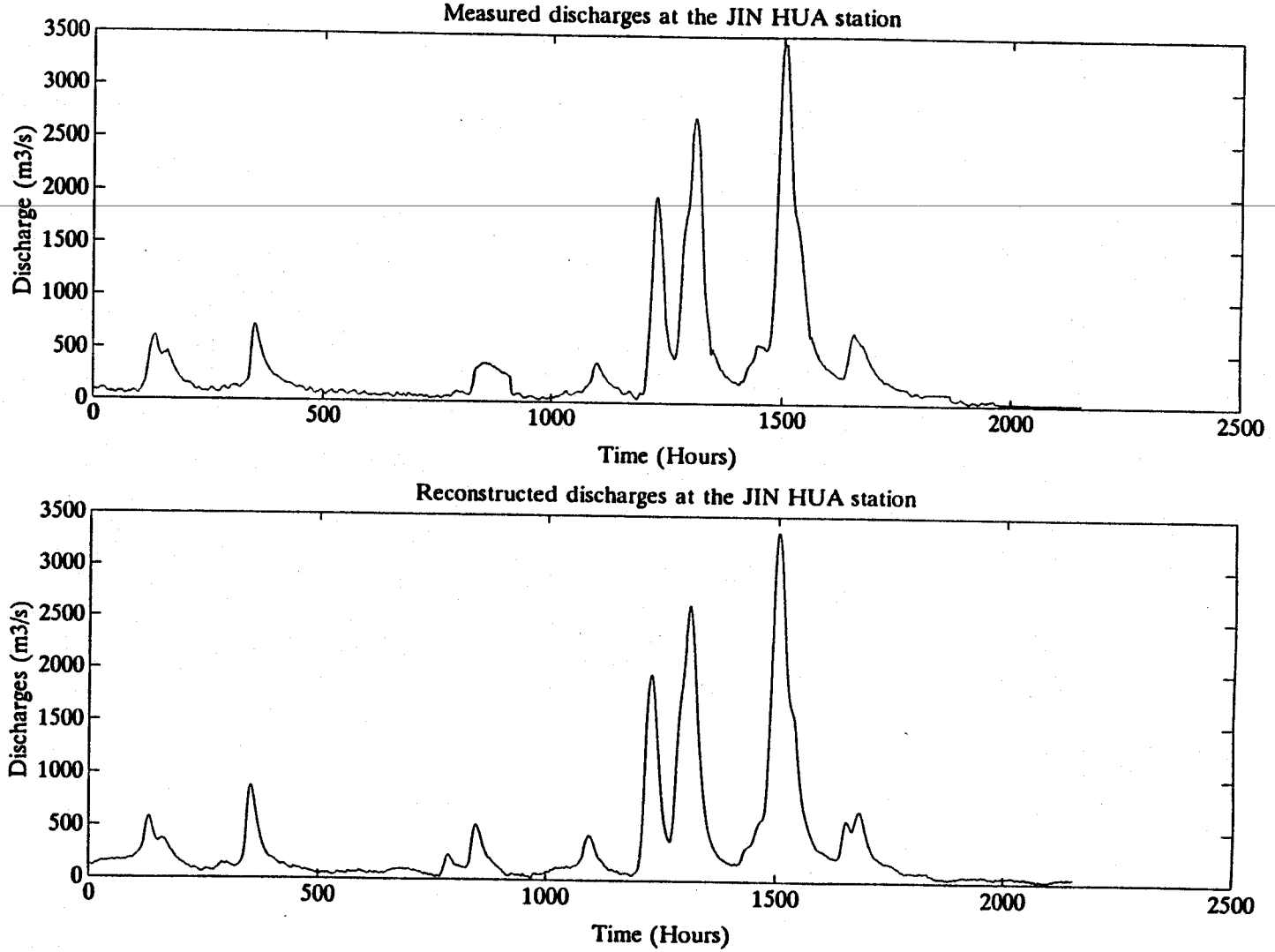

Figure 4.3.8 Reconstruction of discharge data at Jin Hua assuming that the measurements were not available for the entire period

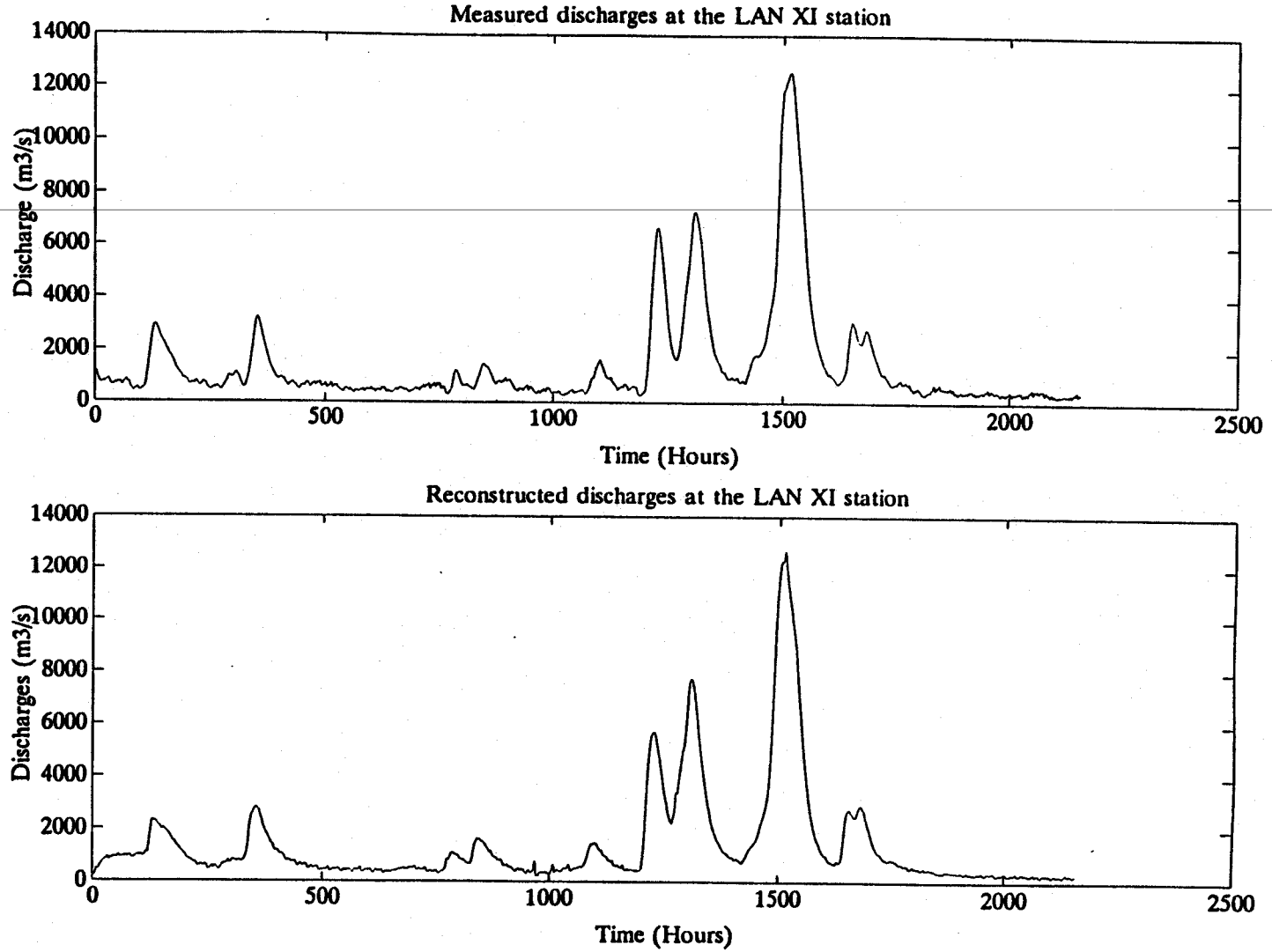

Figure 4.3.9 Reconstruction of discharge data at Lan Xi assuming that the measurements were not available for the entire period

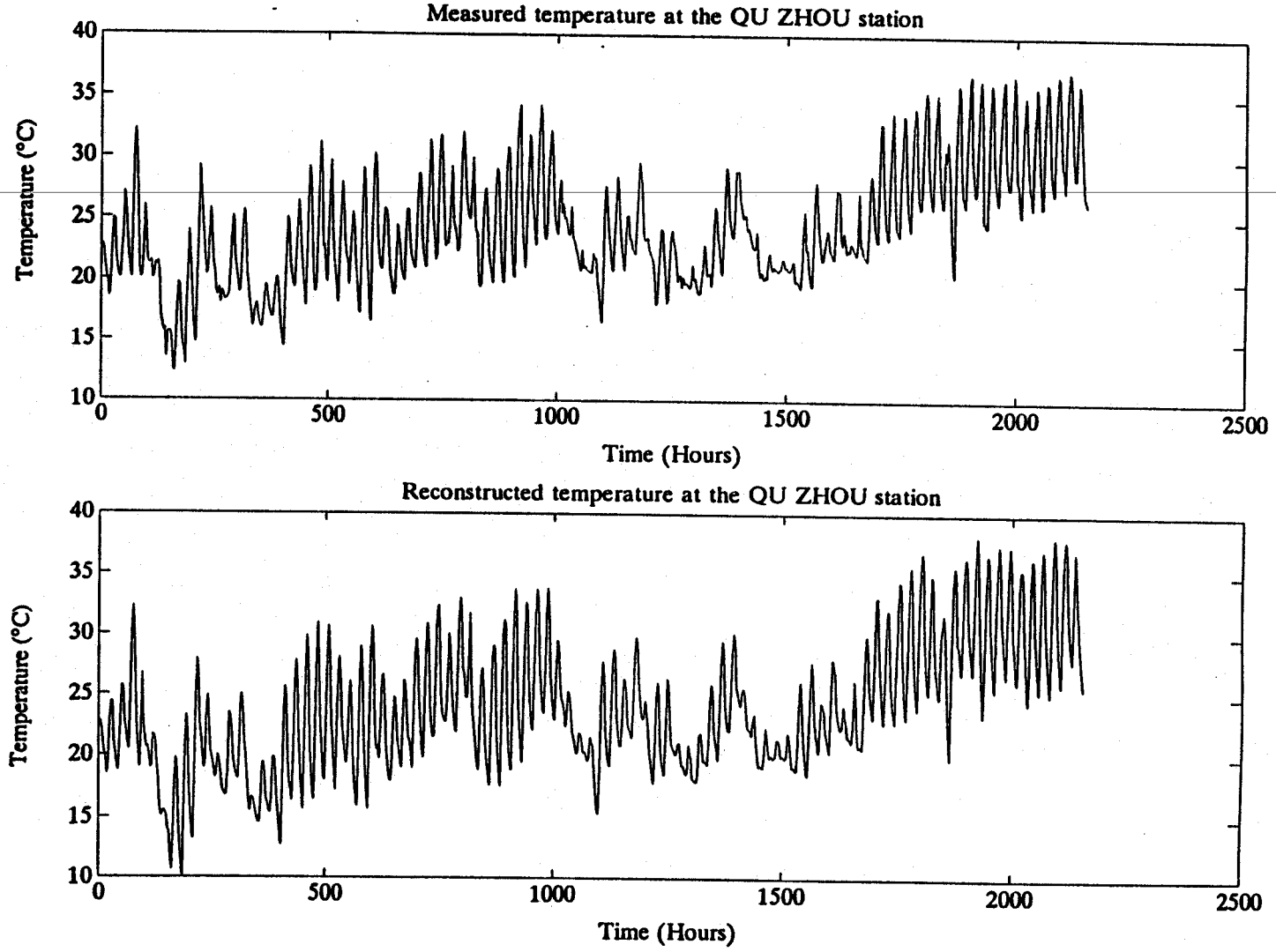

Figure 4.3.10 Reconstruction of temperature data at Qu Zhou assuming that the measurements were not available for the entire period

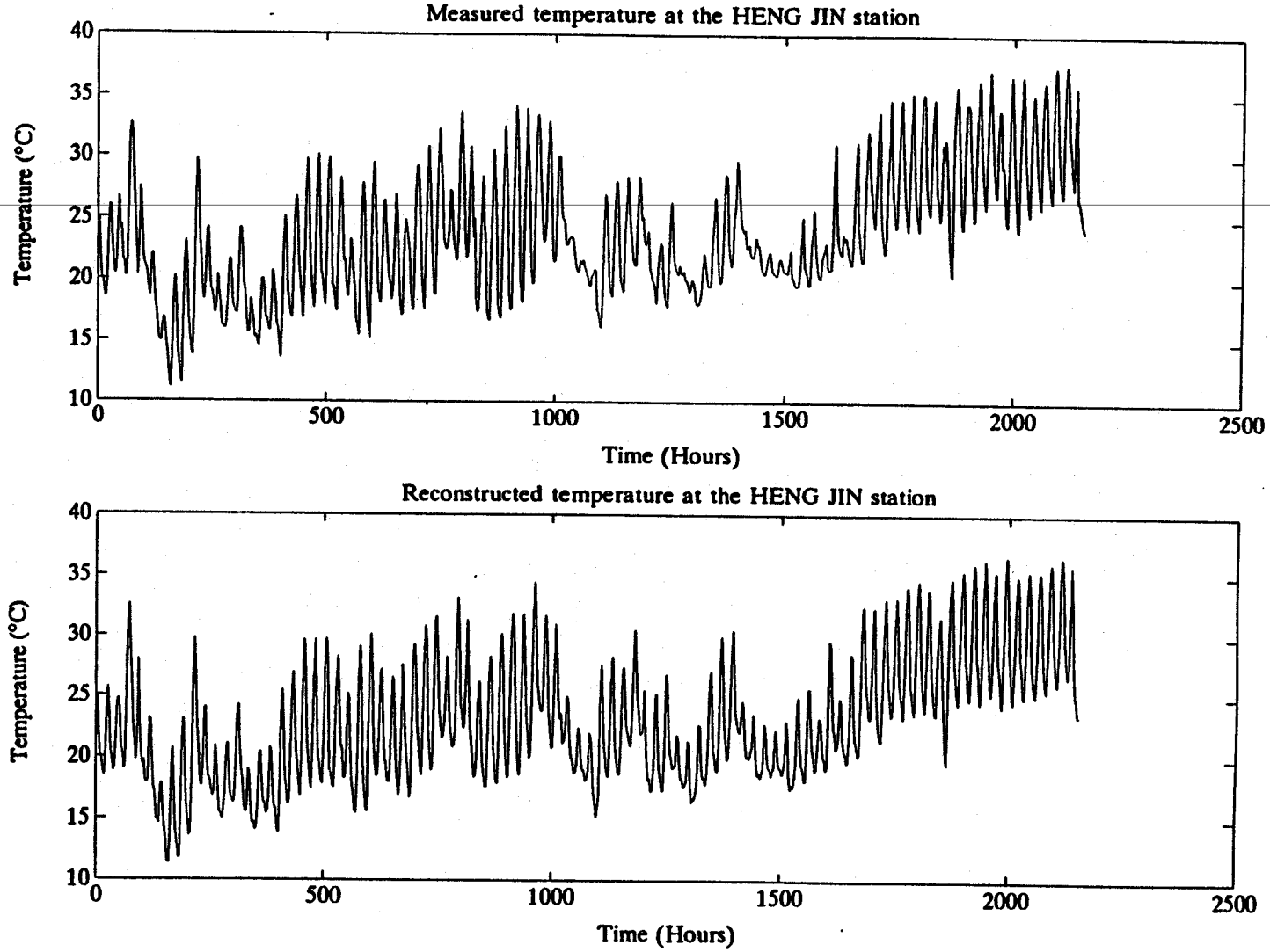

Figure 4.3.11 Reconstruction of temperature data at Heng Jin assuming that the measurements were not available for the entire period

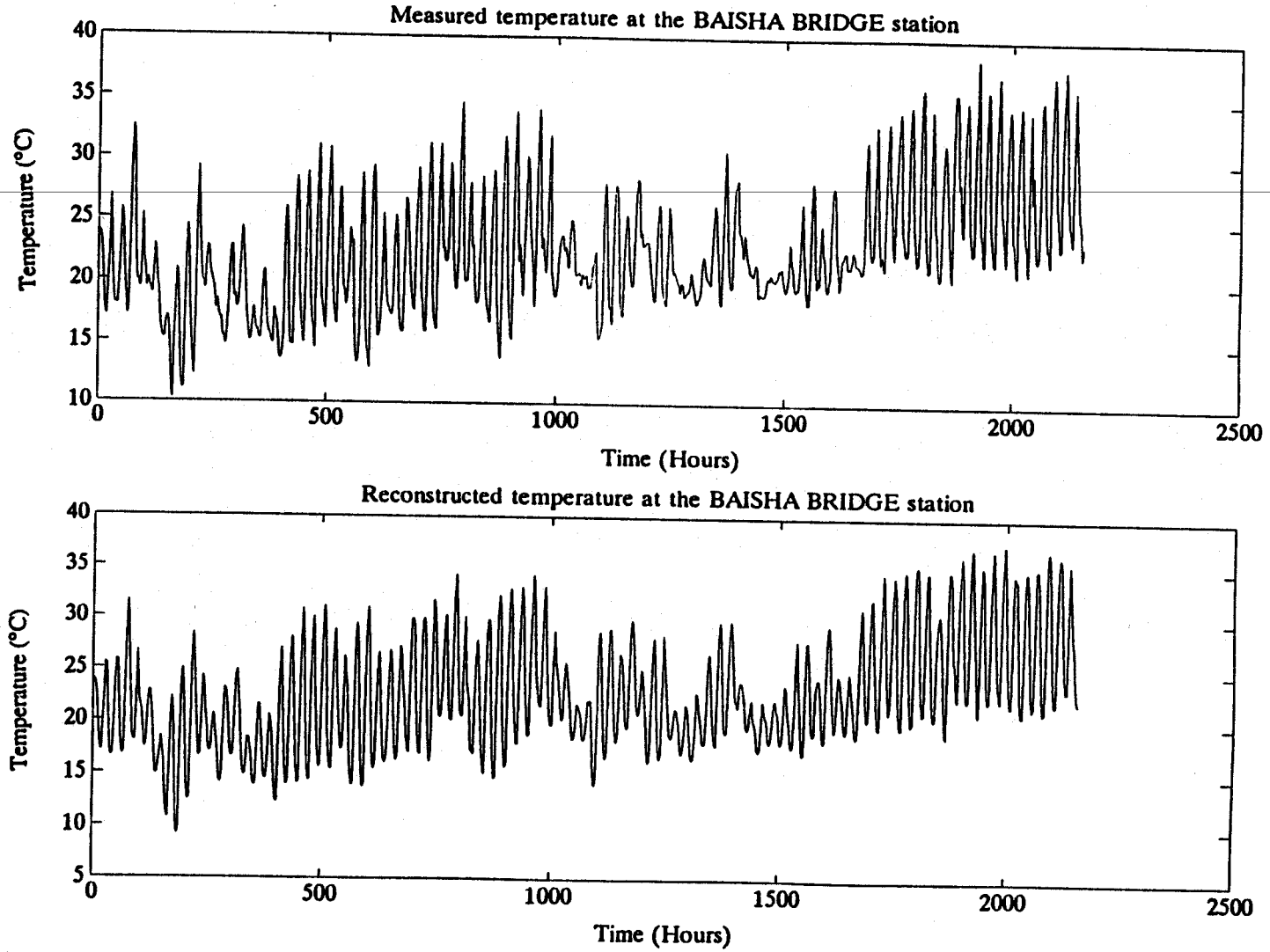

Figure 4.3.12 Reconstruction of temperature data at Baisha Bridge assuming that the measurements were not available for the entire period

4.3.3 Coupling rainfall forecasts with rainfall runoff models

Although this idea has been proposed a long time ago (Lebel 1984), it has received interest only recently (Brath et al. 1988, Bertoni et al. 1992). It simply consists of linking a synthetic rainfall generator with a rainfall runoff model to compensate for the lack of knowledge on future incoming rainfalls (see Figure 4.3.13 (a)). In this work, a simplified lumped version of TOPMODEL (renamed since TOPSIMPL - see paragraph 4.2.4) has been used. Rainfall generator outputs, i.e. scenarios of future rainfall amounts (see Chapter 2, paragraph 2.3.1.2 of this report for details), were considered as possible inputs for TOPMODEL, therefore producing future discharges scenarios at the outlet of the catchment (see Figure 4.3.13(b)).

A lead-time of 12 hours (i.e. a scenario length of 12 hours) was considered a good compromise between operational requirements (warning message to be sent early enough) and performance of the rainfall generator.

It must be remembered that the generator was used in a conditional mode, i.e. scenarios for the coming 12 hours were constrained by the observed basin averaged rainfalls until the current time t. They are therefore possible future sequences based on what has already been observed. Given the correlation structure of rainfall, there is little information to constrain the scenario beyond 12 hours ahead. However, this could be improved by using information on 12 or 24 hours rainfall totals if available, and this will be tested in the future. However, the first goal was already to test if conditioning scenarios from past rainfalls can improve the discharge forecast.

The system of coupling a rainfall generator with a rainfall-runoff model produces, at each timestep of a flood event, a bunch of scenarios representing a wide range of possible future discharges actually conditionned by the past meteorological situation.

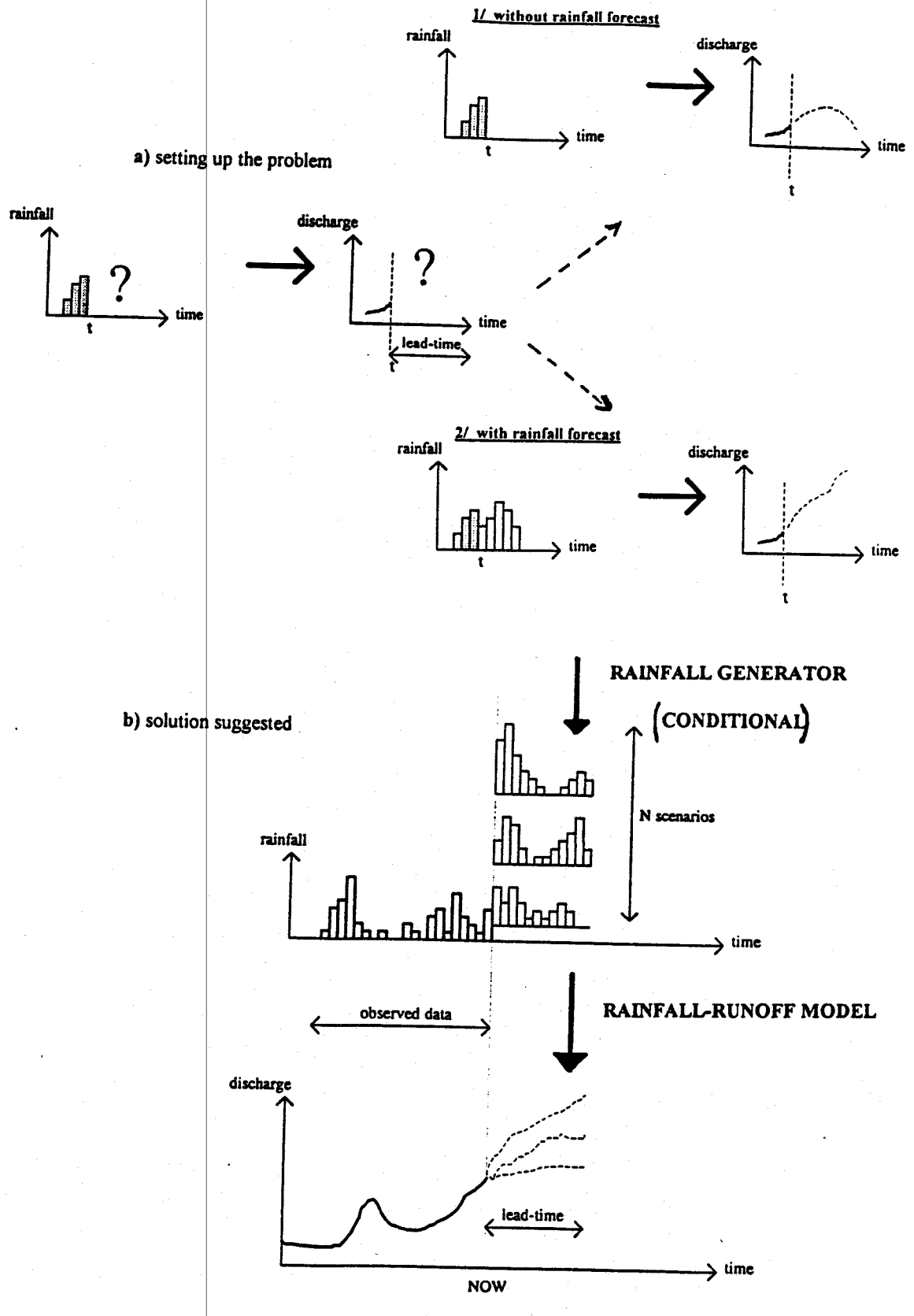

Figure 4.3.13 - Coupling Rainfall scenarios with a rainfall runoff model